Materials Horizons

ROYAL SOCIETY OF CHEMISTRY

COMMUNICATION

View Article Online
View Journal | View Issue

Cite this: *Mater. Horiz.*, 2024, **11**, 3662

Received 18th April 2024,
Accepted 10th May 2024

DOI: 10.1039/d4mh00464g

rsc.li/materials-horizons

High-entropy alloy screening for halide perovskites†

Christopher P. Muzzillo, *[a] Cristian V. Ciobanu [b] and David T. Moore [a]

As the concept of high-entropy alloying (HEA) extends beyond metals, new materials screening methods are needed. Halide perovskites (HP) are a prime case study because greater stability is needed for photovoltaics applications, and there are 322 experimentally observed HP end-members, which leads to more than 10^{57} potential alloys. We screen HEAHP by first calculating the configurational entropy of 10^6 equimolar alloys with experimentally observed end-members. To estimate enthalpy at low computational cost, we turn to the delta-lattice parameter approach, a well-known method for predicting III–V alloy miscibility. To generalize the approach for non-cubic crystals, we introduce the parameter of unit cell volume coefficient of variation (UCV), which does a good job of predicting the experimental HP miscibility data. We use plots of entropy stabilization *versus* UCV to screen promising alloys and identify 10^2 HEAHP of interest.

New concepts

We demonstrate the new concept of using unit cell volume coefficient of variation to approximate the enthalpic penalty of a given high-entropy alloy candidate, and use it along with ideal sublattice configurational entropy to map promising high-entropy alloy halide perovskites. While lattice parameter differences have been used for 50 years to predict III–V alloy miscibility, we extend this approach to non-cubic crystals for the first time, and introduce it as a metric for high-entropy alloy materials screening. This new approach is particularly valuable for guiding the search for nonmetallic high-entropy alloys, which is in its infancy for covalent-bonded and semiconducting materials.

1. Introduction

Halide perovskites (HP) are a broad class of materials spanning 322 inorganic and hybrid organic–inorganic crystals. The prototypical ABX_3 HP has oxidation states of A^+, B^{2+} and X^-. The HP's divalent metal (B^{2+}) constituent is octahedrally coordinated to 6 halide ions (X^-). These octahedra share corners to form a three-dimensional inorganic framework that surrounds the weakly-bonded A^+ constituents in cuboctahedral sites.[1,2] Entropy stabilization (ES) is an emerging method[3–5] where components are added to a given material until its configurational entropy meaningfully alters its Gibbs free energy.

ES of HP is of interest for their many applications: for electrochemical energy storage materials, ES can enhance ion transport.[6,7] For thermoelectrics, ES reduces thermal conductivity.[8] For photovoltaics (PV), the enhanced stability of ES is desirable: the photoactive polytypes of the prototypical inorganic HP PV absorber $CsPbI_3$ are metastable below ~375 K.[9] However, the negative impact of ES on charge carrier transport or recombination may limit its use to non-absorbing PV functions such as buffer layers, transport layers or mechanical anchors.[10] For other HP applications such as light-emitting diodes (LEDs), lasers, neuromorphics, scintillators, *etc.*, the role of entropy is less clear, but such an extensively inhabited class of crystals make HEAHP of general interest for engineering, such that the boundaries of what is possible, feasible, and useful warrant exploration.

Density functional theory (DFT) is currently being used to screen HEA boride, carbide, and carbonitride ceramics.[11] We stress that computationally efficient *pre*screening methods are needed even for choosing alloys for DFT because HEA have large unit cells, and the 322 experimentally observed HP can combine to form 10^{57} alloys (considering equimolar compositions with up to 48 end-members). In our first screening, we report the 10^6 HEAHP consisting entirely of experimentally observed end-members. We then further screen by quantifying their ideal mixing ES and estimate enthalpic penalty using end-member unit cell volume coefficient of variation (UCV), identifying 10^2 alloys with promising UCV-ES tradeoffs.

2. Results

Metal alloys are the prototypical ES case because they commonly have single site lattice structures. This makes metals

[a] *National Renewable Energy Laboratory, Golden, CO, USA.*
E-mail: christopher.muzzillo@nrel.gov
[b] *Colorado School of Mines, Golden, CO, USA*

† Electronic supplementary information (ESI) available. See DOI: https://doi.org/10.1039/d4mh00464g

behave like ideal solid solutions, so their entropies increase dramatically as components are added: the configurational entropy of a 6-component equimolar mixture of (metal) elements on a single sublattice is −4.5 kJ mol^{-1} at 300 K.[12] ES of oxides has been demonstrated in $Mg_{0.2}Co_{0.2}Ni_{0.2}Cu_{0.2}Zn_{0.2}O$[13] and many other oxides.[14] Although MgO, NiO, CuO, and ZnO have different structures and a mean Gibbs energy of formation of −307 kJ mol^{-1},[15] the thermodynamics of $Mg_{0.2}Co_{0.2}Ni_{0.2}Cu_{0.2}Zn_{0.2}O$ were predominated by entropy,[13] despite possessing ES of only −2.0 kJ mol^{-1} at 300 K. By comparison, HP ES should be relatively large and easy to measure. We find 282 inorganic HP that have been experimentally observed[16–24] and theory suggests that many more may exist,[23–27] so a staggeringly wide combinatorial chemical space can be drawn on to realize this potential. Moreover, weak bonding allows entropy to dominate HP Gibbs energies.[28]

A given alloy composition change can be net stabilizing if that change's configurational ES outweighs any enthalpic destabilization. In order to screen for promising alloy compositions, we assume each sublattice (A cation, B cation, and X anion) behaves like an ideal solid solution[12] to calculate the entropy of mixing (configurational entropy; S/R), as well as the ES term in the Gibbs energy equation at 300 K:

$$S/R = -\left(\frac{1}{5}\sum_i y_i^{\mathrm{A}} \ln\left(y_i^{\mathrm{A}}\right) + \frac{1}{5}\sum_j y_j^{\mathrm{B}} \ln\left(y_j^{\mathrm{B}}\right) + \frac{3}{5}\sum_k y_k^{\mathrm{X}} \ln\left(y_k^{\mathrm{X}}\right)\right) \quad (1)$$

$$\text{ES term} = -TS = RT\left(\frac{1}{5}\sum_i y_i^{\mathrm{A}} \ln\left(y_i^{\mathrm{A}}\right) + \frac{1}{5}\sum_j y_j^{\mathrm{B}} \ln\left(y_j^{\mathrm{B}}\right) + \frac{3}{5}\sum_k y_k^{\mathrm{X}} \ln\left(y_k^{\mathrm{X}}\right)\right) \quad (2)$$

R is the gas constant, T is temperature (K), and y_i^{A} is the mole fraction of the ith constituent on the A sublattice in ABX_3. Actual atomic distributions in (metal) HEA have been considered,[29,30] and simple scaling rules have been developed to predict HEA stability for metals.[31–37] Unlike metals, ABX_3 HP have covalent to ionic bonding and 3 distinct lattice sites (A, B, and X), which limits how much they can be stabilized with configurational entropy.[38]

In contrast to ES, estimating enthalpy for screening HEAHP is challenging, leading to a tradeoff between accuracy and computational (or experimental) cost. Experimentally screening HEA is most accurate and most expensive. The next most accurate and expensive method combines DFT with the special quasirandom structures approach.[39–44] Alternative approaches have been developed to screen alloys[45–48] and HEA,[49–53] but these are either too computationally expensive,[49,51] need too much experimental data,[53] or use experiment-free phase diagrams to predict HEA with machine learning, which has limited interpretability.[50,52] An approach with even lower computational cost is to estimate mixing enthalpy, which is proportional to the difference between the lattice parameters of a III–V alloy's constitutive end-members.[54] Based on the Hume–Rothery rules for metal alloying (minimize atomic radii differences, match crystal structures, keep valency constant, and keep electronegativity constant),[55] Foster showed that lattice parameter differences could be used to predict miscibility in III–Vs and II–VIs.[56] Foster and Stringfellow used this "delta-lattice parameter" approach to correctly group the miscibility of 9 ternary II–VI[56] and 9 quaternary III–V[57] alloy systems, respectively, and the method was recently extended to correctly group the miscibility of 18 ternary III–V alloy systems,[58] confirming broad accuracy in spite of its low computational cost. To extend the delta-lattice parameter method to non-cubic structures, we draw on Zen's law: there is an empirical linear relation between molar volume and composition of a solid solution.[59] (Zen's law simplifies to Vegard's law[60] for cubic structures with similar molar volumes.) Therefore, an HP alloy's unit cell volume is its weighted mean ($\bar{V}_{\mathrm{w}}$):

$$\bar{V}_{\mathrm{w}} = \sum_i \sum_j \sum_k y_i^{\mathrm{A}} y_j^{\mathrm{B}} y_k^{\mathrm{X}} V_{ijk_3} \quad (3)$$

Here V_{ijk_3} is the unit cell volume of the end-member with the ith, jth and kth constituent on the A, B and X sublattices, respectively. To reduce complexity, we consider only equimolar compositions, which have the greatest ES term. (A semiconductor alloy's density of states can shift its entropic minimum away from the equimolar composition,[61] so other compositions should be considered after the initial screening.) The equimolar unit cell volume's mean, standard deviation, and coefficient of variation are:

$$\bar{V} = \frac{\sum_i \sum_j \sum_k V_{ijk_3}}{N} \quad (4)$$

$$\sigma = \sqrt{\frac{\sum_i \sum_j \sum_k \left(V_{ijk_3} - \bar{V}\right)^2}{N}} \quad (5)$$

$$\mathrm{UCV} = \frac{\sigma}{\bar{V}} \quad (6)$$

Here $\bar{V}$ is equimolar unit cell volume, σ is equimolar alloy unit cell volume standard deviation, UCV is equimolar alloy unit cell volume coefficient of variation, and N is the number of end-members. Atomic radius differences,[62–64] lattice parameter differences,[65,66] and atomic position differences[67] have been previously parameterized to screen metal HEA. We instead parameterize unit cell volume to extend the approach to non-cubic crystals. Although perovskite lattice parameter was previously shown to correlate with ionic radii,[68,69] we use eqn (6) for enthalpic penalty in HEA for the first time. We confirm agreement with 42 out of 45 room temperature miscibility gap data from III–V (Fig. 1 and Table S1, ESI†)[57,58] and II–VI (Table S1, ESI†)[56] material systems. UCV correlates well with experimental III–V and II–VI mixing enthalpy (Table S1 and Fig. S1, ESI†), although future work using the elastic modulus or melting temperature are expected to improve the fit.[70] Using the phase

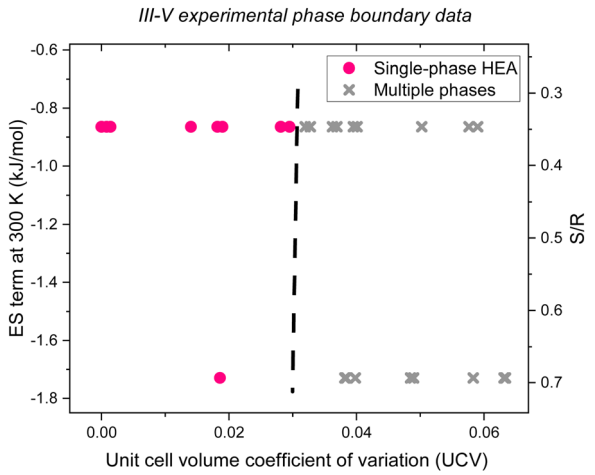

Fig. 1 Experimental III–V single-phase alloy (pink circles) and multiple phase (gray Xs) data,[57,58] confirming that plotting the ES term at 300 K (or *S*/*R*) as a function of UCV leads to a phase boundary near UCV of 0.03 (black dashed line) which is useful for screening HEA that have not yet been experimentally synthesized.

boundary for HP in Fig. 2,[71] 22 out of 26 experimental HEAHP data are grouped correctly. Mapping the boundary between single-phase and multiple phase alloys with UCV-ES plots also works for boride, carbide, and carbonitride ceramics: Fig. S2 and Tables S2, S3 (ESI†) show correct grouping of 56 out of the 64 miscibility data (88% accuracy). Good agreement with such broad experimental data and no fitting parameters suggests the UCV approach has sufficient accuracy despite its low computational cost. UCV allows us to directly compare cubic and hettotype perovskites—the latter have distortions that reduce symmetry, but are more common (*e.g.*, $CsPbI_3$'s metastable polymorphs).[1,2] There are more reports of single-phase inorganic HEAHP (Table S4, ESI†)[71–219] and hybrid organic–inorganic

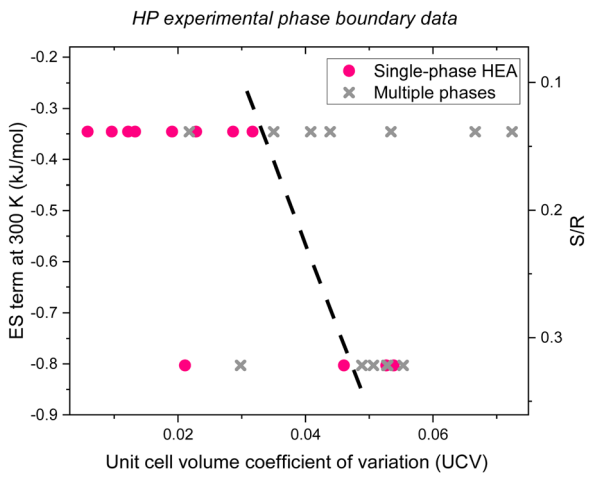

Fig. 2 Experimental HP single-phase alloy (pink circles) and multiple phase (gray Xs) data,[71] confirming that plotting the ES term at 300 K (or *S*/*R*) as a function of UCV leads to a phase boundary near UCV of 0.04 (black dashed line) which correctly groups 22 of the 26 data. Binary copper alloys are excluded because the synthesis method did not produce phase pure $KCuF_3$.[71]

HEAHP (Table S5, ESI†),[220–285] but more investigation into single-phase boundaries is needed to confirm the broadscale applicability of UCV for screening HEAHP.

Using DFT we calculate mixing enthalpy of 6 HEAHP compositions. To make the computations tractable we approximate a HEA's mixing enthalpy by calculating the energy of 8 distinct configurations of 40-atom unit cells and reference their mean to that alloy's constitutive end-members. The results in Fig. 3 and Table S6 (ESI†) confirm that UCV correlates with DFT mixing enthalpy for HEAHP.

It was argued that for thermoelectric devices ES can enhance crystal symmetry to preserve charge carrier transport despite the disordered nuclei that impede phonons and reduce thermal conductance.[8,286] In $CH_3NH_3PbI_3$ phonon lifetimes are shortened by the organic cation's entropy, which may improve charge carrier recombination properties.[287] HP's peculiar semiconductor physics have been attributed to dynamic disorder,[288] lattice softness and anharmonicity.[289]

Beyond PV absorbers, ES HP may be useful as oxygen evolution electrocatalysis,[71] electrochemical energy storage,[86] thermoelectrics,[8] light emitting diodes, photodetectors, PV buffers, contacts, solid state radiation detectors, scintillators, fuel cells, lasers, high temperature electronic components, barocaloric materials for use in refrigeration, ferroelectrics, and neuromorphic computers.

The disordered nuclei in ES HP may alter phonons, possibly reducing thermal conductance. Restricted phonons can result in slow cooling of hot charge carriers, similar to what is already observed in HP as a result of light-induced lattice distortions.[290,291] On the other hand, local bonding distortions in ES crystals should disrupt electron band energies, creating a distribution of local energy states similar to what was described for ion conductivity through ES materials.[7] Thus, bulk 3D carrier transport may suffer, but there may good charge carrier transport along specific crystal directions.

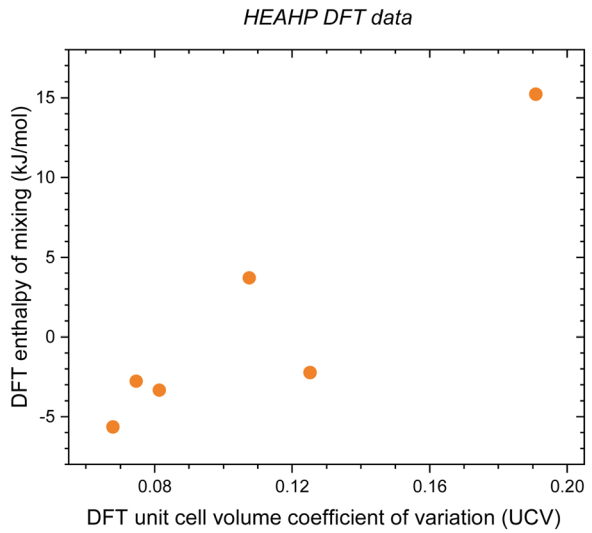

Fig. 3 DFT enthalpy of mixing as a function of UCV from DFT for the HEAHP in Table S6 (ESI†), showing that UCV correlates with DFT mixing enthalpy.

2.1 Mixing on all sublattices

Assuming equimolar compositions on each sublattice (A^+, B^{2+}, and X^- in ABX_3), we calculate the 1 340 752 possible combinations of the 282 experimentally observed inorganic HP with 5 or more components (Table S7, ESI†). The compositions with the greatest ES are in Table 1. HP are mostly composed of halides, so most of the compounds in Table 1 have 4 halide components. The greatest ES, −3.22 kJ mol^{-1}, is for $CsB(Br,Cl,F,I)_3$ with 10 B-site components. The next greatest ES, −3.17 kJ mol^{-1}, is for $(Cs,K,Rb)(Ca,Cd,Sn)(Br,Cl,F,I)_3$, as well as $CsB(Br,Cl,F,I)_3$ with 9 B-site components. $(Cs,Rb)(Ca,Cd,Pb,Sn)(Br,Cl,F,I)_3$ has ES of −3.11 kJ mol^{-1}. $CsB(Br,Cl,I)_3$ with 15 B-site components has ES of −3.00 kJ mol^{-1}.

Next, we calculate most of the combinations of the 282 inorganic HP with known lattice parameters in Fig. 4, where the ES term at 300 K is plotted as a function of UCV. As Fig. 4(b) and Table 2 show, HP are mostly composed of halides, so the greatest ES comes from X-site mixing. However, X-site mixing drives UCV higher: when all 4 halides are used, the ES term reaches −3.17 kJ mol^{-1} but has UCV of 0.283 for $Cs(Ca,Eu,Mg,Mn,Ni,Pb,Sn,Sr,Yb)(Br,Cl,F,I)_3$. When only 3 halides are used, an ES term of −2.96 kJ mol^{-1} is achieved at the much lower UCV of 0.156 for $Cs(Au,Ca,Eu,Ge,Mg,Mn,Ni,Pb,Sn,Sr,Ti,Tm,V,Yb)(Br,Cl,I)_3$. When only 2 halides are used, an ES term of only −2.28 kJ mol^{-1} is possible, but at UCV of only 0.106 for $(Cs,K,Rb,Tl)(Ca,Cd,Mn)(Br,Cl)_3$, while an ES term of −2.19 kJ mol^{-1} is reached at a UCV of only 0.073 for $(Cs,Rb)(Ca,Ge,Pb,Sn,Sr)(Br,Cl)_3$. We examine 1-halide compounds in the next section. Other compounds with attractive UCV-ES term tradeoffs are in Fig. 4(b) and Table 3. These specific compositions demonstrate that in general, mixing Br, Cl, and I on the X-site, Cs and Rb on the A-site and Ge, Pb, and Sn on the B-site are all promising. Less obvious constituents include F on the X-site, K and Tl on the A-site and Ca, Cd, Eu, and Sr on the B-site. Former work found the prospect of using hetero-valent substitutes on the B site to be promising.[292]

2.2 Mixing on only A and B sublattices (ordered valence band)

HP valence band maximum is dominated by (X) halide with minor B cation contributions, while the conduction band minimum is mostly determined by the B cation with small X contributions.[293] Therefore, to preserve order in the valence band and keep valence band energy constant to facilitate hole transport, A- and B-site cations can both be alloyed while the halide is kept pure (1 component on the X sublattice). In this case, the greatest ES term is only −1.68 kJ mol^{-1} for $CsBCl_3$ with 29 B-site components (Fig. 5). Other noteworthy compositions are shown in Fig. 5(b) and Table 4. As discussed in the previous section, less halide mixing translates to less ES but also lower UCV. Halide segregation is a known issue in HP[294] that could prevent the use of mixing on the X-site for ES. If that is a limitation, then the compounds in this section can still be used to achieve moderate ES at low enthalpic penalties (low UCV), all while maintaining an ordered valence band valuable for hole transport.

2.3 Mixing on only A and X sublattices (ordered conduction band)

To preserve order in the conduction band and conduction band energy alignment to facilitate electron transport, mixing on the A- and X-sites can be used. In this case, the greatest ES term is −2.77 kJ mol^{-1} for $(Cs,K,Rb,Tl)Cd(Br,Cl,F,I)_3$. Other noteworthy compositions are shown in Fig. 6(b) and Table 5. We note that 3 of the compounds are entirely composed of end-members whose experimental band gaps are known. The compounds' band gaps are estimated by averaging end-member values: 1.95 eV for CsSnBrClI, 2.31 eV for CsPbBrClI, and 2.48 eV for CsGeBrClI.

2.4 Mixing on only A sublattice (ordered valence and conduction bands)

To preserve order in the valence and conduction bands and prevent changes in the valence and conduction band energy as well as band gap, alloying on only the A-site should be used. In this case, the greatest ES term is only −0.97 kJ mol^{-1} with UCV of 0.063 for $(Cs,In,K,Li,Na,Rb,Tl)CaBr_3$. Other compositions of interest are shown in Fig. 7(b) and Table 6.

A-site and X-site segregation are both known issues in HP[295] that could prevent the use of mixing on the A- and X-sites for ES. If those are limitations, then the compounds in this section can still be used to achieve weak ES at low enthalpic penalties (low UCV), all while maintaining ordered valence and conduction bands valuable for both hole and electron transport.

Table 1 Inorganic HP compositions with the most negative ES term at 300 K whose end-members are all experimentally observed. We omit compositions with an ellipsis (...) that are analogous to the row above them and have the same A- and X-site occupation

Alloy composition	ES term (kJ mol^{-1})	S/R
$CsCa_{0.1}Cd_{0.1}Eu_{0.1}Mg_{0.1}Mn_{0.1}Ni_{0.1}Pb_{0.1}Sn_{0.1}Sr_{0.1}Yb_{0.1}Br_{0.75}Cl_{0.75}F_{0.75}I_{0.75}$	−3.22	1.29
$Cs_{0.33}K_{0.33}Rb_{0.33}Ca_{0.33}Cd_{0.33}Sn_{0.33}Br_{0.75}Cl_{0.75}F_{0.75}I_{0.75}$	−3.17	1.27
$CsCa_{0.11}Cd_{0.11}Eu_{0.11}Mg_{0.11}Mn_{0.11}Ni_{0.11}Pb_{0.11}Sn_{0.11}Sr_{0.11}Br_{0.75}Cl_{0.75}F_{0.75}I_{0.75}$	−3.17	1.27
...		
$Cs_{0.5}Rb_{0.5}Ca_{0.25}Cd_{0.25}Pb_{0.25}Sn_{0.25}Br_{0.75}Cl_{0.75}F_{0.75}I_{0.75}$	−3.11	1.25
$CsCa_{0.13}Cd_{0.13}Eu_{0.13}Mg_{0.13}Mn_{0.13}Ni_{0.13}Pb_{0.13}Sn_{0.13}Br_{0.75}Cl_{0.75}F_{0.75}I_{0.75}$	−3.11	1.25
...		
$CsCa_{0.14}Cd_{0.14}Eu_{0.14}Mg_{0.14}Mn_{0.14}Ni_{0.14}Pb_{0.14}Br_{0.75}Cl_{0.75}F_{0.75}I_{0.75}$	−3.05	1.22
...		
$CsAu_{0.07}Ca_{0.07}Cd_{0.07}Eu_{0.07}Ge_{0.07}Mg_{0.07}Mn_{0.07}Ni_{0.07}Pb_{0.07}Sn_{0.07}Sr_{0.07}Ti_{0.07}Tm_{0.07}V_{0.07}Yb_{0.07}BrClI$	−3.00	1.20
$Cs_{0.33}K_{0.33}Rb_{0.33}Ca_{0.5}Cd_{0.5}Br_{0.75}Cl_{0.75}F_{0.75}I_{0.75}$	−2.97	1.19
...		
$Cs_{0.5}K_{0.5}Ca_{0.33}Cd_{0.33}Sn_{0.33}Br_{0.75}Cl_{0.75}F_{0.75}I_{0.75}$	−2.97	1.19
$Cs_{0.5}Rb_{0.5}Ca_{0.33}Cd_{0.33}Pb_{0.33}Br_{0.75}Cl_{0.75}F_{0.75}I_{0.75}$	−2.97	1.19
...		

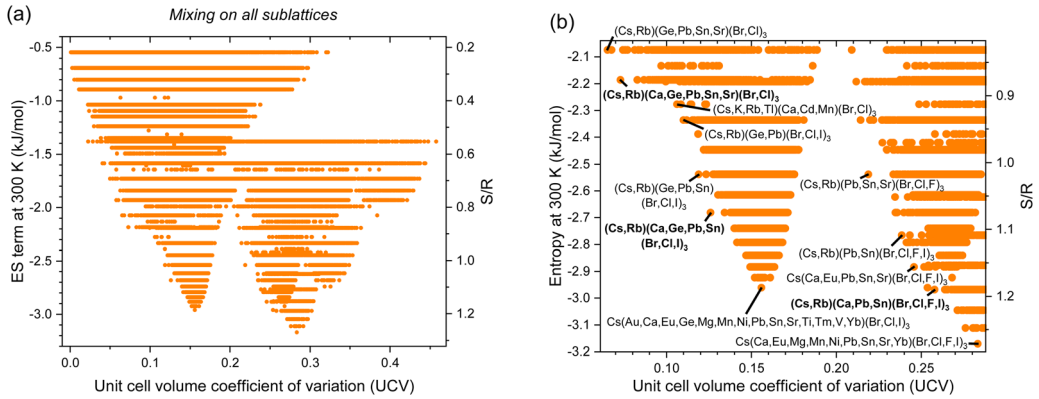

Fig. 4 Entropy stabilization (ES term at 300 K) as a function of enthalpic penalties, or unit cell volume coefficient of variation (UCV), for all equimolar inorganic HP compositions with experimentally observed constitutive end-members with mixing on all sublattices: (a) all data and (b) zoomed in, with promising alloys labeled and in bold.

Table 2 Inorganic HP compositions with the greatest ES term at 300 K whose lattice parameters are known and end-members are all experimentally observed with mixing on all sublattices. We omit compositions with an ellipsis (...) that are analogous to the row above them and have the same A- and X-site occupation

Alloy composition	ES term (kJ mol^{-1})	S/R	UCV
$CsCa_{0.11}Eu_{0.11}Mg_{0.11}Mn_{0.11}Ni_{0.11}Pb_{0.11}Sn_{0.11}Sr_{0.11}Yb_{0.11}Br_{0.75}Cl_{0.75}F_{0.75}I_{0.75}$	−3.17	1.27	0.283
$CsCa_{0.13}Eu_{0.13}Mn_{0.13}Ni_{0.13}Pb_{0.13}Sn_{0.13}Sr_{0.13}Yb_{0.13}Br_{0.75}Cl_{0.75}F_{0.75}I_{0.75}$	−3.11	1.25	0.276
...			
$CsCa_{0.14}Eu_{0.14}Mn_{0.14}Pb_{0.14}Sn_{0.14}Sr_{0.14}Yb_{0.14}Br_{0.75}Cl_{0.75}F_{0.75}I_{0.75}$	−3.05	1.22	0.271
...			
$Cs_{0.5}Rb_{0.5}Ca_{0.33}Pb_{0.33}Sn_{0.33}Br_{0.75}Cl_{0.75}F_{0.75}I_{0.75}$	−2.97	1.19	0.258
$CsCa_{0.17}Eu_{0.17}Pb_{0.17}Sn_{0.17}Sr_{0.17}Yb_{0.17}Br_{0.75}Cl_{0.75}F_{0.75}I_{0.75}$	−2.97	1.19	0.264
...			
$Cs_{0.33}K_{0.33}Rb_{0.33}Ca_{0.5}Sn_{0.5}Br_{0.75}Cl_{0.75}F_{0.75}I_{0.75}$	−2.97	1.19	0.273
$CsCa_{0.17}Eu_{0.17}Mn_{0.17}Sn_{0.17}Sr_{0.17}Yb_{0.17}Br_{0.75}Cl_{0.75}F_{0.75}I_{0.75}$	−2.97	1.19	0.276
...			
$CsAu_{0.07}Ca_{0.07}Eu_{0.07}Ge_{0.07}Mg_{0.07}Mn_{0.07}Ni_{0.07}Pb_{0.07}Sn_{0.07}Sr_{0.07}Ti_{0.07}Tm_{0.07}V_{0.07}Yb_{0.07}BrClI$	−2.96	1.19	0.156
$Cs_{0.5}Rb_{0.5}Ca_{0.14}Cd_{0.14}Mn_{0.14}Ni_{0.14}Pb_{0.14}Sn_{0.14}Sr_{0.14}BrClF$	−2.96	1.19	0.254
$CsAu_{0.08}Ca_{0.08}Eu_{0.08}Ge_{0.08}Mg_{0.08}Mn_{0.08}Pb_{0.08}Sn_{0.08}Sr_{0.08}Ti_{0.08}Tm_{0.08}V_{0.08}Yb_{0.08}BrClI$	−2.92	1.17	0.152
...			
$CsCa_{0.08}Cd_{0.08}Eu_{0.08}Fe_{0.08}Hg_{0.08}Mg_{0.08}Mn_{0.08}Ni_{0.08}Pb_{0.08}Pd_{0.08}Sn_{0.08}Sr_{0.08}Yb_{0.08}BrClF$	−2.92	1.17	0.268
$CsAu_{0.08}Ca_{0.08}Eu_{0.08}Ge_{0.08}Mg_{0.08}Mn_{0.08}Pb_{0.08}Sn_{0.08}Sr_{0.08}Tm_{0.08}V_{0.08}Yb_{0.08}BrClI$	−2.88	1.16	0.149
...			
$Cs_{0.5}Rb_{0.5}Ca_{0.17}Ge_{0.17}Pb_{0.17}Sn_{0.17}Ti_{0.17}V_{0.17}BrClI$	−2.88	1.16	0.152
$CsAu_{0.08}Eu_{0.08}Ge_{0.08}Mg_{0.08}Mn_{0.08}Pb_{0.08}Sn_{0.08}Sr_{0.08}Ti_{0.08}Tm_{0.08}V_{0.08}Yb_{0.08}BrClI$	−2.88	1.16	0.152
...			
$Cs_{0.5}Rb_{0.5}Ca_{0.17}Cd_{0.17}Ni_{0.17}Pb_{0.17}Sn_{0.17}Sr_{0.17}BrClF$	−2.88	1.16	0.246
...			
$CsCa_{0.08}Cd_{0.08}Eu_{0.08}Fe_{0.08}Hg_{0.08}Mn_{0.08}Ni_{0.08}Pb_{0.08}Pd_{0.08}Sn_{0.08}Sr_{0.08}Yb_{0.08}BrClF$	−2.88	1.16	0.263
...			
$Cs_{0.33}K_{0.33}Rb_{0.33}Ca_{0.25}Cd_{0.25}Mn_{0.25}Sn_{0.25}BrClF$	−2.88	1.16	0.265
$CsCa_{0.08}Cd_{0.08}Eu_{0.08}Hg_{0.08}Mg_{0.08}Mn_{0.08}Ni_{0.08}Pb_{0.08}Pd_{0.08}Sn_{0.08}Sr_{0.08}Yb_{0.08}BrClF$	−2.88	1.16	0.266
...			
$CsCa_{0.2}Eu_{0.2}Pb_{0.2}Sn_{0.2}Sr_{0.2}Br_{0.75}Cl_{0.75}F_{0.75}I_{0.75}$	−2.88	1.16	0.254
...			

2.5 Organic A-site components (hybrid organic–inorganic HP)

The previous sections have only considered inorganic compounds, but there are at least 22 organic cations that can substitute on the A-site: methylammonium (MA; CH_3NH_3), formamidinium (FA; $HC(NH_2)_2$), guanidinium (GA; $C(NH_2)_3$), dimethylammonium (DMA; $(CH_3)_2NH_2$), ethylammonium (EA; $CH_3CH_2NH_3$), acetamidinium (ACA; $CH_3C(NH_2)_2$), ammonium (NH_4), hydrazinium (HA; N_2H_5), azetidinium (AZ; $C_3H_6NH_2$), imidazolium (IM; $C_3N_2H_5$), trimethylammonium (TMA; $(CH_3)_3NH$), tetramethylammonium (TEMA; $(CH_3)_4N$), arsonium, methylarsonium, methylphosphonium, aziridine, hydroxylammonium, phosphonium, antimonium, PF_4, NH_2CHPH_2, and NH_2CHAsH_2.[296] Therefore, hybrid organic–inorganic halide perovskites have an even larger chemical space that can be tapped for ES than the pure inorganics.

Previous work found ES in $(Cs,FA)PbI_3$,[297] $(FA,GA)PbBr_3$,[298] $(Cs,FA,MA)PbI_3$,[299] $(Cs,FA,MA)Pb(Br,I)_3$,[221,300] and $(Cs,FA,MA,Rb)PbI_3$,[220,222] and ES was also recently demonstrated in double HP[28,301] and "hollow" HP.[302] Long anneals of $CH_3NH_3PbI_3$ were argued to maximize configurational entropy of the organic cation, which was found to stabilize the cubic polytype and improve

Table 3 Inorganic HP compositions with attractive UCV-ES term at 300 K tradeoffs whose lattice parameters are known and end-members are all experimentally observed with mixing on all sublattices

Alloy composition	ES term (kJ mol^{-1})	S/R	UCV
$Cs_{0.5}Rb_{0.5}Ca_{0.33}Pb_{0.33}Sn_{0.33}Br_{0.75}Cl_{0.75}F_{0.75}I_{0.75}$	−2.97	1.19	0.258
$CsCa_{0.2}Eu_{0.2}Pb_{0.2}Sn_{0.2}Sr_{0.2}Br_{0.75}Cl_{0.75}F_{0.75}I_{0.75}$	−2.88	1.15	0.254
$Cs_{0.5}Rb_{0.5}Pb_{0.5}Sn_{0.5}Br_{0.75}Cl_{0.75}F_{0.75}I_{0.75}$	−2.77	1.11	0.239
$Cs_{0.5}Rb_{0.5}Ca_{0.25}Ge_{0.25}Pb_{0.25}Sn_{0.25}BrClI$	−2.68	1.08	0.126
$Cs_{0.5}Rb_{0.5}Ge_{0.33}Pb_{0.33}Sn_{0.33}BrClI$	−2.54	1.02	0.119
$Cs_{0.5}Rb_{0.5}Pb_{0.33}Sn_{0.33}Sr_{0.33}BrClF$	−2.54	1.02	0.219
$Cs_{0.5}Rb_{0.5}Ge_{0.5}Pb_{0.5}BrClI$	−2.34	0.94	0.112
$Cs_{0.25}K_{0.25}Rb_{0.25}Tl_{0.25}Ca_{0.33}Cd_{0.33}Mn_{0.33}Br_{1.5}Cl_{1.5}$	−2.28	0.91	0.106
$Cs_{0.5}Rb_{0.5}Ca_{0.2}Ge_{0.2}Pb_{0.2}Sn_{0.2}Sr_{0.2}Br_{1.5}Cl_{1.5}$	−2.19	0.88	0.073
$Cs_{0.5}Rb_{0.5}Ge_{0.25}Pb_{0.25}Sn_{0.25}Sr_{0.25}Br_{1.5}Cl_{1.5}$	−2.07	0.83	0.065

electrical properties.[303] Entropy stabilization of HP nanocrystals was recently demonstrated: Pb was substituted for Mg, Zn, and Cd in $CH_3NH_3PbBr_3$ to enhance stability, while narrow band emission was retained.[304] Unlike former reports,[297,298] here we consider the maximum feasible configurational ES, which restricts our focus to alloys with a minimum of 5 components.

Mixing the 40 organic and 282 inorganic HP end-members, we find 14 270 hybrid organic–inorganic HEAHPs consisting of 5 or more experimentally observed end-members (Fig. 8 and Table S8, ESI†). Attractive UCV-ES term tradeoffs are in Table 7. In general, smaller ES are possible at a given UCV, relative to the inorganic HEAHPs in the previous sections. Table 7 mostly consists of well-studied alloys based on Cs, MA, and FA, but the less-studied Rb and K are also present. For PV-related Br, Cl, and I systems, the B-site constituents are Ge, Sn and Pb. The F systems are of interest for electrochemical applications and have smaller unit cells, so NH_4 and Na are allowed, Cd, Fe, and Mn are prevalent while Tl, Co, Cu Fe, Mg, Ni and Zn are possible. $(Cs,K,NH_4,Rb,Tl)(Cd,Fe,Mn)(Cl,F)_3$ and $(K,NH_4,Rb,Tl)(Cd,Co,Cr,Cu,Fe,Mg,Mn,Ni,Sn,Zn)F_3$ have ES terms at 300 K of −2.39 and −1.84 kJ mol^{-1}, respectively. While inorganic HEAHP have more negative ES terms as temperature increases, the organic components' volatility may limit this effect for organic HEAHP.

2.6 Non-equimolar compositions

For non-equimolar compositions, weighted standard deviation (σ_w) and weighted coefficient of variation (UCV_w) are:

$$\sigma_w = \sqrt{\frac{\sum_i \sum_j \sum_k y_i^A y_j^B y_k^X \left(V_{ijk_3} - \bar{V}_w\right)^2}{\sum_i \sum_j \sum_k y_i^A y_j^B y_k^X}} = \sqrt{\sum_i \sum_j \sum_k y_i^A y_j^B y_k^X \left(V_{ijk_3} - \bar{V}_w\right)^2} \quad (7)$$

$$UCV_w = \frac{\sigma_w}{\bar{V}_w} \quad (8)$$

The boundary between single-phase and multiple phase

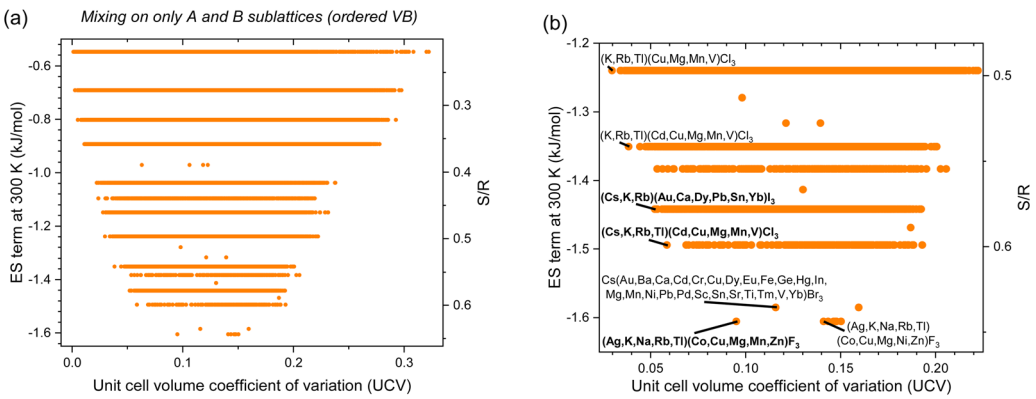

Fig. 5 Entropy stabilization (ES term at 300 K) as a function of enthalpic penalties, or unit cell volume coefficient of variation (UCV), for equimolar inorganic HP compositions with experimentally observed constitutive end-members with mixing on only A and B sublattices (ordered valence band): (a) all data and (b) zoomed in, with promising alloys labeled and in bold.

Table 4 Inorganic HP compositions with attractive UCV-ES term at 300 K tradeoffs whose lattice parameters are known and end-members are all experimentally observed with mixing on only A and B sublattices (ordered valence band)

Alloy composition	ES term (kJ mol^{-1})	S/R	UCV
$Ag_{0.2}K_{0.2}Na_{0.2}Rb_{0.2}Tl_{0.2}Co_{0.2}Cu_{0.2}Mg_{0.2}Mn_{0.2}Zn_{0.2}F_3$	−1.61	0.64	0.095
$Ag_{0.2}K_{0.2}Na_{0.2}Rb_{0.2}Tl_{0.2}Co_{0.2}Cu_{0.2}Mg_{0.2}Ni_{0.2}Zn_{0.2}F_3$	−1.61	0.64	0.141
$CsAu_{0.04}Ba_{0.04}Ca_{0.04}Cd_{0.04}Cr_{0.04}Cu_{0.04}Dy_{0.04}Eu_{0.04}Fe_{0.04}Ge_{0.04}Hg_{0.04}In_{0.04}Mg_{0.04}Mn_{0.04}Ni_{0.04}Pb_{0.04}Pd_{0.04}Sc_{0.04}Sn_{0.04}Sr_{0.04}Ti_{0.04}Tm_{0.04}V_{0.04}Yb_{0.04}Br_3$	−1.59	0.64	0.116
$Cs_{0.25}K_{0.25}Rb_{0.25}Tl_{0.25}Cd_{0.2}Cu_{0.2}Mg_{0.2}Mn_{0.2}V_{0.2}Cl_3$	−1.49	0.60	0.059
$Cs_{0.33}K_{0.33}Rb_{0.33}Au_{0.17}Ca_{0.17}Dy_{0.17}Pb_{0.17}Sn_{0.17}Yb_{0.17}I_3$	−1.44	0.58	0.052
$K_{0.33}Rb_{0.33}Tl_{0.33}Cd_{0.2}Cu_{0.2}Mg_{0.2}Mn_{0.2}V_{0.2}Cl_3$	−1.35	0.54	0.038
$K_{0.33}Rb_{0.33}Tl_{0.33}Cu_{0.25}Mg_{0.25}Mn_{0.25}V_{0.25}Cl_3$	−1.24	0.50	0.030

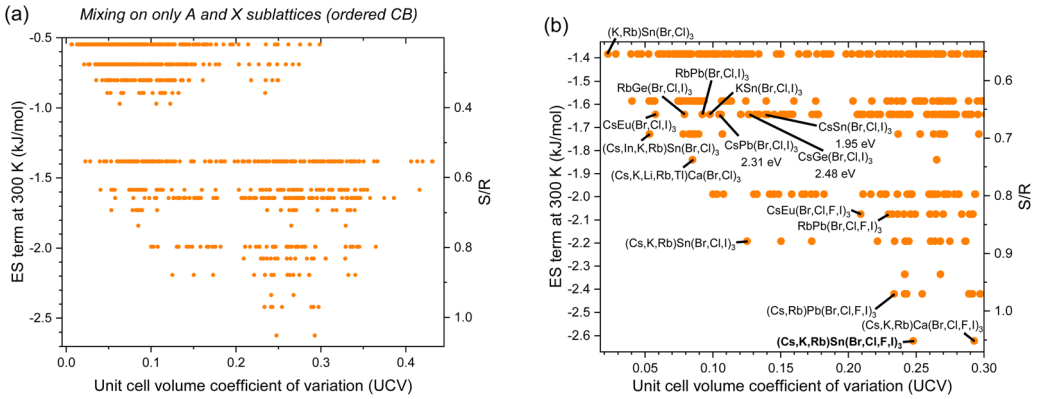

Fig. 6 Entropy stabilization (ES term at 300 K) as a function of enthalpic penalties, or unit cell volume coefficient of variation (UCV), for equimolar inorganic HP compositions with experimentally observed constitutive end-members with mixing on only A and X sublattices (ordered conduction band): (a) all data and (b) zoomed in, with promising alloys labeled and in bold.

Table 5 Inorganic HP compositions with attractive UCV-ES term at 300 K tradeoffs whose lattice parameters are known and end-members are all experimentally observed with mixing on only A and X sublattices (ordered conduction band)

Alloy composition	ES term (kJ mol^{-1})	S/R	UCV
$Cs_{0.33}K_{0.33}Rb_{0.33}SnBr_{0.75}Cl_{0.75}F_{0.75}I_{0.75}$	−2.62	1.05	0.248
$Cs_{0.33}K_{0.33}Rb_{0.33}CaBr_{0.75}Cl_{0.75}F_{0.75}I_{0.75}$	−2.62	1.05	0.293
$Cs_{0.5}Rb_{0.5}PbBr_{0.75}Cl_{0.75}F_{0.75}I_{0.75}$	−2.42	0.97	0.234
$K_{0.5}Rb_{0.5}SnBr_{0.75}Cl_{0.75}F_{0.75}I_{0.75}$	−2.42	0.97	0.242
$Cs_{0.33}K_{0.33}Rb_{0.33}SnBrClI$	−2.19	0.88	0.125
$CsEuBr_{0.75}Cl_{0.75}F_{0.75}I_{0.75}$	−2.07	0.83	0.209
$RbPbBr_{0.75}Cl_{0.75}F_{0.75}I_{0.75}$	−2.07	0.83	0.230
$RbSnBr_{0.75}Cl_{0.75}F_{0.75}I_{0.75}$	−2.07	0.83	0.232
$CsPbBr_{0.75}Cl_{0.75}F_{0.75}I_{0.75}$	−2.07	0.83	0.236
$Cs_{0.2}K_{0.2}Li_{0.2}Rb_{0.2}Tl_{0.2}CaBr_{1.5}Cl_{1.5}$	−1.84	0.74	0.085
$Cs_{0.25}In_{0.25}K_{0.25}Rb_{0.25}SnBr_{1.5}Cl_{1.5}$	−1.73	0.69	0.053
CsEuBrClI	−1.64	0.66	0.058
RbGeBrClI	−1.64	0.66	0.079
RbPbBrClI	−1.64	0.66	0.092
KSnBrClI	−1.64	0.66	0.098
CsPbBrClI (2.31 eV)	−1.64	0.66	0.105
CsGeBrClI (2.48 eV)	−1.64	0.66	0.127
CsSnBrClI (1.95 eV)	−1.64	0.66	0.138
$K_{0.5}Rb_{0.5}SnBr_{1.5}Cl_{1.5}$	−1.38	0.55	0.023

compositions has been mapped experimentally for MAPb(Br,Cl,I)$_3$.[223] We calculate ES term at 300 K and UCV$_w$ for MAPb(Br,Cl,I)$_3$ in Fig. 8(a) and (b). While UCV$_w$ predicts the general shape of the data, multiplying UCV$_w$ by a constant (C) and adding it to ES term accurately predicts 52 out of the 56 data (93%; Fig. 9(c)). ES′ combined effect on Gibbs energy (G_{ES}) is:

$$G_{ES} = \text{ES term} + \text{UCV}_w C = RT\left(\frac{1}{5}\sum_i y_i^A \ln\left(y_i^A\right) + \frac{1}{5}\sum_j y_j^B \ln\left(y_j^B\right) + \frac{3}{5}\sum_k y_k^X \ln\left(y_k^X\right)\right) + \left(\frac{\sqrt{\sum_i\sum_j\sum_k y_i^A y_j^B y_k^X \left(V_{ijk_3} - \bar{V}_w\right)^2}}{\sum_i\sum_j\sum_k y_i^A y_j^B y_k^X V_{ijk_3}}\right) C \quad (9)$$

This new equation is Calphad with crystal structure inputs. Empirically fitting C to the MAPb(Br,Cl,I)$_3$ data yields C of 23 kJ mol^{-1}. On the other hand, a C value of 40 kJ mol^{-1} matches the experimental data for CsPb(Br,Cl,I)$_3$ (Fig. S3, ESI†), suggesting

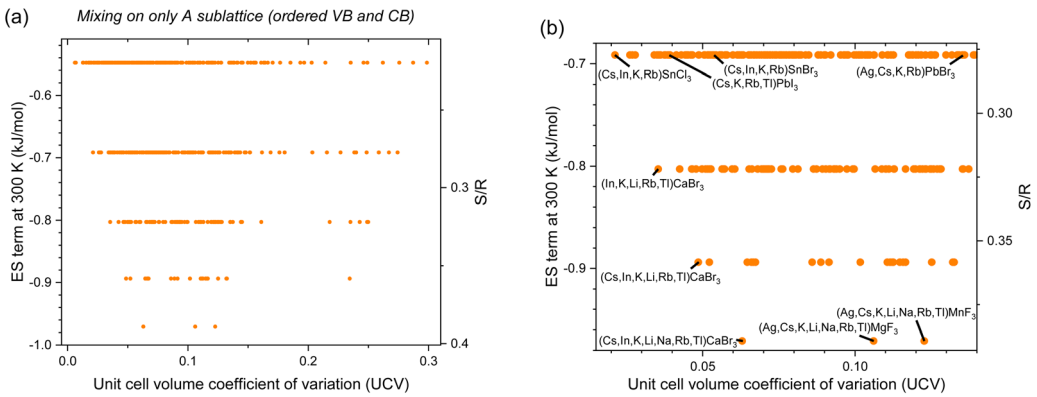

Fig. 7 Entropy stabilization (ES term at 300 K) as a function of enthalpic penalties, or unit cell volume coefficient of variation (UCV), for equimolar inorganic HP compositions with experimentally observed constitutive end-members with mixing on only the A sublattice (ordered valence and conduction bands): (a) all data and (b) zoomed in, with promising alloys labeled and in bold.

Table 6 Inorganic HP compositions with attractive UCV-ES term at 300 K tradeoffs whose lattice parameters are known and end-members are all experimentally observed with mixing on only the A sublattice (ordered valence and conduction bands)

Alloy composition	ES term (kJ mol^{-1})	S/R	UCV
$Cs_{0.14}In_{0.14}K_{0.14}Li_{0.14}Na_{0.14}Rb_{0.14}Tl_{0.14}CaBr_3$	−0.97	0.39	0.063
$Ag_{0.14}Cs_{0.14}K_{0.14}Li_{0.14}Na_{0.14}Rb_{0.14}Tl_{0.14}MgF_3$	−0.97	0.39	0.106
$Ag_{0.14}Cs_{0.14}K_{0.14}Li_{0.14}Na_{0.14}Rb_{0.14}Tl_{0.14}MnF_3$	−0.97	0.39	0.123
$Cs_{0.17}In_{0.17}K_{0.17}Li_{0.17}Rb_{0.17}Tl_{0.17}CaBr_3$	−0.89	0.36	0.049
$In_{0.2}K_{0.2}Li_{0.2}Rb_{0.2}Tl_{0.2}CaBr_3$	−0.80	0.32	0.035
$Cs_{0.25}In_{0.25}K_{0.25}Rb_{0.25}SnCl_3$	−0.69	0.28	0.021
$Cs_{0.25}K_{0.25}Rb_{0.25}Tl_{0.25}PbI_3$	−0.69	0.28	0.039
$Cs_{0.25}In_{0.25}K_{0.25}Rb_{0.25}SnBr_3$	−0.69	0.28	0.053
$Ag_{0.25}Cs_{0.25}K_{0.25}Rb_{0.25}PbBr_3$	−0.69	0.28	0.135

enthalpic penalty plays more of a role in the latter. Altogether we accurately predict 75 out of the 83 ternary data (91%), showing that UCV-ES maps can rank alloys with different constituents *and* different compositions.

2.7 Known experimental band gaps

Of the 282 experimentally observed inorganic HP compounds, we find experimental band gaps for 19. Of the 1 340 752 alloy compositions we consider, 73 are entirely composed of end-members whose experimental band gaps are known. Fig. S4 and Table S9 (ESI†) show that they all contain Cs, most have Ge, Pb or Sn, and most band gaps are wider than 2 eV. Bowing can shift these band gap values, and experimental bowing data is in Table 7 and Fig. S9 (ESI†).

2.8 Overall accuracy

Finally, we note the high accuracy of UCV separating experimental miscibility data across crystal systems with a spectrum of bonding character: from *weak ionic* HP (89% of 109 data) to *weak covalent* II–VIs (83% of 18 data), *covalent* III–Vs (100% of 27 data), and finally to *strong covalent* boride, carbide, and carbonitride ceramics (88% of 64 data). Overall accuracy for the 218 data is 89.4%. For comparison, the accuracy of Materials Project DFT unit cell volumes relative to experiment is 92.6%.[305] There are exceptions to UCV predicting miscibility: $KCo_{0.2}Fe_{0.2}Mg_{0.2}Ni_{0.2}Zn_{0.2}F_3$ in Fig. 2, $Hf_{0.2}Mo_{0.2}Nb_{0.2}Ta_{0.2}W_{0.2}C_{0.5}N_{0.5}$ in Fig. S2 (ESI†), and $CsPb_{0.5}Zn_{0.5}Cl_3$, $CsPb_{0.5}Zn_{0.5}Br_3$, and $CsPb_{0.5}Zn_{0.5}I_3$ in Table S4 (ESI†). These exceptions show that crystal structure and Gibbs energy are more nuanced than a single parameter can describe, but UCV captures 89% of HEA mixing behavior.

3. Conclusions

We take a low computational cost approach to screening HEA and employ it to identify promising inorganic and hybrid organic–inorganic HEAHP. Drawing from the pool of 322 experimentally observed HP, we compute configurational entropy stabilization (ES) of equimolar HEA. Starting with the delta-lattice parameter approach for predicting III–V miscibility, we introduce the more generally applicable unit cell volume coefficient of variation (UCV) to estimate enthalpic penalty of HEA. UCV predicts the existing experimental III–V, II–VI, boride, carbide, carbonitride, and HP data well. We screen the 10^{57} possible HEAHP to report the 10^6 alloys consisting entirely of experimentally observed end-members, then identify 10^2 HEAHP with promising UCV-ES tradeoffs. These results can serve as a first screen for guiding more costly calculations and experiments.

4. Methods

Throughout the literature, the boundary between what is considered perovskite and not considered perovskite is ambiguous.[1,2] We limit our search to the 282 inorganic and 40 organic ABX_3 compounds that have been experimentally observed and previously labeled as "perovskites" (Tables S10[18–20,27,111,112,115,123,179,306–539] and S11 (ESI†),[315,466,524,526,540–558] respectively). We exclude the 90 inorganic HP that have been proposed but not synthesized (Table S12, ESI†).[23,24,307,430] In order to use a self-consistent database, where possible we use lattice parameters from the Materials Project[559] for the *Pnma*

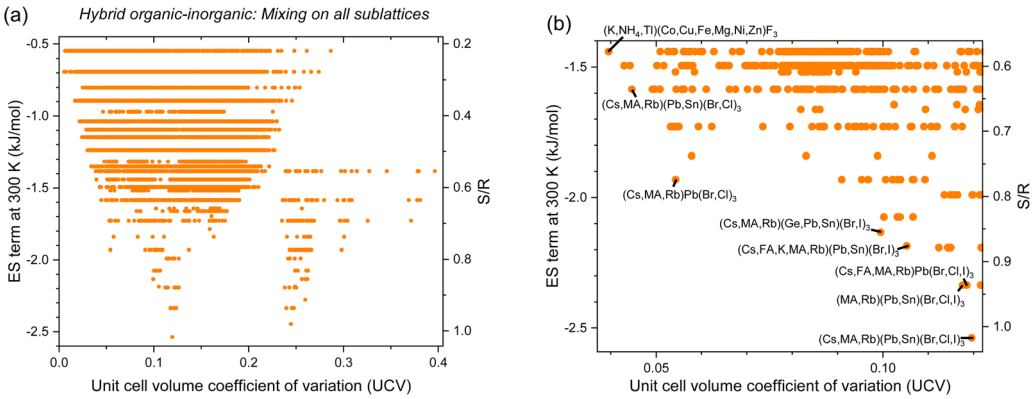

Fig. 8 Entropy stabilization (ES term at 300 K) as a function of enthalpic penalties, or unit cell volume coefficient of variation (UCV), for all equimolar hybrid organic–inorganic HP compositions with experimentally observed constitutive end-members with mixing on all sublattices: (a) all data and (b) zoomed in, with promising alloys labeled and in bold.

Table 7 Hybrid organic–inorganic HP compositions with the greatest ES term at 300 K whose lattice parameters are known and end-members are all experimentally observed with mixing on all sublattices. Calculated band gaps are included along with the maximum experimental band gap bowing (the difference between the linearly-interpolated-band gap and the actual band gap) and references

Alloy composition	ES term (kJ mol^{-1})	S/R	UCV	Band gap (eV)	Exp. bowing (eV)
$Cs_{0.33}MA_{0.33}Rb_{0.33}Pb_{0.5}Sn_{0.5}BrClI$	−2.54	1.02	0.120	—	—
$Cs_{0.2}K_{0.2}(NH_4)_{0.2}Rb_{0.2}Tl_{0.2}CdBrClF$	−2.45	0.98	0.245	—	—
$MA_{0.5}Rb_{0.5}Pb_{0.5}Sn_{0.5}BrClI$	−2.34	0.94	0.118	—	—
$Cs_{0.25}FA_{0.25}MA_{0.25}Rb_{0.25}PbBrClI$	−2.34	0.94	0.119	—	—
$Cs_{0.5}MA_{0.5}Pb_{0.5}Sn_{0.5}BrClI$	−2.34	0.94	0.122	2.24	$MA(Pb,Sn)(Br,I)_3 \leq 0.11$;[243] $(Cs,MA)(Pb,Sn)I_3 \leq 0.11$;[243] $(Cs,FA)PbI_3 \leq 0.02$;[249] $MAPb(Br,Cl)_3 \leq 0.17$[242]
$Cs_{0.25}K_{0.25}MA_{0.25}Rb_{0.25}SnBrClI$	−2.34	0.94	0.124	—	—
...					
$Cs_{0.25}K_{0.25}(NH_4)_{0.25}Rb_{0.25}Cd_{0.33}Fe_{0.33}Mn_{0.33}Cl_{1.5}F_{1.5}$	−2.28	0.91	0.260	—	—
$Cs_{0.33}FA_{0.33}Rb_{0.33}PbBrClI$	−2.19	0.88	0.112	2.31	$(Cs,Rb)PbBr_3 = 0$;[125] $(Cs,Rb)PbCl_3 = 0$[125]
...					
$Cs_{0.33}FA_{0.33}MA_{0.33}PbBrClI$	−2.19	0.88	0.122	2.28	$(FA,MA)Pb(Br,I)_3 \leq 0.10$;[230,243,245,261] $MAPb(Br,Cl)_3 \leq 0.17$[242]
...					
$Cs_{0.2}FA_{0.2}K_{0.2}MA_{0.2}Rb_{0.2}Pb_{0.5}Sn_{0.5}Br_{1.5}I_{1.5}$	−2.19	0.88	0.105	—	—
...					
$Cs_{0.33}MA_{0.33}Rb_{0.33}Ge_{0.33}Pb_{0.33}Sn_{0.33}Br_{1.5}I_{1.5}$	−2.13	0.86	0.099	—	—
...					
$Cs_{0.5}FA_{0.5}PbBrClI$	−1.99	0.80	0.115	2.27	—
...					
$MAPb_{0.5}Sn_{0.5}BrClI$	−1.99	0.80	0.120	2.34	$MA(Pb,Sn)(Br,I)_3 \leq 0.11$;[243] $MAPb(Br,Cl)_3 \leq 0.17$[242]
...					
$Cs_{0.5}MA_{0.5}PbBrClI$	−1.99	0.80	0.121	2.31	$MAPb(Br,I)_3 \leq 0.07$;[243,245] $MAPb(Br,Cl)_3 \leq 0.17$[242]
$Cs_{0.5}MA_{0.5}SnBrClI$	−1.99	0.80	0.122	2.16	$MASn(Br,I)_3 \leq 0.03$[243]
$FA_{0.5}MA_{0.5}PbBrClI$	−1.99	0.80	0.127	2.27	$MAPb(Br,I)_3 \leq 0.07$;[243,245] $MAPb(Br,Cl)_3 \leq 0.17$;[242] $(FA,MA)PbI_3 \leq 0.02$[261]
...					
$Cs_{0.33}MA_{0.33}Rb_{0.33}Pb_{0.5}Sn_{0.5}Br_{1.5}Cl_{1.5}$	−1.93	0.77	0.054	—	—
...					
$K_{0.25}Na_{0.25}(NH_4)_{0.25}Tl_{0.25}Co_{0.14}Cu_{0.14}Fe_{0.14}Mg_{0.14}Mn_{0.14}Ni_{0.14}Zn_{0.14}F_3$	−1.66	0.67	0.082	—	—
...					
$Cs_{0.33}MA_{0.33}Rb_{0.33}PbBr_{1.5}Cl_{1.5}$	−1.59	0.64	0.045	—	—

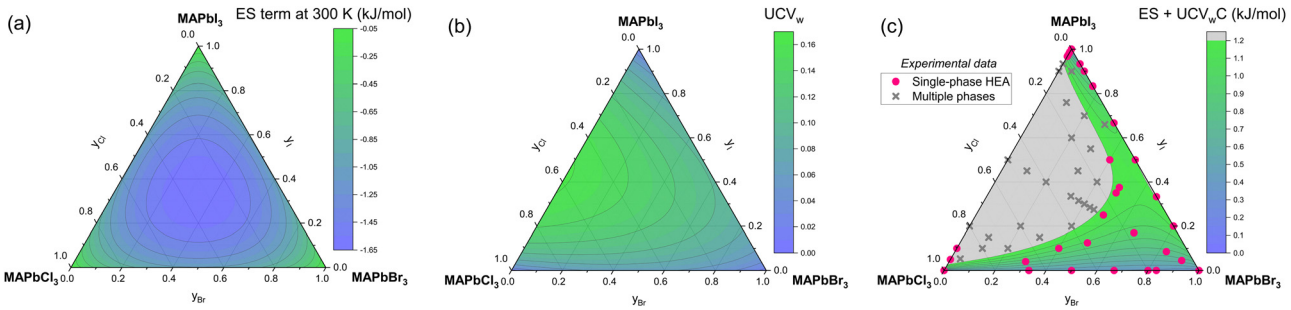

Fig. 9 (a) ES term at 300 K contours, (b) UCV_w contours, and (c) ES + UCV_wC contours for $MAPb(Br,Cl,I)_3$. Experimental HP single-phase alloy (pink circles) and multiple phase (gray Xs) data are in (c),[223] confirming that C = 23 kJ mol^{-1} leads to a phase boundary at G_{ES} = 1.22 kJ mol^{-1} that correctly groups 52 of the 56 data (93%).

orthorhombic perovskite structure (space group #62; 20 constituents per unit cell; 4 formula units per unit cell). Many HP have different structural symmetry (*e.g.*, $Pm\bar{3}m$ cubic with 5 constituents per unit cell or 1 formula unit per unit cell), and in such cases we consider the unit cell volume for which the number of atoms would be 20 (for $Pm\bar{3}m$ the unit cell volume is

multiplied by 4). Materials Project[559] unit cell volumes are well correlated with Inorganic Crystal Structure Database (ICSD) values.[305,560] We find lattice parameters for 265 of the inorganic HP. We also tabulate experimental band gaps where available. We first consider all possible equimolar alloys with 3 end-members, then check if a possible HEA consists entirely of experimentally observed end-members. If it does then we tabulate it after calculating the ES term at 300 K, UCV (if available), and mean band gap (if available). We provide example code with extensive comments as an ESI† file (Mathematica notebook). We execute the notebook on a personal computer using a built-in parallel do statement and consider alloys with up to 48 end-members. There are 10^{57} ways to combine 48 of the 322 end-members (322!/(48! (322-48)!) $\sim 10^{57}$), so to avoid checking every combination of the 9 A-site, 32 B-site and 4 X-site inorganic constituents and 10 additional A-site organic constituents, we examine the simpler alloy systems first to determine which complex alloys can possibly be built from the existing results. In other words, the computation can be simplified by only checking a higher order system's potential constituents if their constitutive lower order systems exist. Eventually, the number of constituents on a sublattice reaches a maximum, beyond which no more can be added without including an end-member that has not been experimentally observed, and then the search can stop. Here we examine only HP, but our approach has value for the closely related double perovskites[301] and the 76 experimentally observed chalcogenide (sulfur, selenium, and tellurium) perovskites,[24] although chalcogenide perovskites are less developed than the halides.[561]

DFT calculations: in order to verify that compositions with small (large) UCV are stable (unstable), we carry out geometric relaxations for the selected compositions in Table S6 (ESI†). We carry out these DFT calculations using the Vienna Ab initio Software Package (VASP, version 5.4),[562,563] in the framework of the generalized gradient approximation (GGA), with the Perdew, Burke and Ernzerhof (PBE) functional.[564] We use a plane wave energy cutoff of 400 eV and the following Brillouin zone grids, depending on the size of the supercell: $2 \times 2 \times 2$ k-point grids (8 irreducible k points) for $2 \times 2 \times 2$ supercells (40 atoms), $1 \times 2 \times 2$ k-point grids for $4 \times 2 \times 2$ supercells (80 atoms), and $1 \times 1 \times 1$ k-point grids for $3 \times 3 \times 3$ supercells (135 atoms). All the relaxations are started from ideal cubic perovskite structures and are fully relaxed (unit cell shape and atomic coordinates) using the conjugate-gradient algorithm until residual forces become smaller than 0.004 eV Å^{-1}. The electronic relaxations at each ionic step are stopped when the energy difference between consecutive self-consistency iterations reaches 10^{-7} eV. In order to improve convergence to equilibrium, we scale the displacement steps by 0.1 and declare 180 bands (20 more than the default). To assess mixing effects of various ions on the A-, B-, and X-sites, we include 8 distinct configurations for each composition, and average the final energy and final cell volume across these configurations. The DFT mixing enthalpy is the mean DFT energy of the 8 HEA configurations referenced to the DFT energy of the HEA's end-members:

$$H_{\mathrm{mix,DFT}} = \frac{E_{\mathrm{HEA,conf.1}}}{8} + \frac{E_{\mathrm{HEA,conf.2}}}{8} + \frac{E_{\mathrm{HEA,conf.3}}}{8} + \frac{E_{\mathrm{HEA,conf.4}}}{8} + \frac{E_{\mathrm{HEA,conf.5}}}{8} + \frac{E_{\mathrm{HEA,conf.6}}}{8} + \frac{E_{\mathrm{HEA,conf.7}}}{8} + \frac{E_{\mathrm{HEA,conf.8}}}{8} - \frac{\sum_i \sum_j \sum_k E_{ijk_3}}{N} \quad (10)$$

Conflicts of interest

There are no conflicts to declare.

Acknowledgements

This work was authored by the National Renewable Energy Laboratory, operated by Alliance for Sustainable Energy, LLC, for the U.S. Department of Energy (DOE) under contract no. DE-AC36-08GO28308. The views expressed in the article do not necessarily represent the views of the DOE or the U.S. Government. The U.S. Government retains and the publisher, by accepting the article for publication, acknowledges that the U.S. Government retains a nonexclusive, paid-up, irrevocable, worldwide license to publish or reproduce the published form of this work, or allow others to do so, for U.S. Government purposes. Funding was provided by the U.S. Army Research Office through grant no. W911NF2210273 (Dr Hugh C. DeLong).

References

1 Q. A. Akkerman and L. Manna, What Defines a Halide Perovskite, *ACS Energy Lett.*, 2020, **5**(2), 604–610, DOI: **10.1021/acsenergylett.0c00039**.
2 R. H. Mitchell, M. D. Welch and A. R. Chakhmouradian, Nomenclature of the perovskite supergroup: A hierarchical system of classification based on crystal structure and composition, *Mineral. Mag.*, 2017, **81**(3), 411–461, DOI: **10.1180/minmag.2016.080.156**.
3 V. Dusastre, Gaining from mixing, *Nat. Mater.*, 2023, **22**(4), 401, DOI: **10.1038/s41563-023-01530-3**.
4 Y. Wang, M. J. Robson, A. Manzotti and F. Ciucci, High-entropy perovskites materials for next-generation energy applications, *Joule*, 2023, **7**(5), 848–854, DOI: **10.1016/j.joule.2023.03.020**.
5 Z. Du, C. Wu, Y. Chen, Z. Cao, R. Hu, Y. Zhang, J. Gu, Y. Cui, H. Chen, Y. Shi, J. Shang, B. Li and S. Yang, High-Entropy Atomic Layers of Transition-Metal Carbides (MXenes), *Adv. Mater.*, 2021, **33**(39), 2101473, DOI: **10.1002/adma.202101473**.
6 S. Schweidler, M. Botros, F. Strauss, Q. Wang, Y. Ma, L. Velasco, G. Cadilha Marques, A. Sarkar, C. Kübel, H. Hahn, J. Aghassi-Hagmann, T. Brezesinski and B. Breitung, High-entropy materials for energy and electronic applications, *Nat. Rev. Mater.*, 2024, **9**, 266–281, DOI: **10.1038/s41578-024-00654-5**.
7 Y. Zeng, B. Ouyang, J. Liu, Y.-W. Byeon, Z. Cai, L. J. Miara, Y. Wang and G. Ceder, High-entropy mechanism to boost

ionic conductivity, *Science*, 2022, **378**(6626), 1320–1324, DOI: 10.1126/science.abq1346.

8 B. Jiang, Y. Yu, J. Cui, X. Liu, L. Xie, J. Liao, Q. Zhang, Y. Huang, S. Ning, B. Jia, B. Zhu, S. Bai, L. Chen, S. J. Pennycook and J. He, High-entropy-stabilized chalcogenides with high thermoelectric performance, *Science*, 2021, **371**(6531), 830–834, DOI: 10.1126/science.abe1292.

9 H.-Y. Gu, W.-J. Yin and X.-G. Gong, Significant phonon anharmonicity drives phase transitions in $CsPbI_3$, *Appl. Phys. Lett.*, 2021, **119**(19), 191101, DOI: 10.1063/5.0072367.

10 J. A. Steele, T. Braeckevelt, V. Prakasam, G. Degutis, H. Yuan, H. Jin, E. Solano, P. Puech, S. Basak, M. I. Pintor-Monroy, H. Van Gorp, G. Fleury, R. X. Yang, Z. Lin, H. Huang, E. Debroye, D. Chernyshov, B. Chen, M. Wei, Y. Hou, R. Gehlhaar, J. Genoe, S. De Feyter, S. M. J. Rogge, A. Walsh, E. H. Sargent, P. Yang, J. Hofkens, V. Van Speybroeck and M. B. J. Roeffaers, An embedded interfacial network stabilizes inorganic $CsPbI_3$ perovskite thin films, *Nat. Commun.*, 2022, **13**(1), 7513, DOI: 10.1038/s41467-022-35255-9.

11 S. Divilov, H. Eckert, D. Hicks, C. Oses, C. Toher, R. Friedrich, M. Esters, M. J. Mehl, A. C. Zettel, Y. Lederer, E. Zurek, J.-P. Maria, D. W. Brenner, X. Campilongo, S. Filipović, W. G. Fahrenholtz, C. J. Ryan, C. M. DeSalle, R. J. Crealese, D. E. Wolfe, A. Calzolari and S. Curtarolo, Disordered enthalpy–entropy descriptor for high-entropy ceramics discovery, *Nature*, 2024, **625**(7993), 66–73, DOI: 10.1038/s41586-023-06786-y.

12 H. L. Lukas, S. G. Fries and B. Sundman, *Computational thermodynamics: the Calphad method*, Cambridge University Press, Cambridge, 2007, p. 324.

13 C. M. Rost, E. Sachet, T. Borman, A. Moballegh, E. C. Dickey, D. Hou, J. L. Jones, S. Curtarolo and J.-P. Maria, Entropy-stabilized oxides, *Nat. Commun.*, 2015, **6**(1), 8485, DOI: 10.1038/ncomms9485.

14 Y. Wang, J. Liu, Y. Song, J. Yu, Y. Tian, M. J. Robson, J. Wang, Z. Zhang, X. Lin, G. Zhou, Z. Wang, L. Shen, H. Zhao, S. Grasso and F. Ciucci, High-Entropy Perovskites for Energy Conversion and Storage: Design, Synthesis, and Potential Applications, *Small Methods*, 2023, **7**(4), 2201138, DOI: 10.1002/smtd.202201138.

15 P. Villars, *Thermodynamic Properties of Compounds: Datasheet from Landolt-Börnstein – Group IV Physical Chemistry, Pure Substances*, Springer-Verlag, Berlin, Heidelberg, 2022, vol. **19**A3, DOI: 10.1007/10551582_9.

16 C. Li, X. Lu, W. Ding, L. Feng, Y. Gao and Z. Guo, Formability of ABX_3 (X = F, Cl, Br, I) halide perovskites, *Acta Crystallogr., Sect. B: Struct. Sci.*, 2008, **64**(6), 702–707, DOI: 10.1107/S0108768108032734.

17 W. Travis, E. N. K. Glover, H. Bronstein, D. O. Scanlon and R. G. Palgrave, On the application of the tolerance factor to inorganic and hybrid halide perovskites: a revised system, *Chem. Sci.*, 2016, **7**(7), 4548–4556, DOI: 10.1039/C5SC04845A.

18 Z.-G. Lin, L.-C. Tang and C.-P. Chou, Study on mid-IR NLO crystals $CsGe(Br_xCl_{1-x})_3$, *Opt. Mater.*, 2008, **31**(1), 28–34, DOI: 10.1016/j.optmat.2008.01.004.

19 T. Krishnamoorthy, H. Ding, C. Yan, W. L. Leong, T. Baikie, Z. Zhang, M. Sherburne, S. Li, M. Asta, N. Mathews and S. G. Mhaisalkar, Lead-free germanium iodide perovskite materials for photovoltaic applications, *J. Mater. Chem. A*, 2015, **3**(47), 23829–23832, DOI: 10.1039/C5TA05741H.

20 L. Debbichi, S. Lee, H. Cho, A. M. Rappe, K.-H. Hong, M. S. Jang and H. Kim, Mixed Valence Perovskite $Cs_2Au_2I_6$: A Potential Material for Thin-Film Pb-Free Photovoltaic Cells with Ultrahigh Efficiency, *Adv. Mater.*, 2018, **30**(12), 1707001, DOI: 10.1002/adma.201707001.

21 M. R. Filip and F. Giustino, Computational Screening of Homovalent Lead Substitution in Organic–Inorganic Halide Perovskites, *J. Phys. Chem. C*, 2016, **120**(1), 166–173, DOI: 10.1021/acs.jpcc.5b11845.

22 M. Kar and T. Körzdörfer, Computational high throughput screening of inorganic cation based halide perovskites for perovskite only tandem solar cells, *Mater. Res. Express*, 2020, **7**(5), 055502, DOI: 10.1088/2053-1591/ab8c0d.

23 S. Lu, Q. Zhou, L. Ma, Y. Guo and J. Wang, Rapid Discovery of Ferroelectric Photovoltaic Perovskites and Material Descriptors *via* Machine Learning, *Small Methods*, 2019, **3**(11), 1900360, DOI: 10.1002/smtd.201900360.

24 Q. Xu, Z. Li, M. Liu and W.-J. Yin, Rationalizing Perovskite Data for Machine Learning and Materials Design, *J. Phys. Chem. Lett.*, 2018, **9**(24), 6948–6954, DOI: 10.1021/acs.jpclett.8b03232.

25 C. J. Bartel, C. Sutton, B. R. Goldsmith, R. Ouyang, C. B. Musgrave, L. M. Ghiringhelli and M. Scheffler, New tolerance factor to predict the stability of perovskite oxides and halides, *Sci. Adv.*, 2019, **5**(2), eaav0693, DOI: 10.1126/sciadv.aav0693.

26 G. H. Gu, J. Jang, J. Noh, A. Walsh and Y. Jung, Perovskite synthesizability using graph neural networks, *npj Comput. Mater.*, 2022, **8**(1), 71, DOI: 10.1038/s41524-022-00757-z.

27 G. Pilania, P. V. Balachandran, C. Kim and T. Lookman, Finding New Perovskite Halides *via* Machine Learning, *Front. Mater.*, 2016, 3, DOI: 10.3389/fmats.2016.00019.

28 X. Wang, J. Yang, X. Wang, M. Faizan, H. Zou, K. Zhou, B. Xing, Y. Fu and L. Zhang, Entropy-Driven Stabilization of Multielement Halide Double-Perovskite Alloys, *J. Phys. Chem. Lett.*, 2022, **13**(22), 5017–5024, DOI: 10.1021/acs.jpclett.2c01180.

29 I. Toda-Caraballo, J. S. Wróbel, S. L. Dudarev, D. Nguyen-Manh and P. E. J. Rivera-Díaz-del-Castillo, Interatomic spacing distribution in multicomponent alloys, *Acta Mater.*, 2015, **97**, 156–169, DOI: 10.1016/j.actamat.2015.07.010.

30 B. Wu, Y. Zhao, H. Ali, R. Chen, H. Chen, J. Wen, Y. Liu, L. Liu, K. Yang, L. Zhang, Z. He, Q. Yao, H. Zhang, B. Sa, C. Wen, Y. Qiu, H. Xiong, M. Lin, Y. Liu, C. Wang and H. Su, A reasonable approach to describe the atom distributions and configurational entropy in high entropy alloys based on site preference, *Intermetallics*, 2022, **144**, 107489, DOI: 10.1016/j.intermet.2022.107489.

31 O. N. Senkov, G. B. Wilks, D. B. Miracle, C. P. Chuang and P. K. Liaw, Refractory high-entropy alloys, *Intermetallics*, 2010, **18**(9), 1758–1765, DOI: 10.1016/j.intermet.2010.05.014.

32 A. Takeuchi, K. Amiya, T. Wada, K. Yubuta, W. Zhang and A. Makino, Entropies in Alloy Design for High-Entropy and

Bulk Glassy Alloys, *Entropy*, 2013, **15**(9), 3810–3821, DOI: 10.3390/e15093810.

33 A. Takeuchi and A. Inoue, Calculations of Mixing Enthalpy and Mismatch Entropy for Ternary Amorphous Alloys, *Mater. Trans., JIM*, 2000, **41**(11), 1372–1378, DOI: 10.2320/matertrans1989.41.1372.

34 Z. Wang, Y. Huang, Y. Yang, J. Wang and C. T. Liu, Atomic-size effect and solid solubility of multicomponent alloys, *Scr. Mater.*, 2015, **94**, 28–31, DOI: 10.1016/j.scriptamat.2014.09.010.

35 Y. F. Ye, Q. Wang, J. Lu, C. T. Liu and Y. Yang, The generalized thermodynamic rule for phase selection in multicomponent alloys, *Intermetallics*, 2015, **59**, 75–80, DOI: 10.1016/j.intermet.2014.12.011.

36 Y. F. Ye, Q. Wang, J. Lu, C. T. Liu and Y. Yang, Design of high entropy alloys: A single-parameter thermodynamic rule, *Scr. Mater.*, 2015, **104**, 53–55, DOI: 10.1016/j.scriptamat.2015.03.023.

37 O. N. Senkov, J. D. Miller, D. B. Miracle and C. Woodward, Accelerated exploration of multi-principal element alloys with solid solution phases, *Nat. Commun.*, 2015, **6**(1), 6529, DOI: 10.1038/ncomms7529.

38 S. J. McCormack and A. Navrotsky, Thermodynamics of high entropy oxides, *Acta Mater.*, 2021, **202**, 1–21, DOI: 10.1016/j.actamat.2020.10.043.

39 Z. Rák, J. P. Maria and D. W. Brenner, Evidence for Jahn-Teller compression in the (Mg, Co, Ni, Cu, Zn)O entropy-stabilized oxide: A DFT study, *Mater. Lett.*, 2018, **217**, 300–303, DOI: 10.1016/j.matlet.2018.01.111.

40 Z. Rak, C. M. Rost, M. Lim, P. Sarker, C. Toher, S. Curtarolo, J.-P. Maria and D. W. Brenner, Charge compensation and electrostatic transferability in three entropy-stabilized oxides: Results from density functional theory calculations, *J. Appl. Phys.*, 2016, **120**(9), 095105, DOI: 10.1063/1.4962135.

41 Y.-P. Wang, G.-Y. Gan, W. Wang, Y. Yang and B.-Y. Tang, *Ab Initio* Prediction of Mechanical and Electronic Properties of Ultrahigh Temperature High-Entropy Ceramics $(Hf_{0.2}Zr_{0.2}Ta_{0.2}M_{0.2}Ti_{0.2})B_2$ (M = Nb, Mo, Cr), *Phys. Status Solidi B*, 2018, **255**(8), 1800011, DOI: 10.1002/pssb.201800011.

42 B. Ye, T. Wen, M. C. Nguyen, L. Hao, C.-Z. Wang and Y. Chu, First-principles study, fabrication and characterization of $(Zr_{0.25}Nb_{0.25}Ti_{0.25}V_{0.25})C$ high-entropy ceramics, *Acta Mater.*, 2019, **170**, 15–23, DOI: 10.1016/j.actamat.2019.03.021.

43 A. Zunger, S. H. Wei, L. G. Ferreira and J. E. Bernard, Special quasirandom structures, *Phys. Rev. Lett.*, 1990, **65**(3), 353–356, DOI: 10.1103/PhysRevLett.65.353.

44 J. Yang, P. Manganaris and A. Mannodi-Kanakkithodi, A high-throughput computational dataset of halide perovskite alloys, *Digital Discovery*, 2023, **2**(3), 856–870, DOI: 10.1039/D3DD00015J.

45 J. D. Gale, GULP: A computer program for the symmetry-adapted simulation of solids, *J. Chem. Soc., Faraday Trans.*, 1997, **93**(4), 629–637, DOI: 10.1039/A606455H.

46 Y.-X. Guo, Y.-B. Zhuang, J. Shi and J. Cheng, ChecMatE: A workflow package to automatically generate machine learning potentials and phase diagrams for semiconductor alloys, *J. Chem. Phys.*, 2023, **159**(9), 094801, DOI: 10.1063/5.0166858.

47 G. V. Lewis and C. R. A. Catlow, Potential models for ionic oxides, *J. Phys. C-Solid State Phys.*, 1985, **18**(6), 1149, DOI: 10.1088/0022-3719/18/6/010.

48 W. Smith and T. R. Forester, DL_POLY_2.0: A general-purpose parallel molecular dynamics simulation package, *J. Mol. Graphics*, 1996, **14**(3), 136–141, DOI: 10.1016/S0263-7855(96)00043-4.

49 G. Anand, A. P. Wynn, C. M. Handley and C. L. Freeman, Phase stability and distortion in high-entropy oxides, *Acta Mater.*, 2018, **146**, 119–125, DOI: 10.1016/j.actamat.2017.12.037.

50 C. Oses, C. Toher and S. Curtarolo, Data-driven design of inorganic materials with the Automatic Flow Framework for Materials Discovery, *MRS Bull.*, 2018, **43**(9), 670–675, DOI: 10.1557/mrs.2018.207.

51 P. Sarker, T. Harrington, C. Toher, C. Oses, M. Samiee, J.-P. Maria, D. W. Brenner, K. S. Vecchio and S. Curtarolo, High-entropy high-hardness metal carbides discovered by entropy descriptors, *Nat. Commun.*, 2018, **9**(1), 4980, DOI: 10.1038/s41467-018-07160-7.

52 C. Toher, C. Oses, D. Hicks and S. Curtarolo, Unavoidable disorder and entropy in multi-component systems, *npj Comput. Mater.*, 2019, **5**(1), 69, DOI: 10.1038/s41524-019-0206-z.

53 Y. Zhong, H. Sabarou, X. Yan, M. Yang, M. C. Gao, X. Liu and R. D. Sisson, Exploration of high entropy ceramics (HECs) with computational thermodynamics – A case study with $LaMnO_{3\pm\delta}$, *Mater. Des.*, 2019, **182**, 108060, DOI: 10.1016/j.matdes.2019.108060.

54 G. B. Stringfellow, Calculation of regular solution interaction parameters in semiconductor solid solutions, *J. Phys. Chem. Solids*, 1973, **34**(10), 1749–1751, DOI: 10.1016/S0022-3697(73)80140-4.

55 F. Otto, Y. Yang, H. Bei and E. P. George, Relative effects of enthalpy and entropy on the phase stability of equiatomic high-entropy alloys, *Acta Mater.*, 2013, **61**(7), 2628–2638, DOI: 10.1016/j.actamat.2013.01.042.

56 L. M. Foster, A Lattice Parameter Criterion for Miscibility Gaps in the III–V and II–VI Pseudobinary Solid Solutions, *J. Electrochem. Soc.*, 1974, **121**(12), 1662, DOI: 10.1149/1.2401764.

57 G. B. Stringfellow, Miscibility gaps in quaternary III/V alloys, *J. Cryst. Growth*, 1982, **58**(1), 194–202, DOI: 10.1016/0022-0248(82)90226-3.

58 G. Han, I. W. Yeu, J. Park, K. H. Ye, S.-C. Lee, C. S. Hwang and J.-H. Choi, Effect of local strain energy to predict accurate phase diagram of III–V pseudobinary systems: case of Ga(As,Sb) and (In,Ga)As, *J. Phys. D: Appl. Phys.*, 2021, **54**(4), 045104, DOI: 10.1088/1361-6463/abbf78.

59 E.-A. Zen, Validity of "Vegard's law", *Am. Mineral.*, 1956, **41**(5–6), 523–524.

60 L. Vegard and H. Dale, VIII. Untersuchungen über Mischkristalle und Legierungen, *Z. Kristallogr. – Cryst. Mater.*, 1928, **67**(1–6), 148–162, DOI: 10.1524/zkri.1928.67.1.148.

61 S. D. Baranovskii, A. V. Nenashev, D. Hertel, F. Gebhard and K. Meerholz, Energy Scales of Compositional Disorder in Alloy Semiconductors, *ACS Omega*, 2022, **7**(50), 45741–45751, DOI: 10.1021/acsomega.2c05426.

62 M. Rittiruam, J. Noppakhun, S. Setasuban, N. Aumnongpho, A. Sriwattana, S. Boonchuay, T. Saelee, C. Wangphon, A. Ektarawong, P. Chammingkwan, T. Taniike, S. Praserthdam and P. Praserthdam, High-throughput materials screening algorithm based on first-principles density functional theory and artificial neural network for high-entropy alloys, *Sci. Rep.*, 2022, **12**(1), 16653, DOI: 10.1038/s41598-022-21209-0.

63 Y. Zhang, Y. J. Zhou, J. P. Lin, G. L. Chen and P. K. Liaw, Solid-Solution Phase Formation Rules for Multi-component Alloys, *Adv. Eng. Mater.*, 2008, **10**(6), 534–538, DOI: 10.1002/adem.200700240.

64 X. D. Xu, S. Guo, T. G. Nieh, C. T. Liu, A. Hirata and M. W. Chen, Effects of mixing enthalpy and cooling rate on phase formation of Al_xCoCrCuFeNi high-entropy alloys, *Materialia*, 2019, **6**, 100292, DOI: 10.1016/j.mtla.2019.100292.

65 W. Q. Feng, S. M. Zheng, Y. Qi and S. Q. Wang, Periodic Maximum Entropy Random Structure Models for High-Entropy Alloys, *Mater. Sci. Forum*, 2017, **898**, 611–621, DOI: 10.4028/www.scientific.net/MSF.898.611.

66 S.-m Zheng, W.-q Feng and S.-q Wang, Elastic properties of high entropy alloys by MaxEnt approach, *Comput. Mater. Sci.*, 2018, **142**, 332–337, DOI: 10.1016/j.commatsci.2017.09.060.

67 S. Yang and Y. Zhong, *Ab Initio* Modeling of fcc Fe-Co-Cr-Ni High Entropy Alloys with Full Composition Range, *J. Phase Equilib. Diffus.*, 2021, **42**(5), 656–672, DOI: 10.1007/s11669-021-00905-w.

68 L. Q. Jiang, J. K. Guo, H. B. Liu, M. Zhu, X. Zhou, P. Wu and C. H. Li, Prediction of lattice constant in cubic perovskites, *J. Phys. Chem. Solids*, 2006, **67**(7), 1531–1536, DOI: 10.1016/j.jpcs.2006.02.004.

69 C. Ye, J. Yang, L. Yao and N. Chen, Regularities of formation and lattice distortion of perovskite-type compounds, *Chin. Sci. Bull.*, 2002, **47**(6), 458–460, DOI: 10.1360/02tb9105.

70 H. Ohtani, K. Kojima, K. Ishida and T. Nishizawa, Miscibility gap in II–VI alloy semiconductor systems, *J. Alloys Compd.*, 1992, **182**(1), 103–114, DOI: 10.1016/0925-8388(92)90579-X.

71 T. Wang, H. Chen, Z. Yang, J. Liang and S. Dai, High-Entropy Perovskite Fluorides: A New Platform for Oxygen Evolution Catalysis, *J. Am. Chem. Soc.*, 2020, **142**(10), 4550–4554, DOI: 10.1021/jacs.9b12377.

72 Y. Huang, R. Ding, D. Ying, Y. Huang, C. Tan, T. Yan, X. Sun and E. Liu, A F-deficient and high-Mn ternary perovskite fluoride anode with a dominant conversion mechanism for advanced Li-ion batteries, *Chem. Commun.*, 2021, **57**(62), 7705–7708, DOI: 10.1039/D1CC00910A.

73 Y.-F. Huang, R. Ding, D.-F. Ying, Y.-X. Huang, T. Yan, C.-N. Tan, X.-J. Sun and E.-H. Liu, A novel Li-ion supercapattery by K-ion vacant ternary perovskite fluoride anode with pseudocapacitive conversion/insertion dual mechanisms, *Rare Met.*, 2022, **41**(7), 2491–2504, DOI: 10.1007/s12598-022-01979-2.

74 Z. Jia, R. Ding, W. Yu, Y. Li, A. Wang, M. Liu, F. Yang, X. Sun and E. Liu, Unraveling the Charge Storage and Activity-Enhancing Mechanisms of Zn-Doping Perovskite Fluorides and Engineering the Electrodes and Electrolytes for Wide-Temperature Aqueous Supercabatteries, *Adv. Funct. Mater.*, 2022, **32**(1), 2107674, DOI: 10.1002/adfm.202107674.

75 Z. Jia, W. Shi, R. Ding, W. Yu, Y. Li, C. Tan, X. Sun and E. Liu, Conversion-type NiCoMn triple perovskite fluorides for advanced aqueous supercapacitors, batteries and supercapatteries, *Chem. Commun.*, 2021, **57**(64), 7962–7965, DOI: 10.1039/D1CC02488D.

76 Y. Li, R. Ding, Z. Jia, W. Yu, A. Wang, M. Liu, F. Yang, Y. Zhang, Q. Fang, M. Yan, J. Xie, X. Sun and E. Liu, Unlocking the intrinsic mechanisms of A-site K/Na doped perovskite fluorides pseudocapacitive cathode materials for enhanced aqueous zinc-based batteries, *Energy Storage Mater.*, 2023, **57**, 334–345, DOI: 10.1016/j.ensm.2023.02.020.

77 H. Mao, L. Wang, J. Li, X. Jiang, S. Xue, M. Li, J. Zhu, B. Fan, T. Xu, G. Shao, H. Xu, H. Wang, R. Zhang and H. Lu, High-Entropy $Cs(Pb_{1/3}Mn_{1/3}Ni_{1/3})Br_3$ Perovskite Nanocrystals Prepared by High Energy Ball Milling and their Luminescence Properties, *Part. Part. Syst. Charact.*, 2022, **39**(9), 2200073, DOI: 10.1002/ppsc.202200073.

78 W. Shi, W. Yu, R. Ding, Z. Jia, Y. Li, Y. Huang, C. Tan, X. Sun and E. Liu, Bipolar redox electrolyte-synergistically mediated NiCoMn-811 high-Ni ternary perovskite fluorides for advanced supercapacitors in both alkaline and neutral media, *J. Mater. Chem. A*, 2021, **9**(15), 9624–9633, DOI: 10.1039/D1TA01156A.

79 C. Tan, R. Ding, Y. Huang, T. Yan, Y. Huang, F. Yang, X. Sun, P. Gao and E. Liu, A vacancy-rich perovskite fluoride $K_{0.79}Ni_{0.25}Co_{0.36}Mn_{0.39}F_{2.83}$@rGO anode for advanced Na-based dual-ion batteries, *Chem. Commun.*, 2021, **57**(47), 5830–5833, DOI: 10.1039/D1CC01477C.

80 A. Wang, R. Ding, Y. Li, M. Liu, F. Yang, Y. Zhang, Q. Fang, M. Yan, J. Xie, Z. Chen, Z. Yan, Y. He, J. Guo, X. Sun and E. Liu, Redox Electrolytes-Assisting Aqueous Zn-Based Batteries by Pseudocapacitive Multiple Perovskite Fluorides Cathode and Charge Storage Mechanisms, *Small*, 2023, 2302333, DOI: 10.1002/smll.202302333.

81 T. Wang, J. Fan, C.-L. Do-Thanh, X. Suo, Z. Yang, H. Chen, Y. Yuan, H. Lyu, S. Yang and S. Dai, Perovskite Oxide–Halide Solid Solutions: A Platform for Electrocatalysts, *Angew. Chem., Int. Ed.*, 2021, **60**(18), 9953–9958, DOI: 10.1002/anie.202101120.

82 X. Wang, G. Liu, C. Tang, H. Tang, W. Zhang, Z. Ju, J. Jiang, Q. Zhuang and Y. Cui, A novel high entropy perovskite fluoride anode with 3D cubic framework for advanced lithium-ion battery, *J. Alloys Compd.*, 2023, **934**, 167889, DOI: 10.1016/j.jallcom.2022.167889.

83 T. Yan, R. Ding, Y. Huang, D. Ying, C. Tan, Y. Huang, F. Yang, X. Sun, P. Gao and E. Liu, A novel sodium-ion supercabattery based on vacancy defective Ni–Co–Mn ternary perovskite fluoride electrode materials, *J. Mater. Chem. A*, 2021, **9**(25), 14276–14284, DOI: 10.1039/D1TA02894D.

84 T. Yan, Y. Huang, R. Ding, W. Shi, D. Ying, Z. Jia, C. Tan, Y. Huang, X. Sun and E. Liu, Pseudocapacitive trimetallic NiCoMn-111 perovskite fluorides for advanced Li-ion

supercabatteries, *Nanoscale Adv.*, 2021, **3**(19), 5703–5710, DOI: 10.1039/D1NA00329A.

85 F. Yang, R. Ding, Z. Jia, W. Yu, Y. Li, A. Wang, M. Liu, J. Xie, M. Yan, Q. Fang, Y. Zhang, X. Sun and E. Liu, High specific energy and power sodium-based dual-ion supercabatteries by pseudocapacitive Ni-Zn-Mn ternary perovskite fluorides@reduced graphene oxides anodes with conversion-alloying-intercalation triple mechanisms, *Energy Storage Mater.*, 2022, **53**, 222–237, DOI: 10.1016/j.ensm.2022.08.049.

86 D. Ying, Y. Li, R. Ding, W. Shi, Q. Xu, Y. Huang, Z. Jia, W. Yu, X. Sun, P. Gao, E. Liu and X. Wang, Nanosilver-Promoted Trimetallic Ni–Co–Mn Perovskite Fluorides for Advanced Aqueous Supercabatteries with Pseudocapacitive Multielectrons Phase Conversion Mechanisms, *Adv. Funct. Mater.*, 2021, **31**(24), 2101353, DOI: 10.1002/adfm.202101353.

87 W. Yu, R. Ding, Z. Jia, Y. Li, A. Wang, M. Liu, F. Yang, X. Sun and E. Liu, Pseudocapacitive Co-Free Trimetallic Ni-Zn-Mn Perovskite Fluorides Enable Fast-Rechargeable Zn-Based Aqueous Batteries, *Adv. Funct. Mater.*, 2022, **32**(19), 2112469, DOI: 10.1002/adfm.202112469.

88 J. Jung, Y. Yun, S. W. Yang, H. G. Oh, A. Y. Jeon, Y. Nam, Y.-W. Heo, W.-S. Chae and S. Lee, Ternary diagrams of phase, stability, and optical properties of cesium lead mixed-halide perovskites, *Acta Mater.*, 2023, **246**, 118661, DOI: 10.1016/j.actamat.2022.118661.

89 W. Zhang, H. Liu, Y. Qu, J. Cui, W. Zhang, T. Shi and H.-L. Wang, B-Site Co-Doping Coupled with Additive Passivation Pushes the Efficiency of Pb–Sn Mixed Inorganic Perovskite Solar Cells to Over 17%, *Adv. Mater.*, 2023, 2309193, DOI: 10.1002/adma.202309193.

90 S. Baek, S. Kim, J. Y. Noh, J. H. Heo, S. H. Im, K.-H. Hong and S.-W. Kim, Development of Mixed-Cation $Cs_xRb_{1-x}PbX_3$ Perovskite Quantum Dots and Their Full-Color Film with High Stability and Wide Color Gamut, *Adv. Opt. Mater.*, 2018, **6**(15), 1800295, DOI: 10.1002/adom.201800295.

91 M. Zirak, E. Moyen, H. Alehdaghi, A. Kanwat, W.-C. Choi and J. Jang, Anion- and Cation-Codoped All-Inorganic Blue-Emitting Perovskite Quantum Dots for Light-Emitting Diodes, *ACS Appl. Nano Mater.*, 2019, **2**(9), 5655–5662, DOI: 10.1021/acsanm.9b01187.

92 L. Stand, M. Zhuravleva, B. Chakoumakos, H. Wei, J. Johnson, V. Martin, M. Loyd, D. Rutstrom, W. McAlexander, Y. Wu, M. Koschan and C. L. Melcher, Characterization of mixed halide scintillators: $CsSrBrI_2$:Eu, $CsCaBrI_2$:Eu and $CsSrClBr_2$:Eu, *J. Lumin.*, 2019, **207**, 70–77, DOI: 10.1016/j.jlumin.2018.10.108.

93 T. Wen, G. Gu, B. Wang, W. Zhang and R. Wang, Cyan-rich sunlight-like spectra from Mn^{2+}-doped $CsCd(Cl_{1-y}Br_y)_3$ perovskites with dual tunable emissions and high stability, *J. Mater. Chem. C*, 2023, **11**(21), 6989–6998, DOI: 10.1039/D2TC05455H.

94 Y. Ji, M. Wang, Z. Yang, H. Wang, M. A. Padhiar, J. Shi, H. Qiu and A. S. Bhatti, *In Situ* Synthesis of UltraStable TiO_2 Coating Rb^+-Doped Red Emitting $CsPbBrI_2$ Perovskite Quantum Dots, *J. Phys. Chem. C*, 2022, **126**(3), 1542–1551, DOI: 10.1021/acs.jpcc.1c09945.

95 Y.-H. Lin, Z.-H. Qiu, S.-H. Wang, X.-H. Zhang and S.-F. Wu, All-inorganic $Rb_xCs_{1-x}PbBrI_2$ perovskite nanocrystals with wavelength-tunable properties for red light-emitting, *Inorg. Chem. Commun.*, 2019, **103**, 47–52, DOI: 10.1016/j.inoche.2019.03.007.

96 S. Lee, J. Moon, J. Ryu, B. Parida, S. Yoon, D.-G. Lee, J. S. Cho, S. Hayase and D.-W. Kang, Inorganic narrow bandgap $CsPb_{0.4}Sn_{0.6}I_{2.4}Br_{0.6}$ perovskite solar cells with exceptional efficiency, *Nano Energy*, 2020, **77**, 105309, DOI: 10.1016/j.nanoen.2020.105309.

97 N. Li, Z. Zhu, J. Li, A. K.-Y. Jen and L. Wang, Inorganic $CsPb_{1-x}Sn_xIBr_2$ for Efficient Wide-Bandgap Perovskite Solar Cells, *Adv. Energy Mater.*, 2018, **8**(22), 1800525, DOI: 10.1002/aenm.201800525.

98 Y. Shang, X. Li, W. Lian, X. Jiang, X. Wang, T. Chen, Z. Xiao, M. Wang, Y. Lu and S. Yang, Lead acetate as a superior lead source enables highly efficient and stable all-inorganic lead-tin perovskite solar cells, *Chem. Eng. J.*, 2023, **457**, 141246, DOI: 10.1016/j.cej.2022.141246.

99 Q. Wen, C. Duan, F. Zou, D. Luo, J. Li, Z. Liu, J. Wang and K. Yan, All-inorganic $CsPb_{1-x}Sn_xI_2Br$ perovskites mediated by dicyandiamide additive for efficient 4-terminal tandem solar cell, *Chem. Eng. J.*, 2023, **452**, 139697, DOI: 10.1016/j.cej.2022.139697.

100 W. Zhang, H. Liu, X. Qi, Y. Yu, Y. Zhou, Y. Xia, J. Cui, Y. Shi, R. Chen and H.-L. Wang, Oxalate Pushes Efficiency of $CsPb_{0.7}Sn_{0.3}IBr_2$ Based All-Inorganic Perovskite Solar Cells to over 14%, *Adv. Sci.*, 2022, **9**(11), 2106054, DOI: 10.1002/advs.202106054.

101 Z. Zhang, L. Dai, M. Zhang, H. Ban, Z. Liu, H. Yu, A. Gu, X.-L. Zhang, S. Chen, Y. Wang, Y. Shen and M. Wang, Surface Modification in $CsPb_{0.5}Sn_{0.5}I_2Br$ Inorganic Perovskite Solar Cells: Effects of Bifunctional Dipolar Molecules on Photovoltaic Performance, *ACS Appl. Mater. Interfaces*, 2023, **15**(30), 36594–36601, DOI: 10.1021/acsami.3c07018.

102 F. Yang, D. Hirotani, G. Kapil, M. A. Kamarudin, C. H. Ng, Y. Zhang, Q. Shen and S. Hayase, All-Inorganic $CsPb_{1-x}Ge_xI_2Br$ Perovskite with Enhanced Phase Stability and Photovoltaic Performance, *Angew. Chem., Int. Ed.*, 2018, **57**(39), 12745–12749, DOI: 10.1002/anie.201807270.

103 Y. Hu, Y. Zhang, C. Yang, J. Li and L. Wang, The cation–anion co-exchange in $CsPb_{1-x}Fe_x(Br_{1-y}Cl_y)_3$ nanocrystals prepared using a hot injection method, *RSC Adv.*, 2020, **10**(55), 33080–33085, DOI: 10.1039/D0RA06238C.

104 C. Wu, Y. Li, Z. Xia, C. Ji, Y. Tang, J. Zhang, C. Ma and J. Gao, Enhancing Photoluminescence of $CsPb(Cl_xBr_{1-x})_3$ Perovskite Nanocrystals by Fe^{2+} Doping, *Nanomaterials*, 2023, **13**(3), 533, DOI: 10.3390/nano13030533.

105 V. Naresh and N. Lee, Zn(II)-Doped Cesium Lead Halide Perovskite Nanocrystals with High Quantum Yield and Wide Color Tunability for Color-Conversion Light-Emitting Displays, *ACS Appl. Nano Mater.*, 2020, **3**(8), 7621–7632, DOI: 10.1021/acsanm.0c01254.

106 H. Sun, J. Zhang, X. Gan, L. Yu, H. Yuan, M. Shang, C. Lu, D. Hou, Z. Hu, Y. Zhu and L. Han, Pb-Reduced $CsPb_{0.9}Zn_{0.1}I_2Br$ Thin Films for Efficient Perovskite Solar

Cells, *Adv. Energy Mater.*, 2019, **9**(25), 1900896, DOI: 10.1002/aenm.201900896.

107 I. N. Belyaev and E. A. Shurginov, *Zh. Neorg. Khim.*, 1970, **15**, 1401.

108 H. M. Ghaithan, S. M. H. Qaid, Z. A. Alahmed, M. Hezam, A. Lyras, M. Amer and A. S. Aldwayyan, Anion Substitution Effects on the Structural, Electronic, and Optical Properties of Inorganic $CsPb(I_{1-x}Br_x)_3$ and $CsPb(Br_{1-x}Cl_x)_3$ Perovskites: Theoretical and Experimental Approaches, *J. Phys. Chem. C*, 2021, **125**(1), 886–897, DOI: 10.1021/acs.jpcc.0c07983.

109 H. M. Ghaithan, S. M. H. Qaid, K. K. AlHarbi, A. F. Bin Ajaj, B. A. Al-Asbahi and A. S. Aldwayyan, Amplified Spontaneous Emission from Thermally Evaporated High-Quality Thin Films of $CsPb(Br_{1-x}Y_x)_3$ (Y = I, Cl) Perovskites, *Langmuir*, 2022, **38**(28), 8607–8613, DOI: 10.1021/acs.langmuir.2c00861.

110 T. C. Jellicoe, J. M. Richter, H. F. J. Glass, M. Tabachnyk, R. Brady, S. E. Dutton, A. Rao, R. H. Friend, D. Credgington, N. C. Greenham and M. L. Böhm, Synthesis and Optical Properties of Lead-Free Cesium Tin Halide Perovskite Nanocrystals, *J. Am. Chem. Soc.*, 2016, **138**(9), 2941–2944, DOI: 10.1021/jacs.5b13470.

111 L. Peedikakkandy and P. Bhargava, Composition dependent optical, structural and photoluminescence characteristics of cesium tin halide perovskites, *RSC Adv.*, 2016, **6**(24), 19857–19860, DOI: 10.1039/C5RA22317B.

112 D. E. Scaife, P. F. Weller and W. G. Fisher, Crystal preparation and properties of cesium tin(II) trihalides, *J. Solid State Chem.*, 1974, **9**(3), 308–314, DOI: 10.1016/0022-4596(74)90088-7.

113 S. Sharma, N. Weiden and A. Weiss, Phase Diagrams Of Quasibinary Systems Of The Type: Abx3-A′bx3; Abx3-Ab′x3 And Abx3-Abx′3; X = Halogen, *Z. Phys. Chem.*, 1992, **175**(1), 63–80.

114 Z.-G. Lin, L.-C. Tang and C.-P. Chou, Infrared properties of $CsGe(Br_xCl_{1-x})_3$, nonlinear optical rhombohedral semiconductor, *J. Phys.: Condens. Matter*, 2007, **19**(47), 476209, DOI: 10.1088/0953-8984/19/47/476209.

115 Z.-G. Lin, L.-C. Tang and C.-P. Chou, Characterization and properties of infrared NLO crystals: $AGeX_3$ (A = Rb, Cs; X = Cl, Br), *J. Cryst. Growth*, 2008, **310**(13), 3224–3229, DOI: 10.1016/j.jcrysgro.2008.03.018.

116 S. R. Lüthi and M. J. Riley, Ni(II)-Doped $CsCdBrCl_2$: Variation of Spectral and Structural Properties *via* Mixed-Halide Coordination, *Inorg. Chem.*, 2001, **40**(2), 196–207, DOI: 10.1021/ic000899l.

117 M. P. Plokker, D. A. Biner, N. Dusoswa, P. Dorenbos, K. W. Krämer and E. Van Der Kolk, Photoluminescence and excited states dynamics of Tm^{2+}-doped $CsCa(Cl/Br)_3$ and $CsCa(Br/I)_3$ perovskites, *J. Phys.: Mater.*, 2021, **4**(4), 045004, DOI: 10.1088/2515-7639/ac24ed.

118 H. Näsström, P. Becker, J. A. Márquez, O. Shargaieva, R. Mainz, E. Unger and T. Unold, Dependence of phase transitions on halide ratio in inorganic $CsPb(Br_xI_{1-x})_3$ perovskite thin films obtained from high-throughput experimentation, *J. Mater. Chem. A*, 2020, **8**(43), 22626–22631, DOI: 10.1039/D0TA08067E.

119 L. Yuan, M. Yuan, H. Xu, C. Hou and X. Meng, Moisture-stimulated reversible thermochromic $CsPbI_{3-x}Br_x$ films: In-situ spectroscopic-resolved structure and optical properties, *Appl. Surf. Sci.*, 2022, **573**, 151484, DOI: 10.1016/j.apsusc.2021.151484.

120 G. Natta and L. Passerini, Isomorfismo, polimorfismo e morfotropia I. Composti del tipo ABX_3, *Gazz. Chim. Ital.*, 1928, **58**, 472–484.

121 N. Bontemps, C. Grisolia, M. Nerozzi and B. Briat, Optical and magneto-optical study of the magnetic properties of $RbFeCl_3$, $RbFeBr_3$, and disordered materials of intermediate composition, *J. Appl. Phys.*, 1982, **53**(3), 2710–2712, DOI: 10.1063/1.330940.

122 A. Harrison and D. Visser, Magnetic ordering effects in the random mixed one-dimensional ferromagnet-antiferromagnet system $RbFeCl_{3-x}Br_x$, *J. Phys.: Condens. Matter*, 1989, **1**(4), 733, DOI: 10.1088/0953-8984/1/4/008.

123 H. P. Beck, M. Schramm and R. Haberkorn, The $InSnCl_3$-Type Arrangement: II. High Pressure Synthesis of $TlPbCl_3$ and of Solid Solutions Containing Rb or Br, *J. Solid State Chem.*, 1999, **146**(2), 351–354, DOI: 10.1006/jssc.1999.8361.

124 D. Amgar, T. Binyamin, V. Uvarov and L. Etgar, Near ultra-violet to mid-visible band gap tuning of mixed cation $Rb_xCs_{1-x}PbX_3$ (X = Cl or Br) perovskite nanoparticles, *Nanoscale*, 2018, **10**(13), 6060–6068, DOI: 10.1039/C7NR09607K.

125 M. R. Linaburg, E. T. McClure, J. D. Majher and P. M. Woodward, $Cs_{1-x}Rb_xPbCl_3$ and $Cs_{1-x}Rb_xPbBr_3$ Solid Solutions: Understanding Octahedral Tilting in Lead Halide Perovskites, *Chem. Mater.*, 2017, **29**(8), 3507–3514, DOI: 10.1021/acs.chemmater.6b05372.

126 W. Jia, Q. Wei, S. Ge, C. Peng, T. Huang, S. Yao, Y. Tian, T. Chang, R. Zeng and B. Zou, Polaronic Magnetic Excitons and Photoluminescence in Mn^{2+}-Doped $CsCdBr_3$ Metal Halides, *J. Phys. Chem. C*, 2021, **125**(32), 18031–18039, DOI: 10.1021/acs.jpcc.1c05127.

127 F. Lahoz, P. J. Alonso, B. Villacampa and R. Alcala, Spectroscopic properties of Mn^{2+} ions in mixed fluoroperovskites, *Radiat. Eff. Defects Solids*, 1995, **135**(1–4), 163–167, DOI: 10.1080/10420159508229827.

128 F. Lahoz, M. Díaz, B. Villacampa, R. Cases and R. Alcalá, Influence of the host lattice on the photoluminescence of Ni^{2+} ions in $Rb_{1-x}Cs_xCaF_3$ and $RbCa_{1-x}Cd_xF_3$ crystals, *J. Appl. Phys.*, 1997, **82**(10), 5121–5125, DOI: 10.1063/1.366314.

129 P. Ghigna, M. Scavini, C. Mazzoli, M. Brunelli, C. Laurenti and C. Ferrero, Experimental disentangling of orbital and lattice energy scales by inducing cooperative Jahn-Teller melting in $KCu_{1-x}Mg_xF_3$ solid solutions, *Phys. Rev. B: Condens. Matter Mater. Phys.*, 2010, **81**(7), 073107, DOI: 10.1103/PhysRevB.81.073107.

130 C. Oliva, M. Scavini, S. Cappelli, C. Bottalo, C. Mazzoli and P. Ghigna, Melting of Orbital Ordering in $KMg_xCu_{1-x}F_3$ Solid Solution, *J. Phys. Chem. B*, 2007, **111**(21), 5976–5983, DOI: 10.1021/jp067539p.

131 P. A. Fleury, W. Hayes and H. J. Guggenheim, Magnetic scattering of light in $K(NiMg)F_3$, *J. Phys. C-Solid State Phys.*, 1975, **8**(13), 2183, DOI: 10.1088/0022-3719/8/13/027.

132 A. Karmakar, A. Bhattacharya, G. M. Bernard, A. Mar and V. K. Michaelis, Revealing the Local Sn and Pb

Arrangements in $CsSn_xPb_{1-x}Br_3$ Perovskites with Solid-State NMR Spectroscopy, *ACS Mater. Lett.*, 2021, **3**(3), 261–267, DOI: 10.1021/acsmaterialslett.0c00596.

133 X. Zhang, W. Cao, W. Wang, B. Xu, S. Liu, H. Dai, S. Chen, K. Wang and X. W. Sun, Efficient light-emitting diodes based on green perovskite nanocrystals with mixed-metal cations, *Nano Energy*, 2016, **30**, 511–516, DOI: 10.1016/j.nanoen.2016.10.039.

134 T. Suzuki, H. Guo, I. Kawasaki, I. Watanabe, T. Goto, K. Katayama and H. Tanaka, Disappearance of Gapped Mott Insulating Phase Neighboring Bose Glass Phase in $Tl_{1-x}K_xCuCl_3$ Detected by Longitudinal-Field Muon Spin Relaxation, *J. Phys. Soc. Jpn.*, 2014, **83**(8), 084703, DOI: 10.7566/JPSJ.83.084703.

135 T. Suzuki, F. Yamada, I. Watanabe, T. Goto, A. Oosawa and H. Tanaka, Bond-randomness effect on the quantum spin system $Tl_{1-x}K_xCuCl_3$ probed by muon-spin-relaxation method, *Phys. B*, 2009, **404**(5), 590–593, DOI: 10.1016/j.physb.2008.11.108.

136 F. Yamada, H. Tanaka, T. Ono and H. Nojiri, Transition from Bose glass to a condensate of triplons in $Tl_{1-x}K_xCuCl_3$, *Phys. Rev. B: Condens. Matter Mater. Phys.*, 2011, **83**(2), 020409, DOI: 10.1103/PhysRevB.83.020409.

137 P. Chartrand and A. D. Pelton, Thermodynamic Evaluation and Optimization of the LiCl–NaCl–KCl–RbCl–CsCl–$MgCl_2$–$CaCl_2$–$SrCl_2$ System Using The Modified Quasi-chemical Model, *Can. Metall. Q.*, 2000, **39**(4), 405–420, DOI: 10.1179/cmq.2000.39.4.405.

138 Y. Chornodolskyy, G. Stryganyuk, S. Syrotyuk, A. Voloshinovskii and P. Rodnyi, Features of the core–valence luminescence and electron energy band structure of $A_{1-x}Cs_xCaCl_3$ (A = K,Rb) crystals, *J. Phys.: Condens. Matter*, 2007, **19**(47), 476211, DOI: 10.1088/0953-8984/19/47/476211.

139 K. Takahashi, M. Koshimizu, Y. Fujimoto, T. Yanagida and K. Asai, Auger-free luminescence characteristics of $Rb_{1-x}Cs_xCaCl_3$, *J. Ceram. Soc. Jpn.*, 2018, **126**(10), 755–760, DOI: 10.2109/jcersj2.18051.

140 V. Vaněček, J. Páterek, R. Král, R. Kučerková, V. Babin, J. Rohlíček, R. Cala', N. Kratochwil, E. Auffray and M. Nikl, (INVITED) Ultraviolet cross-luminescence in ternary chlorides of alkali and alkaline-earth metals, *Opt. Mater.: X*, 2021, **12**, 100103, DOI: 10.1016/j.omx.2021.100103.

141 Q. Dong, B. Tian, W. Zhang and L. He, Facile synthesis of $K_aCs_{1-a}PbBr_3$@ molecular sieve SBA-15 composite with improved luminescence and wet/thermal stability, *Colloids Surf., A*, 2022, **648**, 129258, DOI: 10.1016/j.colsurfa.2022.129258.

142 G. Shao, S. Liu, L. Ding, Z. Zhang, W. Xiang and X. Liang, $K_xCs_{1-x}PbBr_3$ NCs glasses possessing super optical properties and stability for white light emitting diodes, *Chem. Eng. J.*, 2019, **375**, 122031, DOI: 10.1016/j.cej.2019.122031.

143 S. H. S. S. Dintakurti, *Phase evolution and local structure in [Cs, MA][Pb, Sr][Cl, Br]$_3$ perovskites*, Doctoral Thesis, Nanyang Technological University, 2021.

144 J.-M. Dance, J. Grannec and A. Tressand, *C. R. Acad. Sci.*, 1975, **C281**, 91.

145 M. Hu, M. Chen, P. Guo, H. Zhou, J. Deng, Y. Yao, Y. Jiang, J. Gong, Z. Dai, Y. Zhou, F. Qian, X. Chong, J. Feng, R. D. Schaller, K. Zhu, N. P. Padture and Y. Zhou, Sub-1.4eV bandgap inorganic perovskite solar cells with long-term stability, *Nat. Commun.*, 2020, **11**(1), 151, DOI: 10.1038/s41467-019-13908-6.

146 M. Hu, Y. Zhang, J. Gong, H. Zhou, X. Huang, M. Liu, Y. Zhou and S. Yang, Surface Sn(IV) Hydrolysis Improves Inorganic Sn–Pb Perovskite Solar Cells, *ACS Energy Lett.*, 2023, **8**(2), 1035–1041, DOI: 10.1021/acsenergylett.2c02435.

147 M. Liu, H. Pasanen, H. Ali-Löytty, A. Hiltunen, K. Lahtonen, S. Qudsia, J.-H. Smått, M. Valden, N. V. Tkachenko and P. Vivo, B-Site Co-Alloying with Germanium Improves the Efficiency and Stability of All-Inorganic Tin-Based Perovskite Nanocrystal Solar Cells, *Angew. Chem., Int. Ed.*, 2020, **59**(49), 22117–22125, DOI: 10.1002/anie.202008724.

148 F. Borsa, D. J. Benard, W. C. Walker and A. Baviera, NMR and birefringence study of structural transitions in disordered crystals: $Rb_xK_{1-x}MnF_3$, *Phys. Rev. B: Solid State*, 1977, **15**(1), 84–94, DOI: 10.1103/PhysRevB.15.84.

149 J. C. Cousseins, Etude dans l'etat solide de quelques fluorures ternaires: Synthese; identification; filiation; miscibilite, *Rev. Chim. Miner.*, 1964, **1**, 573–616.

150 J. Kapusta, Ph Daniel and A. Ratuszna, Vibrational investigation and phase transitions in the $KMnF_3$ doped perovskite crystals (Li^+, Na^+, Rb^+ and Cs^+), *J. Phys.: Condens. Matter*, 2002, **14**(21), 5433, DOI: 10.1088/0953-8984/14/21/317.

151 P. Todorović, D. Ma, B. Chen, R. Quintero-Bermudez, M. I. Saidaminov, Y. Dong, Z.-H. Lu and E. H. Sargent, Spectrally Tunable and Stable Electroluminescence Enabled by Rubidium Doping of $CsPbBr_3$ Nanocrystals, *Adv. Opt. Mater.*, 2019, **7**(24), 1901440, DOI: 10.1002/adom.201901440.

152 H. Wu, Y. Yang, D. Zhou, K. Li, J. Yu, J. Han, Z. Li, Z. Long, J. Ma and J. Qiu, Rb^+ cations enable the change of luminescence properties in perovskite ($Rb_xCs_{1-x}PbBr_3$) quantum dots, *Nanoscale*, 2018, **10**(7), 3429–3437, DOI: 10.1039/C7NR07776A.

153 F. Lahoz, B. Villacampa, R. Alcalá, C. Marquina and M. R. Ibarra, Cubic-to-tetragonal structural phase transition in $Rb_{1-x}Cs_xCaF_3$ solid solutions: Thermal expansion and EPR studies, *Phys. Rev. B: Condens. Matter Mater. Phys.*, 1997, **55**(13), 8148–8154, DOI: 10.1103/PhysRevB.55.8148.

154 J. Deng, J. Xun, W. Shen, M. Li and R. He, Phase Regulation of $CsPb_2Br_5$/$CsPbBr_3$ Perovskite Nanocrystals by Doping with Divalent Cations: Implications for Optoelectronic Devices with Enhanced Stability and Reduced Toxicity, *ACS Appl. Nano Mater.*, 2021, **4**(9), 9213–9222, DOI: 10.1021/acsanm.1c01737.

155 D. B. Straus and R. J. Cava, Tuning the Band Gap in the Halide Perovskite $CsPbBr_3$ through Sr Substitution, *ACS Appl. Mater. Interfaces*, 2022, **14**(30), 34884–34890, DOI: 10.1021/acsami.2c09275.

156 H. Tanaka, K. Iio and K. Nagata, Magnetic properties of $Rb_{1-x}K_xNiCl_3$, $RbVBr_3$ and $CsNiI_3$, *J. Magn. Magn. Mater.*, 1992, **104–107**, 829–830, DOI: 10.1016/0304-8853(92)90380-7.

157 A. Bernasconi, A. Rizzo, A. Listorti, A. Mahata, E. Mosconi, F. De Angelis and L. Malavasi, Synthesis, Properties, and Modeling of $Cs_{1-x}Rb_xSnBr_3$ Solid Solution: A New Mixed-Cation Lead-Free All-Inorganic Perovskite System, *Chem. Mater.*, 2019, **31**(9), 3527–3533, DOI: 10.1021/acs.chemmater.9b00837.

158 P. Daniel, J. Toulouse and M. Rousseau, Phase transitions in mixed disordered crystals $Rb_{1-x}K_xCaF_3$ ($0 < x < 1$) investigated by Raman spectroscopy, *Eur. Phys. J.: Appl. Phys.*, 1999, **5**(1), 33–44, DOI: 10.1051/epjap:1999109.

159 A. Jouanneaux, Ph Daniel and G. Bushnell-Wye, Structural instabilities in disordered perovskites studied by synchrotron radiation powder diffraction. Proposition for a phase diagram, *J. Phys.: Condens. Matter*, 1998, **10**(24), 5485, DOI: 10.1088/0953-8984/10/24/024.

160 N. V. Rebrova, A. Y. Grippa, I. A. Boiaryntseva, P. Berastegui, T. E. Gorbacheva, Y. N. Datsko, A. L. Rebrov, C. Dujardin, R. Calà, L. Martinazzoli, E. Auffray and V. V. Kononets, Effects of europium concentration on luminescent and scintillation performance of $Cs_{0.2}Rb_{0.8}Ca_{1-x}Eu_xBr_3$ ($0 \leq x \leq 0.08$) crystals, *J. Rare Earths*, 2022, **40**(1), 29–33, DOI: 10.1016/j.jre.2020.08.012.

161 N. V. Rebrova, A. Y. Grippa, I. A. Boiaryntseva, P. Berastegui, T. E. Gorbacheva, V. Y. Pedash, S. N. Galkin, V. V. Kononets, Y. N. Datsko and V. L. Cherginets, Crystal growth and characterization of Eu^{2+} doped $Cs_{1-x}Rb_xCaBr_3$, *J. Alloys Compd.*, 2020, **816**, 152594, DOI: 10.1016/j.jallcom.2019.152594.

162 M. Hidaka, Z. Y. Zhou and S. Yamashita, Structural phase transitions in $KCdF_3$ and $K_{0.5}Rb_{0.5}CdF_3$, *Phase Transitions*, 1990, **20**(1–2), 83–94, DOI: 10.1080/01411599008206869.

163 S. He, Q. Qiang, T. Lang, M. Cai, T. Han, H. You, L. Peng, S. Cao, B. Liu, X. Jing and B. Jia, Highly Stable Orange-Red Long-Persistent Luminescent $CsCdCl_3$:Mn^{2+} Perovskite Crystal, *Angew. Chem., Int. Ed.*, 2022, **61**(48), e202208937, DOI: 10.1002/anie.202208937.

164 W. Jia, Q. Wei, S. Yao, S. Ge, C. Peng, L. Wang, X. Zhong, H. peng and B. Zou, Magnetic coupling for highly efficient and tunable emission in $CsCdX_3$:Mn perovskites, *J. Lumin.*, 2023, **257**, 119657, DOI: 10.1016/j.jlumin.2022.119657.

165 S. Wu, L. Yuan, G. Chen, C. Peng and Y. Jin, All-inorganic Mn^{2+}-doped metal halide perovskite crystals for the late-time detection of X-ray afterglow imaging, *Nanoscale*, 2023, **15**(33), 13628–13634, DOI: 10.1039/D3NR02208K.

166 L. Men, B. A. Rosales, N. E. Gentry, S. D. Cady and J. Vela, Lead-Free Semiconductors: Soft Chemistry, Dimensionality Control, and Manganese-Doping of Germanium Halide Perovskites, *ChemNanoMat*, 2019, **5**(3), 334–339, DOI: 10.1002/cnma.201800497.

167 A. Ratuszna and J. Kapusta, Structural phase transitions in $KMnF_3$ doped by Li^+, Na^+ and Rb^+, *Phase Transitions*, 1997, **62**(3), 181–198, DOI: 10.1080/01411599708220068.

168 M. W. Shafer and T. R. McGuire, Preparation and properties of ferrimagnets in the $RbMgF_3$–$RbCoF_3$ system, *J. Phys. Chem. Solids*, 1969, **30**(8), 1989–1997, DOI: 10.1016/0022-3697(69)90177-2.

169 M. Chen, M.-G. Ju, H. F. Garces, A. D. Carl, L. K. Ono, Z. Hawash, Y. Zhang, T. Shen, Y. Qi, R. L. Grimm, D. Pacifici, X. C. Zeng, Y. Zhou and N. P. Padture, Highly stable and efficient all-inorganic lead-free perovskite solar cells with native-oxide passivation, *Nat. Commun.*, 2019, **10**(1), 16, DOI: 10.1038/s41467-018-07951-y.

170 A. Kama, S. Tirosh, A. Itzhak, M. Ejgenberg and D. Cahen, New Pb-Free Stable Sn–Ge Solid Solution Halide Perovskites Fabricated by Spray Deposition, *ACS Appl. Energy Mater.*, 2022, **5**(3), 3638–3646, DOI: 10.1021/acsaem.1c04115.

171 H. Lv, X. Tang and M. Chen, Ionic Doping of $CsPbI_3$ Perovskite Nanocrystals Improves Luminescence and Stability in Patterned Large-Area Light-Emitting Diodes, *ACS Appl. Nano Mater.*, 2023, **6**(20), 18918–18925, DOI: 10.1021/acsanm.3c03358.

172 W. J. L. Buyers, D. E. Pepper and R. J. Elliott, Theory of spin waves in disordered antiferromagnets. I. Application to (Mn, Co)F_2 and K(Mn, Co)F_3, *J. Phys. C-Solid State Phys.*, 1972, **5**(18), 2611, DOI: 10.1088/0022-3719/5/18/011.

173 I. P. Dzyub, Cluster Theory of Spin Excitations of Mixed Antiferromagnets. Application to $Mn_cCo_{1-c}F_2$ and $KMn_cCo_{1-c}F_3$, *Phys. Status Solidi B*, 1974, **66**(1), 339–347, DOI: 10.1002/pssb.2220660138.

174 H. Komura, M. M. Shapiro and R. Stevenson, Exciton-magnon cross excitation in the mixed substitutional system $KMn_{1-x}Co_xF_3$, *Phys. Rev. B: Solid State*, 1974, **9**(8), 3266–3269, DOI: 10.1103/PhysRevB.9.3266.

175 A. R. Chakhmouradian, K. Ross, R. H. Mitchell and I. Swainson, The crystal chemistry of synthetic potassium-bearing neighborite, $(Na_{1-x}K_x)MgF_3$, *Phys. Chem. Miner.*, 2001, **28**(4), 277–284, DOI: 10.1007/s002690100151.

176 P. Chartrand and A. D. Pelton, Thermodynamic evaluation and optimization of the LiF-NaF-KF-MgF_2-CaF_2 system using the modified quasi-chemical model, *Metall. Mater. Trans. A*, 2001, **32**(6), 1385–1396, DOI: 10.1007/s11661-001-0228-1.

177 C. D. Martin, S. Chaudhur, C. P. Grey and J. B. Parise, Effect of A-site cation radius on ordering of BX_6 octahedra in (K,Na)MgF_3 perovskite, *Am. Mineral.*, 2005, **90**(10), 1522–1533, DOI: 10.2138/am.2005.1693.

178 Y. Zhao, Crystal Chemistry and Phase Transitions of Perovskite in P–T–X Space: Data for $(K_xNa_{1-x})MgF_3$ Perovskites, *J. Solid State Chem.*, 1998, **141**(1), 121–132, DOI: 10.1006/jssc.1998.7927.

179 R. E. Schmidt, M. Welsch, S. Kummer-Dörner and D. Babel, Einkristallstrukturuntersuchungen an hexagonalen Fluorperowskiten $AMIIF_3$ (MII = Mg, Mn, Fe, Co, Ni), *Z. Anorg. Allg. Chem.*, 1999, **625**(4), 637–642, DOI: 10.1002/(SICI)1521-3749(199904)625:4<637::AID-ZAAC637>3.0.CO;2-N.

180 X. Huang, J. Hu, C. Bi, J. Yuan, Y. Lu, M. Sui and J. Tian, B-site doping of $CsPbI_3$ quantum dot to stabilize the cubic structure for high-efficiency solar cells, *Chem. Eng. J.*, 2021, **421**, 127822, DOI: 10.1016/j.cej.2020.127822.

181 I. D. Skurlov, A. V. Sokolova, D. A. Tatarinov, P. S. Parfenov, D. A. Kurshanov, A. O. Ismagilov, A. V. Koroleva,

D. V. Danilov, E. V. Zhizhin, S. V. Mikushev, A. N. Tcypkin, A. V. Fedorov and A. P. Litvin, Engineering the Optical Properties of $CsPbBr_3$ Nanoplatelets through Cd^{2+} Doping, *Materials*, 2022, **15**(21), 7676, DOI: 10.3390/ma15217676.

182 I. D. Skurlov, W. Yin, A. O. Ismagilov, A. N. Tcypkin, H. Hua, H. Wang, X. Zhang, A. P. Litvin and W. Zheng, Improved One- and Multiple-Photon Excited Photoluminescence from Cd^{2+}-Doped $CsPbBr_3$ Perovskite NCs, *Nanomaterials*, 2022, **12**(1), 151, DOI: 10.3390/nano12010151.

183 M. Retuerto, Z. Yin, T. J. Emge, P. W. Stephens, M.-R. Li, T. Sarkar, M. C. Croft, A. Ignatov, Z. Yuan, S. J. Zhang, C. Jin, R. Paria Sena, J. Hadermann, G. Kotliar and M. Greenblatt, Hole Doping and Structural Transformation in $CsTl_{1-x}Hg_xCl_3$, *Inorg. Chem.*, 2015, **54**(3), 1066–1075, DOI: 10.1021/ic502400d.

184 C.-Q. Lin, M.-L. Liu, Z. Yang, H. Wang and C.-Y. Pan, Mn^{2+} doped $CsPbBr_3$ perovskite quantum dots with high quantum yield and stability for flexible array displays, *J. Solid State Chem.*, 2023, **327**, 124295, DOI: 10.1016/j.jssc.2023.124295.

185 Z. Yang, X. Yuan, Y. Song, M. Chen, K. Xing, S. Cao, J. Zheng and J. Zhao, Thickness-Dependent Photoluminescence Properties of Mn-Doped $CsPbBr_3$ Perovskite Nanoplatelets Synthesized at Room Temperature, *J. Phys. Chem. C*, 2023, **127**(43), 21227–21234, DOI: 10.1021/acs.jpcc.3c05639.

186 D. J. Lockwood, G. J. Coombs and R. A. Cowley, Light scattering from the mixed antiferromagnet $KNi_xMn_{1-x}F_3$, *J. Phys. C-Solid State Phys.*, 1979, **12**(21), 4611, DOI: 10.1088/0022-3719/12/21/025.

187 D. Skrzypek, Critical Behaviour of the Magnetic Resonance in $KNi_xMn_{1-x}F_3$, *Phys. Status Solidi B*, 1990, **157**(2), 695–700, DOI: 10.1002/pssb.2221570222.

188 D. Skrzypek, Antiferromagnetic resonance in $KNi_xMn_{1-x}F_3$ crystals, *Phys. B*, 1995, **205**(3), 279–284, DOI: 10.1016/0921-4526(94)00611-X.

189 A. Harrison, D. Visser, P. Day, W. Knop and M. Steiner, Magnetic ordering effects in the random singlet-magnetic ground state system $Rb_{(1-x)}Cs_xFeCl_3$, *J. Phys. C-Solid State Phys.*, 1986, **19**(34), 6811, DOI: 10.1088/0022-3719/19/34/018.

190 A. Ratuszna, The crystal structures of $(K_xNa_{1-x})MnF_3$ perovskite-type compounds, *Phase Transitions*, 1984, **4**(3), 217–223, DOI: 10.1080/01411598408218596.

191 A. Ratuszna, Determination of structure distortions in $KMnF_3$ doped with Na^+, *Z. Kristallogr.*, 1988, **185**, 521.

192 A. Ratuszna, P. Daniel, J. Kapusta and M. Rousseau, Experimental evidence for glasslike behavior in a $KMnF_3$: Na^+ crystal from x-ray diffraction and Raman scattering, *Phys. Rev. B: Condens. Matter Mater. Phys.*, 1998, **57**(17), 10470–10475, DOI: 10.1103/PhysRevB.57.10470.

193 W. E. Vehse, F. A. Sherrill and C. R. Riley, Lattice Constants for $KMg_{(1-x)}Mn_xF_3$ Crystals, *J. Appl. Phys.*, 1972, **43**(3), 1320–1321, DOI: 10.1063/1.1661275.

194 N. Elliott and L. Pauling, The Crystal Structure of Cesium Aurous Auric Chloride, $Cs_2AuAuCl_6$, and Cesium Argentous Auric Chloride, $Cs_2AgAuCl_6$, *J. Am. Chem. Soc.*, 1938, **60**(8), 1846–1851, DOI: 10.1021/ja01275a037.

195 P. Chartrand and A. D. Pelton, Thermodynamic Evaluation and Optimization of the LiCl–NaCl–KCl–RbCl–CsCl–$MgCl_2$–$CaCl_2$–$SrCl_2$–$BaCl_2$ System Using the Modified Quasichemical Model, *Can. Metall. Q.*, 2001, **40**(1), 13–32, DOI: 10.1179/cmq.2001.40.1.13.

196 J. Y. Buzare and P. Foucher, Disorder and phase transitions in $Rb_{1-x}K_xCaF_3$: an electron paramagnetic resonance investigation, *J. Phys.: Condens. Matter*, 1991, **3**(15), 2535, DOI: 10.1088/0953-8984/3/15/009.

197 J. W. Flocken, R. W. Smith, J. R. Hardy, E. S. Stevenson and J. Swearingen, Phase transitions in mixed alkali calcium trifluoride solid solutions, *Mater. Res. Bull.*, 1996, **31**(9), 1093–1099, DOI: 10.1016/0025-5408(96)00099-2.

198 A. Ratuszna, P. Daniel and M. Rousseau, Optical and X-ray evidence of structural phase transitions in mixed $(Rb_{1-x}K_x)CaF_3$ crystals, *Phase Transitions*, 1995, **54**(1), 43–59, DOI: 10.1080/01411599508200403.

199 M. Rousseau, P. Daniel, J. Toulouse and B. Hennion, Evidence of disorder in the perovskite crystals $RbCaF_3$ and $Rb_{0.65}K_{0.35}CaF_3$ investigation of phonon acoustic modes by inelastic neutron scattering, *Phys. B*, 1997, **234–236**, 139–141, DOI: 10.1016/S0921-4526(96)00928-3.

200 L. Shen, Z. Zhang, Y. Zhao, H. Yang, L. Yuan, Y. Chen, W. Xiang and X. Liang, Synthesis and optical properties of novel mixed-metal cation $CsPb_{1-x}Ti_xBr_3$-based perovskite glasses for W-LED, *J. Am. Ceram. Soc.*, 2020, **103**(1), 382–390, DOI: 10.1111/jace.16760.

201 Z. Wu, Q. Zhang, B. Li, Z. Shi, K. Xu, Y. Chen, Z. Ning and Q. Mi, Stabilizing the $CsSnCl_3$ Perovskite Lattice by B-Site Substitution for Enhanced Light Emission, *Chem. Mater.*, 2019, **31**(14), 4999–5004, DOI: 10.1021/acs.chemmater.9b00433.

202 T. Inami, T. Asano, Y. Ajiro and T. Goto, Magnetization process of the one-dimensional Ising-like antiferromagnet with nonmagnetic impurity, $CsCo_{1-x}Mg_xCl_3$, *Phys. B*, 1994, **201**, 204–207, DOI: 10.1016/0921-4526(94)91084-7.

203 H. Ohta, S. Imagawa, M. Motokawa and H. Ikeda, Electron Paramagnetic Resonance of $CsCo_xMg_{1-x}Cl_3$ and the Determination of Exchange Interactions, *J. Phys. Soc. Jpn.*, 1993, **62**(7), 2481–2489, DOI: 10.1143/JPSJ.62.2481.

204 E. Mei, Y. Chen, Y. Chen, Q. He, Y. Tong, P. Yu, X. Liang and W. Xiang, Ba-doped $CsPbBr_3$ with high quantum efficiency for wide color gamut on white light-emitting diodes, *Appl. Phys. Lett.*, 2021, **119**(25), 251103, DOI: 10.1063/5.0070326.

205 H. Liu, Z. Wu, J. Shao, D. Yao, H. Gao, Y. Liu, W. Yu, H. Zhang and B. Yang, $CsPb_xMn_{1-x}Cl_3$ Perovskite Quantum Dots with High Mn Substitution Ratio, *ACS Nano*, 2017, **11**(2), 2239–2247, DOI: 10.1021/acsnano.6b08747.

206 X. Zhang, F. Wang, Y. Wang, X. Wu, Q. Ou and S. Zhang, Boosting the Photoluminescence Quantum Yield and Stability of Lead-Free $CsEuCl_3$ Nanocrystals *via* Ni^{2+} Doping, *J. Phys. Chem. Lett.*, 2023, **14**(24), 5580–5585, DOI: 10.1021/acs.jpclett.3c01046.

207 Y. Hu, X. Zhang, C. Yang, J. Li and L. Wang, Fe^{2+} doped in $CsPbCl_3$ perovskite nanocrystals: impact on the luminescence and magnetic properties, *RSC Adv.*, 2019, **9**(57), 33017–33022, DOI: 10.1039/C9RA07069A.

208 G. Elbinger, A. Funke, P. Kleinert, P. Rosemann and W. Keilig, Präparation und Eigenschaften von Metallfluoridverbindungen des Typs $Me^{I}Me^{II}F_3$, *Z. Anorg. Allg. Chem.*, 1972, **393**(3), 193–206, DOI: 10.1002/zaac.19723930302.

209 W. Shi, X. Zhang, H. S. Chen, K. Matras-Postolek and P. Yang, Transition metal halide derived phase transition from Cs_4PbCl_6 to $CsPb_xM_{1-x}X_3$ for bright white light-emitting diodes, *J. Mater. Chem. C*, 2021, **9**(17), 5732–5739, DOI: 10.1039/D1TC01150B.

210 R. B. Rogge, Y. S. Yang, Z. Tun, B. D. Gaulin, J. A. Fernandez-Baca, R. M. Nicklow and A. Harrison, A neutron scattering study of the quasi-one-dimensional, dilute Ising-like antiferromagnet $CsCo_{0.83}Mg_{0.17}Br_3$, *J. Appl. Phys.*, 1993, **73**(10), 6451–6453, DOI: 10.1063/1.352630.

211 J. van Duijn, B. D. Gaulin, M. A. Lumsden, J. P. Castellan and W. J. L. Buyers, Random Fields and the Partially Paramagnetic State of $CsCo_{0.83}Mg_{0.17}Br_3$: Critical Scattering Study, *Phys. Rev. Lett.*, 2004, **92**(7), 077202, DOI: 10.1103/PhysRevLett.92.077202.

212 Y. S. Yang, F. Marsiglio, M. Madsen, B. D. Gaulin, R. B. Rogge and J. A. Fernandez-Baca, Spin-wave response in the dilute quasi-one-dimensional Ising-like antiferromagnet $CsCo_{0.83}Mg_{0.17}Br_3$, *Phys. Rev. B: Condens. Matter Mater. Phys.*, 2002, **65**(21), 212408, DOI: 10.1103/PhysRevB.65.212408.

213 J.-S. Yao, J. Ge, B.-N. Han, K.-H. Wang, H.-B. Yao, H.-L. Yu, J.-H. Li, B.-S. Zhu, J.-Z. Song, C. Chen, Q. Zhang, H.-B. Zeng, Y. Luo and S.-H. Yu, Ce^{3+}-Doping to Modulate Photoluminescence Kinetics for Efficient $CsPbBr_3$ Nanocrystals Based Light-Emitting Diodes, *J. Am. Chem. Soc.*, 2018, **140**(10), 3626–3634, DOI: 10.1021/jacs.7b11955.

214 R. Chen, Y. Xu, S. Wang, C. Xia, Y. Liu, B. Yu, T. Xuan and H. Li, Zinc ions doped cesium lead bromide perovskite nanocrystals with enhanced efficiency and stability for white light-emitting diodes, *J. Alloys Compd.*, 2021, **866**, 158969, DOI: 10.1016/j.jallcom.2021.158969.

215 K. Cui, Y. Wen, X. Han, Z. Hao, J. Zhang and J. Xie, Intense blue emission from one-pot synthesized quaternary $CsZn_xPb_{1-x}Br_3$ perovskite quantum dots, *Opt. Mater.*, 2023, **136**, 113441, DOI: 10.1016/j.optmat.2023.113441.

216 P.-N. Tran, H.-H. Phan, T.-N. Luu, Q.-H. Tran and T.-T. Duong, Optimizing the single-source flash thermal evaporation process of Zn-doped $CsPbBr_3$ films for enhanced performance in perovskite LEDs, *Appl. Phys. A: Mater. Sci. Process.*, 2023, **130**(1), 20, DOI: 10.1007/s00339-023-07179-8.

217 X. Shen, Y. Zhang, S. V. Kershaw, T. Li, C. Wang, X. Zhang, W. Wang, D. Li, Y. Wang, M. Lu, L. Zhang, C. Sun, D. Zhao, G. Qin, X. Bai, W. W. Yu and A. L. Rogach, Zn-Alloyed $CsPbI_3$ Nanocrystals for Highly Efficient Perovskite Light-Emitting Devices, *Nano Lett.*, 2019, **19**(3), 1552–1559, DOI: 10.1021/acs.nanolett.8b04339.

218 Y. Wu, Q. Li, B. C. Chakoumakos, M. Zhuravleva, A. C. Lindsey, J. A. Johnson II, L. Stand, M. Koschan and C. L. Melcher, Quaternary Iodide $K(Ca,Sr)I_3:Eu^{2+}$ Single-Crystal Scintillators for Radiation Detection: Crystal Structure, Electronic Structure, and Optical and Scintillation Properties, *Adv. Opt. Mater.*, 2016, **4**(10), 1518–1532, DOI: 10.1002/adom.201600239.

219 Y. Wu, M. Zhuravleva, A. C. Lindsey, M. Koschan and C. L. Melcher, Eu^{2+} concentration effects in $KCa_{0.8}Sr_{0.2}I_3:Eu^{2+}$: A novel high-performance scintillator, *Nucl. Instrum. Methods Phys. Res., Sect. A*, 2016, **820**, 132–140, DOI: 10.1016/j.nima.2016.03.027.

220 M. Saliba, T. Matsui, K. Domanski, J.-Y. Seo, A. Ummadisingu, S. M. Zakeeruddin, J.-P. Correa-Baena, W. R. Tress, A. Abate, A. Hagfeldt and M. Grätzel, Incorporation of rubidium cations into perovskite solar cells improves photovoltaic performance, *Science*, 2016, **354**(6309), 206–209, DOI: 10.1126/science.aah5557.

221 M. Saliba, T. Matsui, J.-Y. Seo, K. Domanski, J.-P. Correa-Baena, M. K. Nazeeruddin, S. M. Zakeeruddin, W. Tress, A. Abate, A. Hagfeldt and M. Grätzel, Cesium-containing triple cation perovskite solar cells: improved stability, reproducibility and high efficiency, *Energy Environ. Sci.*, 2016, **9**(6), 1989–1997, DOI: 10.1039/C5EE03874J.

222 S. P. Senanayak, M. Abdi-Jalebi, V. S. Kamboj, R. Carey, R. Shivanna, T. Tian, G. Schweicher, J. Wang, N. Giesbrecht, D. Di Nuzzo, H. E. Beere, P. Docampo, D. A. Ritchie, D. Fairen-Jimenez, R. H. Friend and H. Sirringhaus, A general approach for hysteresis-free, operationally stable metal halide perovskite field-effect transistors, *Sci. Adv.*, 2020, **6**(15), eaaz4948, DOI: 10.1126/sciadv.aaz4948.

223 S.-Y. Kim, H.-C. Lee, Y. Nam, Y. Yun, S.-H. Lee, D. H. Kim, J. H. Noh, J.-H. Lee, D.-H. Kim, S. Lee and Y.-W. Heo, Ternary diagrams of the phase, optical bandgap energy and photoluminescence of mixed-halide perovskites, *Acta Mater.*, 2019, **181**, 460–469, DOI: 10.1016/j.actamat.2019.10.008.

224 F. Meng, X. Liu, X. Cai, Z. Gong, B. Li, W. Xie, M. Li, D. Chen, H.-L. Yip and S.-J. Su, Incorporation of rubidium cations into blue perovskite quantum dot light-emitting diodes *via* FABr-modified multi-cation hot-injection method, *Nanoscale*, 2019, **11**(3), 1295–1303, DOI: 10.1039/C8NR07907B.

225 R. K. Gunasekaran, J. Jung, S. W. Yang, J. Yun, Y. Yun, D. Vidyasagar, W. C. Choi, C.-L. Lee, J. H. Noh, D. H. Kim and S. Lee, High-throughput compositional mapping of triple-cation tin–lead perovskites for high-efficiency solar cells, *InfoMat*, 2023, **5**(4), e12393, DOI: 10.1002/inf2.12393.

226 C. Otero-Martínez, M. Imran, N. J. Schrenker, J. Ye, K. Ji, A. Rao, S. D. Stranks, R. L. Z. Hoye, S. Bals, L. Manna, J. Pérez-Juste and L. Polavarapu, Fast A-Site Cation Cross-Exchange at Room Temperature: Single-to Double- and Triple-Cation Halide Perovskite Nanocrystals, *Angew. Chem., Int. Ed.*, 2022, **61**(34), e202205617, DOI: 10.1002/anie.202205617.

227 A. F. Palmstrom, G. E. Eperon, T. Leijtens, R. Prasanna, S. N. Habisreutinger, W. Nemeth, E. A. Gaulding, S. P. Dunfield, M. Reese, S. Nanayakkara, T. Moot,

J. Werner, J. Liu, B. To, S. T. Christensen, M. D. McGehee, M. F. A. M. van Hest, J. M. Luther, J. J. Berry and D. T. Moore, Enabling Flexible All-Perovskite Tandem Solar Cells, *Joule*, 2019, **3**(9), 2193–2204, DOI: **10.1016/j.joule.2019.05.009**.

228 L. Gao, Y. Zhang, L. Gou, Q. Wang, M. Wang, W. Zheng, Y. Wang, H.-L. Yip and J. Zhang, High efficiency pure blue perovskite quantum dot light-emitting diodes based on formamidinium manipulating carrier dynamics and electron state filling, *Light: Sci. Appl.*, 2022, **11**(1), 346, DOI: **10.1038/s41377-022-00992-5**.

229 T. Nakamura, K. Otsuka, S. Hu, R. Hashimoto, T. Morishita, T. Handa, T. Yamada, M. A. Truong, R. Murdey, Y. Kanemitsu and A. Wakamiya, Composition–Property Mapping in Bromide-Containing Tin Perovskite Using High-Purity Starting Materials, *ACS Appl. Energy Mater.*, 2022, **5**(12), 14789–14798, DOI: **10.1021/acsaem.2c02144**.

230 T. Jesper Jacobsson, J.-P. Correa-Baena, M. Pazoki, M. Saliba, K. Schenk, M. Grätzel and A. Hagfeldt, Exploration of the compositional space for mixed lead halogen perovskites for high efficiency solar cells, *Energy Environ. Sci.*, 2016, **9**(5), 1706–1724, DOI: **10.1039/C6EE00030D**.

231 I. Susic, A. Kama, L. Gil-Escrig, C. Dreessen, F. Palazon, D. Cahen, M. Sessolo and H. J. Bolink, Combinatorial Vacuum-Deposition of Wide Bandgap Perovskite Films and Solar Cells, *Adv. Mater. Interfaces*, 2023, **10**(4), 2202271, DOI: **10.1002/admi.202202271**.

232 H. Xiao, H. Xiong, P. Li, L. Jiang, A. Yang, L. Lin, Z. Kang, Q. Yan and Y. Qiu, Tunable deep-blue luminescence from ball-milled chlorine-rich $Cs_x(NH_4)_{1-x}PbCl_2Br$ nanocrystals by ammonium modulation, *Chem. Commun.*, 2022, **58**(23), 3827–3830, DOI: **10.1039/D1CC07125D**.

233 C. Wang, Y. Liu, X. Feng, C. Zhou, Y. Liu, X. Yu and G. Zhao, Phase Regulation Strategy of Perovskite Nanocrystals from 1D Orthomorphic NH_4PbI_3 to 3D Cubic $(NH_4)_{0.5}Cs_{0.5}Pb(I_{0.5}Br_{0.5})_3$ Phase Enhances Photoluminescence, *Angew. Chem., Int. Ed.*, 2019, **58**(34), 11642–11646, DOI: **10.1002/anie.201903121**.

234 S. Terada, T. Oku, A. Suzuki, M. Okita, S. Fukunishi, T. Tachikawa and T. Hasegawa, Ethylammonium Bromide- and Potassium-Added $CH_3NH_3PbI_3$ Perovskite Solar Cells, *Photonics*, 2022, **9**(11), 791, DOI: **10.3390/photonics9110791**.

235 S. L. Sanchez, E. Foadian, M. Ziatdinov, J. Yang, S. V. Kalinin, Y. Liu and M. Ahmadi, Physics-driven discovery and bandgap engineering of hybrid perovskites, *arXiv*, 2023, preprint, arXiv:2310.06583, DOI: **10.48550/arXiv.2310.06583**.

236 A. Gabriel Tomulescu, L. Nicoleta Leonat, F. Neatu, V. Stancu, V. Toma, S. Derbali, S. Neatu, A. Mihai Rostas, C. Besleaga, R. Pătru, I. Pintilie and M. Florea, Enhancing stability of hybrid perovskite solar cells by imidazolium incorporation, *Sol. Energy Mater. Sol. Cells*, 2021, **227**, 111096, DOI: **10.1016/j.solmat.2021.111096**.

237 R. K. Singh, P. Sharma, C.-H. Lu, R. Kumar, N. Jain and J. Singh, Structural, morphological and thermodynamic parameters investigation of tunable $MAPb_{1-x}Cd_xBr_{3-2x}I_{2x}$ hybrid perovskite, *J. Alloys Compd.*, 2021, **866**, 158936, DOI: **10.1016/j.jallcom.2021.158936**.

238 R. K. Singh, P. Sharma, R. Kumar, S. Som, S. Dutta, N. Jain, R. Chaurasiya, M. L. Meena, J.-S. Ho, S.-W. Dai, J. Singh, C.-H. Lu and H.-W. Lin, $CH_3NH_3Pb_{1-x}Co_xBr_{3-2x}Cl_{2x}$ Perovskite Quantum Dots for Wide-Color Backlighting, *ACS Appl. Nano Mater.*, 2021, **4**(1), 717–728, DOI: **10.1021/acsanm.0c03019**.

239 J. Xun, J. Deng, W. Shen, M. Li and R. He, Highly efficient green-emitting nanocrystals of $MAPb_{1-x}Mn_xBr_3$ perovskite with excellent thermal stability, *Opt. Mater.*, 2021, **122**, 111799, DOI: **10.1016/j.optmat.2021.111799**.

240 C. Lu, J. Zhou, C. Tang, Q. Dai, Y. Peng, W. Lv, L. Sun, S. Xu and W. Hu, Ultranarrow-band filterless photodetectors based on $CH_3NH_3PbCl_xBr_{3-x}$ mixed-halide perovskite single crystals, *Nanotechnology*, 2023, **34**(34), 345705, DOI: **10.1088/1361-6528/acd944**.

241 M. Mazurin, A. Shelestova, D. Tsvetkov, V. Sereda, I. Ivanov, D. Malyshkin and A. Zuev, Thermochemical Study of $CH_3NH_3Pb(Cl_{1-x}Br_x)_3$ Solid Solutions, *Materials*, 2022, **15**(21), 7675, DOI: **10.3390/ma15217675**.

242 Y. Pan, X. Wang, Y. Xu, S. Chai, J. Wu, Z. Zhao, Q. Li, J. Wu, J. Chen, Z. Zhu, B. S. Bae, O. E. Fayemi, J. Zhou, Y. Zhu and W. Lei, Epitaxy growth of $MAPbBr_xCl_{3-x}$ single-crystalline perovskite films toward spectral selective detection in both broadband and narrowband ranges, *J. Mater. Chem. C*, 2023, **11**(40), 13763–13773, DOI: **10.1039/D3TC02300A**.

243 A. Rajagopal, R. J. Stoddard, H. W. Hillhouse and A. K. Y. Jen, On understanding bandgap bowing and optoelectronic quality in Pb–Sn alloy hybrid perovskites, *J. Mater. Chem. A*, 2019, **7**(27), 16285–16293, DOI: **10.1039/C9TA05308E**.

244 F.-X. Liang, L.-L. Zhou, Y. Hu, S.-F. Li, Z.-Y. Zhang, J.-Y. Li, C. Fu, C.-Y. Wu, L. Wang, J.-A. Huang and L.-B. Luo, Self-Driven Narrow-Band Photodetector based on $FAPbBr_{2.5}I_{0.5}$ Single Crystal for Yellow Light Intensity Meter Application, *Adv. Funct. Mater.*, 2023, **33**(36), 2302175, DOI: **10.1002/adfm.202302175**.

245 J. H. Noh, S. H. Im, J. H. Heo, T. N. Mandal and S. I. Seok, Chemical Management for Colorful, Efficient, and Stable Inorganic–Organic Hybrid Nanostructured Solar Cells, *Nano Lett.*, 2013, **13**(4), 1764–1769, DOI: **10.1021/nl400349b**.

246 S. Hu, K. Otsuka, R. Murdey, T. Nakamura, M. A. Truong, T. Yamada, T. Handa, K. Matsuda, K. Nakano, A. Sato, K. Marumoto, K. Tajima, Y. Kanemitsu and A. Wakamiya, Optimized carrier extraction at interfaces for 23.6% efficient tin–lead perovskite solar cells, *Energy Environ. Sci.*, 2022, **15**(5), 2096–2107, DOI: **10.1039/D2EE00288D**.

247 S.-H. Turren-Cruz, J. Pascual, S. Hu, J. Sanchez-Diaz, S. Galve-Lahoz, W. Liu, W. Hempel, V. S. Chirvony, J. P. Martinez-Pastor, P. P. Boix, A. Wakamiya and I. Mora-Seró, Multicomponent Approach for Stable Methylammonium-Free Tin–Lead Perovskite Solar Cells, *ACS Energy Lett.*, 2024, **9**(2), 432–441, DOI: **10.1021/acsenergylett.3c02426**.

248 H. Zhang, Z. Bi, Z. Zhai, H. Gao, Y. Liu, M. Jin, M. Ye, X. Li, H. Liu, Y. Zhang, X. Li, H. Tan, Y. Xu and L. Yang, Revealing Unusual Bandgap Shifts with Temperature and Bandgap Renormalization Effect in Phase-Stabilized Metal Halide Perovskite Thin Films, *Adv. Funct. Mater.*, 2024, **34**(9), 2302214, DOI: **10.1002/adfm.202302214**.

249 R. Prasanna, A. Gold-Parker, T. Leijtens, B. Conings, A. Babayigit, H.-G. Boyen, M. F. Toney and M. D. McGehee, Band Gap Tuning *via* Lattice Contraction and Octahedral Tilting in Perovskite Materials for Photovoltaics, *J. Am. Chem. Soc.*, 2017, **139**(32), 11117–11124, DOI: **10.1021/jacs.7b04981**.

250 J. Wang, M. A. Uddin, B. Chen, X. Ying, Z. Ni, Y. Zhou, M. Li, M. Wang, Z. Yu and J. Huang, Enhancing Photostability of Sn-Pb Perovskite Solar Cells by an Alkylammonium Pseudo-Halogen Additive, *Adv. Energy Mater.*, 2023, **13**(15), 2204115, DOI: **10.1002/aenm.202204115**.

251 J. Guo, Y. Fu, W. Zheng, M. Xie, Y. Huang, Z. Miao, C. Han, W. Yin, J. Zhang, X. Yang, J. Tian and X. Zhang, Entropy-Driven Strongly Confined Low-Toxicity Pure-Red Perovskite Quantum Dots for Spectrally Stable Light-Emitting Diodes, *Nano Lett.*, 2024, **24**(1), 417–423, DOI: **10.1021/acs.nanolett.3c04214**.

252 K.-C. Hsiao, C.-M. Ho, T.-H. Lin, S.-H. Chen, Y.-H. Chang, Y.-H. Liao, J.-M. Chang, T.-F. Lin, Y.-C. Huang, K.-M. Lee and M.-C. Wu, Ceiling of Barium Substitution for B-Site Cation in Organometal Halide Perovskite Solar Cells, *Int. J. Energy Res.*, 2024, **2024**, 9990559, DOI: **10.1155/2024/9990559**.

253 I. Susic, L. Gil-Escrig, K. P. S. Zanoni, C. Roldán-Carmona, M. Sessolo and H. J. Bolink, Pure Iodide Multication Wide Bandgap Perovskites by Vacuum Deposition, *ACS Mater. Lett.*, 2023, **5**(12), 3299–3305, DOI: **10.1021/acsmaterialslett.3c01094**.

254 S. Derbali, K. Nouneh, M. Florea, L. N. Leonat, V. Stancu, A. G. Tomulescu, A. C. Galca, M. Secu, L. Pintilie and M. E. Touhami, Potassium-containing triple-cation mixed-halide perovskite materials: Toward efficient and stable solar cells, *J. Alloys Compd.*, 2021, **858**, 158335, DOI: **10.1016/j.jallcom.2020.158335**.

255 I. Ono, T. Oku, A. Suzuki, S. Fukunishi, T. Tachikawa and T. Hasegawa, Effects of ethylammonium and rubidium addition to guanidinium-based $CH_3NH_3PbI_3$ perovskite photovoltaic devices prepared at 190 °C in ambient air, *Mater. Today Commun.*, 2024, **38**, 107623, DOI: **10.1016/j.mtcomm.2023.107623**.

256 F. B. Minussi, L. A. Silva and E. B. Araújo, Structure, optoelectronic properties and thermal stability of the triple organic cation $GA_xFA_xMA_{1-2x}PbI_3$ system prepared by mechanochemical synthesis, *Phys. Chem. Chem. Phys.*, 2022, **24**(8), 4715–4728, DOI: **10.1039/D1CP04977A**.

257 F. B. Minussi, R. M. Silva Jr. and E. B. Araújo, Composition-Property Relations for $GA_xFA_yMA_{1-x-y}PbI_3$ Perovskites, *Small*, 2024, **20**(7), 2305054, DOI: **10.1002/smll.202305054**.

258 S. Wang, S. Pang, D. Chen, W. Zhu, H. Xi and C. Zhang, Improving perovskite solar cell performance by compositional engineering *via* triple-mixed cations, *Sol. Energy*, 2021, **220**, 412–417, DOI: **10.1016/j.solener.2021.03.036**.

259 M. Badrooj, F. Jamali-Sheini and N. Torabi, Zn-doped Pb/Sn hybrid perovskite solar cells: Towards high photovoltaic performance, *Sol. Energy*, 2022, **236**, 63–74, DOI: **10.1016/j.solener.2022.02.034**.

260 T. Soto-Montero, S. Kralj, W. Soltanpoor, J. S. Solomon, J. S. Gómez, K. P. S. Zanoni, A. Paliwal, H. J. Bolink, C. Baeumer, A. P. M. Kentgens and M. Morales-Masis, Single-Source Vapor-Deposition of $MA_{1-x}FA_xPbI_3$ Perovskite Absorbers for Solar Cells, *Adv. Funct. Mater.*, 2023, 2300588, DOI: **10.1002/adfm.202300588**.

261 O. J. Weber, B. Charles and M. T. Weller, Phase behaviour and composition in the formamidinium–methylammonium hybrid lead iodide perovskite solid solution, *J. Mater. Chem. A*, 2016, **4**(40), 15375–15382, DOI: **10.1039/C6TA06607K**.

262 C. Zhao, C. Cazorla, X. Zhang, H. Huang, X. Zhao, D. Li, J. Shi, Q. Zhao, W. Ma and J. Yuan, Fast Organic Cation Exchange in Colloidal Perovskite Quantum Dots toward Functional Optoelectronic Applications, *J. Am. Chem. Soc.*, 2024, **146**(7), 4913–4921, DOI: **10.1021/jacs.3c14000**.

263 D. Ju, Y. Dang, Z. Zhu, H. Liu, C.-C. Chueh, X. Li, L. Wang, X. Hu, A. K. Y. Jen and X. Tao, Tunable Band Gap and Long Carrier Recombination Lifetime of Stable Mixed $CH_3NH_3Pb_xSn_{1-x}Br_3$ Single Crystals, *Chem. Mater.*, 2018, **30**(5), 1556–1565, DOI: **10.1021/acs.chemmater.7b04565**.

264 S. Kahmann, Z. Chen, O. Hordiichuk, O. Nazarenko, S. Shao, M. V. Kovalenko, G. R. Blake, S. Tao and M. A. Loi, Compositional Variation in $FAPb_{1-x}Sn_xI_3$ and Its Impact on the Electronic Structure: A Combined Density Functional Theory and Experimental Study, *ACS Appl. Mater. Interfaces*, 2022, **14**(30), 34253–34261, DOI: **10.1021/acsami.2c00889**.

265 X. Lü, C. Stoumpos, Q. Hu, X. Ma, D. Zhang, S. Guo, J. Hoffman, K. Bu, X. Guo, Y. Wang, C. Ji, H. Chen, H. Xu, Q. Jia, W. Yang, M. G. Kanatzidis and H.-K. Mao, Regulating off-centering distortion maximizes photoluminescence in halide perovskites, *Natl. Sci. Rev.*, 2020, **8**(9), nwaa288, DOI: **10.1093/nsr/nwaa288**.

266 S. S. H. Dintakurti, D. Walker, T. A. Bird, Y. Fang, T. White and J. V. Hanna, A powder XRD, solid state NMR and calorimetric study of the phase evolution in mechanochemically synthesized dual cation $(Cs_x(CH_3NH_3)_{1-x})PbX_3$ lead halide perovskite systems, *Phys. Chem. Chem. Phys.*, 2022, **24**(30), 18004–18021, DOI: **10.1039/D2CP02131E**.

267 M. Chen, Q. Dong, C. Xiao, X. Zheng, Z. Dai, Y. Shi, J. M. Luther and N. P. Padture, Lead-Free Flexible Perovskite Solar Cells with Interfacial Native Oxide Have >10% Efficiency and Simultaneously Enhanced Stability and Reliability, *ACS Energy Lett.*, 2022, **7**(7), 2256–2264, DOI: **10.1021/acsenergylett.2c01130**.

268 F. Hao, C. C. Stoumpos, R. P. H. Chang and M. G. Kanatzidis, Anomalous Band Gap Behavior in Mixed Sn and Pb Perovskites Enables Broadening of Absorption

Spectrum in Solar Cells, *J. Am. Chem. Soc.*, 2014, **136**(22), 8094–8099, DOI: 10.1021/ja5033259.

269 J. Im, C. C. Stoumpos, H. Jin, A. J. Freeman and M. G. Kanatzidis, Antagonism between Spin–Orbit Coupling and Steric Effects Causes Anomalous Band Gap Evolution in the Perovskite Photovoltaic Materials $CH_3NH_3Sn_{1-x}Pb_xI_3$, *J. Phys. Chem. Lett.*, 2015, **6**(17), 3503–3509, DOI: 10.1021/acs.jpclett.5b01738.

270 Y. Chu, C. Wang, L. Ma, X. Feng, B. Wang, Y. Wu, Y. Jia, M. Zhang, Y. Sun, H. Zhang and G. Zhao, Unveiling the photoluminescence regulation of colloidal perovskite quantum dots *via* defect passivation and lattice distortion by potassium cations doping: Not the more the better, *J. Colloid Interface Sci.*, 2021, **596**, 199–205, DOI: 10.1016/j.jcis.2021.03.128.

271 A. Ali, H. Park, R. Mall, B. Aïssa, S. Sanvito, H. Bensmail, A. Belaidi and F. El-Mellouhi, Machine Learning Accelerated Recovery of the Cubic Structure in Mixed-Cation Perovskite Thin Films, *Chem. Mater.*, 2020, **32**(7), 2998–3006, DOI: 10.1021/acs.chemmater.9b05342.

272 D. Jia, J. Chen, R. Zhuang, Y. Hua and X. Zhang, Antisolvent-Assisted *In Situ* Cation Exchange of Perovskite Quantum Dots for Efficient Solar Cells, *Adv. Mater.*, 2023, **35**(21), 2212160, DOI: 10.1002/adma.202212160.

273 F.-C. Liang, F.-C. Jhuang, Y.-H. Fang, J.-S. Benas, W.-C. Chen, Z.-L. Yan, W.-C. Lin, C.-J. Su, Y. Sato, T. Chiba, J. Kido and C.-C. Kuo, Synergistic Effect of Cation Composition Engineering of Hybrid $Cs_{1-x}FA_xPbBr_3$ Nanocrystals for Self-Healing Electronics Application, *Adv. Mater.*, 2023, **35**(9), 2207617, DOI: 10.1002/adma.202207617.

274 A. Pisanu, *Chemical tuning of hybrid perovskites for solar-driven clean energy technologies*, PhD Thesis, Universita' di Pavia, 2020.

275 S. Nagane, D. Ghosh, R. L. Z. Hoye, B. Zhao, S. Ahmad, A. B. Walker, M. S. Islam, S. Ogale and A. Sadhanala, Lead-Free Perovskite Semiconductors Based on Germanium–Tin Solid Solutions: Structural and Optoelectronic Properties, *J. Phys. Chem. C*, 2018, **122**(11), 5940–5947, DOI: 10.1021/acs.jpcc.8b00480.

276 Y. Liu, Y.-P. Gong, S. Geng, M.-L. Feng, D. Manidaki, Z. Deng, C. C. Stoumpos, P. Canepa, Z. Xiao, W.-X. Zhang and L. Mao, Hybrid Germanium Bromide Perovskites with Tunable Second Harmonic Generation, *Angew. Chem., Int. Ed.*, 2022, **61**(43), e202208875, DOI: 10.1002/anie.202208875.

277 J. Liu, H. Fu, Z. Du, D. Ou, S. Li, Q. Chen, W. Yang, J. Zhao and J. Zheng, Enhanced photothermal stability of *in situ* grown $FAPbBr_3$ nanocrystals in polyvinylidene fluoride by incorporation of Cd^{2+} ions, *J. Mater. Chem. C*, 2022, **10**(46), 17512–17520, DOI: 10.1039/D2TC04100F.

278 T. Oku, S. Uchiya, R. Okumura, A. Suzuki, I. Ono, S. Fukunishi, T. Tachikawa and T. Hasegawa, Effects of Co-Addition of Guanidinium and Cesium to $CH_3NH_3PbI_3$ Perovskite Solar Cells, *Inorganics*, 2023, **11**(7), 273, DOI: 10.3390/inorganics11070273.

279 J. Deng, J. Xun, Y. Qin, M. Li and R. He, Blue-emitting NH_4^+-doped $MAPbBr_3$ perovskite quantum dots with near unity quantum yield and super stability, *Chem. Commun.*, 2020, **56**(79), 11863–11866, DOI: 10.1039/D0CC04912C.

280 C.-H. Lu, R. K. Singh, T.-Y. Chen, S. Som, R. Kumar, S. A. Lu and M. L. Meena, Rapid synthesis and theoretical analysis of $CH_3NH_3Pb_{1-x}Cd_xBr_3$ perovskite quantum dots for backlight LEDs: A step towards enhanced stability, *Org. Electron.*, 2022, **102**, 106444, DOI: 10.1016/j.orgel.2022.106444.

281 M. T. Klug, A. Osherov, A. A. Haghighirad, S. D. Stranks, P. R. Brown, S. Bai, J. T. W. Wang, X. Dang, V. Bulović, H. J. Snaith and A. M. Belcher, Tailoring metal halide perovskites through metal substitution: influence on photovoltaic and material properties, *Energy Environ. Sci.*, 2017, **10**(1), 236–246, DOI: 10.1039/C6EE03201J.

282 J. Yu, H. Xu, L. Wu, Q. Han and W. Wu, Highly sensitive photodetector of Zn/Bi doped $MAPbBr_3$ single crystals formed homojunction, *Mater. Sci. Semicond. Process.*, 2022, **149**, 106824, DOI: 10.1016/j.mssp.2022.106824.

283 Z. Zhou, J. Xu, Y. Liu, C. Wei, H. Zhang and Q. Wang, Zn-alloyed $MAPbBr_3$ crystals with improved thermoelectric and photocatalytic properties, *Mater. Chem. Front.*, 2021, **5**(24), 8319–8332, DOI: 10.1039/D1QM00993A.

284 A. E. Abd El-Samad, N. Gad, M. El-Aasser, M. M. Rashad and A. Mourtada Elseman, Optoelectronic investigation and simulation study of zinc and cobalt doped lead halide perovskite nanocrystals, *Sol. Energy*, 2022, **247**, 553–563, DOI: 10.1016/j.solener.2022.10.061.

285 S. L. Roscoe and H. M. Haendler, Synthesis of fluorometallates in methanol. The solid solution NH_4MnF_3–NH_4ZnF_3, *Inorg. Chim. Acta*, 1967, **1**, 73–75, DOI: 10.1016/S0020-1693(00)93142-6.

286 B. Jiang, Y. Yu, H. Chen, J. Cui, X. Liu, L. Xie and J. He, Entropy engineering promotes thermoelectric performance in p-type chalcogenides, *Nat. Commun.*, 2021, **12**(1), 3234, DOI: 10.1038/s41467-021-23569-z.

287 A. Gold-Parker, P. M. Gehring, J. M. Skelton, I. C. Smith, D. Parshall, J. M. Frost, H. I. Karunadasa, A. Walsh and M. F. Toney, Acoustic phonon lifetimes limit thermal transport in methylammonium lead iodide, *Proc. Natl. Acad. Sci. U. S. A.*, 2018, **115**(47), 11905–11910, DOI: 10.1073/pnas.1812227115.

288 J. M. Frost and A. Walsh, What Is Moving in Hybrid Halide Perovskite Solar Cells?, *Acc. Chem. Res.*, 2016, **49**(3), 528–535, DOI: 10.1021/acs.accounts.5b00431.

289 C. Katan, A. D. Mohite and J. Even, Entropy in halide perovskites, *Nat. Mater.*, 2018, **17**(5), 377–379, DOI: 10.1038/s41563-018-0070-0.

290 S. A. Cuthriell, S. Panuganti, C. C. Laing, M. A. Quintero, B. Guzelturk, N. Yazdani, B. Traore, A. Brumberg, C. D. Malliakas, A. M. Lindenberg, V. Wood, C. Katan, J. Even, X. Zhang, M. G. Kanatzidis and R. D. Schaller, Nonequilibrium Lattice Dynamics in Photoexcited 2D Perovskites, *Adv. Mater.*, 2022, **34**(44), 2202709, DOI: 10.1002/adma.202202709.

291 H. Seiler, D. Zahn, V. C. A. Taylor, M. I. Bodnarchnuk, Y. W. Windsor, M. V. Kovalenko and R. Ernstorfer, Direct observation of ultrafast lattice distortions during exciton-polaron formation in lead-halide perovskite nanocrystals,

arXiv, 2022, preprint, arXiv:2209.05931, DOI: 10.48550/arXiv.2209.05931.

292 R. Nie, R. R. Sumukam, S. H. Reddy, M. Banavoth and S. I. Seok, Lead-free perovskite solar cells enabled by hetero-valent substitutes, *Energy Environ. Sci.*, 2020, **13**(8), 2363–2385, DOI: 10.1039/D0EE01153C.

293 J. Endres, D. A. Egger, M. Kulbak, R. A. Kerner, L. Zhao, S. H. Silver, G. Hodes, B. P. Rand, D. Cahen, L. Kronik and A. Kahn, Valence and Conduction Band Densities of States of Metal Halide Perovskites: A Combined Experimental–Theoretical Study, *J. Phys. Chem. Lett.*, 2016, **7**(14), 2722–2729, DOI: 10.1021/acs.jpclett.6b00946.

294 X. Liu, D. Luo, Z.-H. Lu, J. S. Yun, M. Saliba, S. I. Seok and W. Zhang, Stabilization of photoactive phases for perovskite photovoltaics, *Nat. Rev. Chem.*, 2023, **7**(7), 462–479, DOI: 10.1038/s41570-023-00492-z.

295 S. P. Dunfield, L. Bliss, F. Zhang, J. M. Luther, K. Zhu, M. F. A. M. van Hest, M. O. Reese and J. J. Berry, From Defects to Degradation: A Mechanistic Understanding of Degradation in Perovskite Solar Cell Devices and Modules, *Adv. Energy Mater.*, 2020, **10**(26), 1904054, DOI: 10.1002/aenm.201904054.

296 W. A. Saidi, W. Shadid and I. E. Castelli, Machine-learning structural and electronic properties of metal halide perovskites using a hierarchical convolutional neural network, *npj Comput. Mater.*, 2020, **6**(1), 36, DOI: 10.1038/s41524-020-0307-8.

297 C. Yi, J. Luo, S. Meloni, A. Boziki, N. Ashari-Astani, C. Grätzel, S. M. Zakeeruddin, U. Röthlisberger and M. Grätzel, Entropic stabilization of mixed A-cation ABX_3 metal halide perovskites for high performance perovskite solar cells, *Energy Environ. Sci.*, 2016, **9**(2), 656–662, DOI: 10.1039/C5EE03255E.

298 Y.-H. Kim, S. Kim, A. Kakekhani, J. Park, J. Park, Y.-H. Lee, H. Xu, S. Nagane, R. B. Wexler, D.-H. Kim, S. H. Jo, L. Martínez-Sarti, P. Tan, A. Sadhanala, G.-S. Park, Y.-W. Kim, B. Hu, H. J. Bolink, S. Yoo, R. H. Friend, A. M. Rappe and T.-W. Lee, Comprehensive defect suppression in perovskite nanocrystals for high-efficiency light-emitting diodes, *Nat. Photonics*, 2021, **15**(2), 148–155, DOI: 10.1038/s41566-020-00732-4.

299 I. M. Pavlovetc, M. C. Brennan, S. Draguta, A. Ruth, T. Moot, J. A. Christians, K. Aleshire, S. P. Harvey, S. Toso, S. U. Nanayakkara, J. Messinger, J. M. Luther and M. Kuno, Suppressing Cation Migration in Triple-Cation Lead Halide Perovskites, *ACS Energy Lett.*, 2020, **5**(9), 2802–2810, DOI: 10.1021/acsenergylett.0c01207.

300 S. Kim, T. Eom, Y.-S. Ha, K.-H. Hong and H. Kim, Thermodynamics of Multicomponent Perovskites: A Guide to Highly Efficient and Stable Solar Cell Materials, *Chem. Mater.*, 2020, **32**(10), 4265–4272, DOI: 10.1021/acs.chemmater.0c00893.

301 M. C. Folgueras, Y. Jiang, J. Jin and P. Yang, High-entropy halide perovskite single crystals stabilized by mild chemistry, *Nature*, 2023, **621**, 282–288, DOI: 10.1038/s41586-023-06396-8.

302 K. Jayanthi, I. Spanopoulos, N. Zibouche, A. A. Voskanyan, E. S. Vasileiadou, M. S. Islam, A. Navrotsky and M. G. Kanatzidis, Entropy Stabilization Effects and Ion Migration in 3D "Hollow" Halide Perovskites, *J. Am. Chem. Soc.*, 2022, **144**(18), 8223–8230, DOI: 10.1021/jacs.2c01383.

303 A. Bonadio, C. A. Escanhoela, F. P. Sabino, G. Sombrio, V. G. de Paula, F. F. Ferreira, A. Janotti, G. M. Dalpian and J. A. Souza, Entropy-driven stabilization of the cubic phase of $MaPbI_3$ at room temperature, *J. Mater. Chem. A*, 2021, **9**(2), 1089–1099, DOI: 10.1039/D0TA10492B.

304 S. F. Solari, L.-N. Poon, M. Wörle, F. Krumeich, Y.-T. Li, Y.-C. Chiu and C.-J. Shih, Stabilization of Lead-Reduced Metal Halide Perovskite Nanocrystals by High-Entropy Alloying, *J. Am. Chem. Soc.*, 2022, **144**(13), 5864–5870, DOI: 10.1021/jacs.1c12294.

305 J.-H. Pöhls, M. Heyberger and A. Mar, Comparison of computational and experimental inorganic crystal structures, *J. Solid State Chem.*, 2020, **290**, 121557, DOI: 10.1016/j.jssc.2020.121557.

306 N. Achiwa, Linear Antiferromagnetic Chains in Hexagonal $ABCl_3$-Type Compounds (A; Cs, or Rb, B; Cu, Ni, Co, or Fe), *J. Phys. Soc. Jpn.*, 1969, **27**(3), 561–574, DOI: 10.1143/JPSJ.27.561.

307 M. S. Alam, M. Saiduzzaman, A. Biswas, T. Ahmed, A. Sultana and K. M. Hossain, Tuning band gap and enhancing optical functions of $AGeF_3$ (A = K, Rb) under pressure for improved optoelectronic applications, *Sci. Rep.*, 2022, **12**(1), 8663, DOI: 10.1038/s41598-022-12713-4.

308 P. S. Aleonard, Fluorometallates obtenus par dissolution d'oxydes metalliques dans bain fondu a base de fluoroborate de potassium, *C. R. Seances Acad. Sci., Ser. D*, 1965, **260**, 1977–1980.

309 K. S. Alexandrov, B. V. Besnosikov and L. A. Posdnjakova, Successive phase transitions in perovskites. II. Structures of distorted phases, *Ferroelectrics*, 1976, **12**(1), 197–198, DOI: 10.1080/00150197608241424.

310 E. Alter and R. Hoppe, Uber Fluoropalladate(II): $KPdF_3$, $RbPdF_3$, $TlPdF_3$ und K_2PdF_4, *Z. Anorg. Allg. Chem.*, 1974, **408**(2), 115–120, DOI: 10.1002/zaac.19744080205.

311 M. Arakawa, H. Ebisu and H. Takeuchi, EPR study of Cr^{3+} centres in Tl_2MgF_4 and Tl_2ZnF_4 crystals, in *EPR in the 21st Century*, ed. A. Kawamori, J. Yamauchi and H. Ohta, Elsevier Science B.V., Amsterdam, 2002, pp. 219–224.

312 H. Arif, M. B. Tahir, M. Sagir, S. Znaidia, H. Alrobei and M. Alzaid, First-principles calculations to investigate "H" and "K" doped $RbSrF_3$ for photovoltaic applications, *Optik*, 2022, **271**, 169864, DOI: 10.1016/j.ijleo.2022.169864.

313 E. C. Ashby, R. S. Smith and A. B. Goel, Comparative studies on the addition reactions of the Normant reagent ("CH_3MgBr" + CuBr) and the new tetrahydrofuran-soluble magnesium methylcuprates $Mg_mCu_n(CH_3)_{2m+n}$ with phenylacetylene, *J. Org. Chem.*, 1981, **46**(25), 5133–5139, DOI: 10.1021/jo00338a013.

314 R. W. Asmussen, T. K. Larsen and H. Soling, The crystal structure of $RbNiCl_3$ and $RbNiBr_3$. The Weiss constant in relation to the crystal structure of some double halides of

the type $ANiX_3$, *Acta Chem. Scand.*, 1969, **23**, 2055–2060, DOI: 10.3891/acta.chem.scand.23-2055.

315 D. Babel, in *Structural chemistry of octahedral fluorocomplexes of the transition elements, Structure and Bonding, Berlin, Heidelberg*, ed. C. K. Jørgensen, J. B. Neilands, R. S. Nyholm, D. Reinen and R. J. P. Williams, Springer Berlin Heidelberg, Berlin, Heidelberg, 1967, pp. 1–87.

316 B. Bachmann and B. G. Müller, Einkristalluntersuchungen an Fluoroperowskiten $MPdF_3$ (M = Rb, K) und PdF_2, *Z. Anorg. Allg. Chem.*, 1993, **619**(2), 387–391, DOI: 10.1002/zaac.19936190225.

317 C. Baopeng, W. Shihua and Z. Xinhua, Synthesis and structure of $AEuI_3$ (A = Rb, Cs) and AEu_2I_5 (A = K, Rb, Cs), *J. Alloys Compd.*, 1992, **181**(1), 511–514, DOI: 10.1016/0925-8388(92)90348-D.

318 H. P. Beck, H. Tratzky, V. Kallmayer and K. Stöwe, The $InSnCl_3$-Type Arrangement: I. A New ABX_3 Structure Type with Close Cation–Cation Contacts, *J. Solid State Chem.*, 1999, **146**(2), 344–350, DOI: 10.1006/jssc.1999.8360.

319 M. Belabbas, N. Marbouh, O. Arbouche and A. Hussain, Optoelectronic properties of the novel perovskite materials $LiPb(Cl:Br:I)_3$ for enhanced hydrogen production by visible photo-catalytic activity: Theoretical prediction based on empirical formulae and DFT, *Int. J. Hydrogen Energy*, 2020, **45**(58), 33466–33477, DOI: 10.1016/j.ijhydene.2020.09.066.

320 F. L. M. Bernal, J. Sottmann, D. S. Wragg, H. Fjellvåg, Ø. S. Fjellvåg, C. Drathen, W. A. Sławiński and O. M. Løvvik, Structural and magnetic characterization of the elusive Jahn-Teller active $NaCrF_3$, *Phys. Rev. Mater.*, 2020, **4**(5), 054412, DOI: 10.1103/PhysRevMaterials.4.054412.

321 J. Bill, K. Lerch and W. Laqua, $Cs_2Ag^{I}Ag^{III}Cl_6$. Eine gemischtvalente Verbindung mit dreiwertigem Silber, *Z. Anorg. Allg. Chem.*, 1990, **589**(1), 7–11, DOI: 10.1002/zaac.19905890102.

322 S. R. A. Bird, J. D. Donaldson and J. Silver, The Mössbauer effect in tin(II) compounds. Part XII. The spectra of the chloro- and bromo-stannates(II), *J. Chem. Soc., Dalton Trans.*, 1972, (18), 1950–1953, DOI: 10.1039/DT9720001950.

323 A. V. Bogdanova, N. P. Zaslavskaya, E. V. Sinichka, M. F. Fedyna, I. R. Mokra and S. M. Gasinets, Synthesis and Crystal Structure of Compounds $TlCdCl_3$ and $TlCdBr_3$, *Inorg. Mater.*, 1993, **29**, 664–666, DOI: 10.1002/chin.199346021.

324 A. I. Boltalin and Y. M. Korenev, Reaction between KF and PbF_2 in Solid and Gas Phases, *J. Inorg. Chem.*, 1996, **41**(6), 924–927.

325 E. D. Bourret-Courchesne, G. A. Bizarri, R. Borade, G. Gundiah, E. C. Samulon, Z. Yan and S. E. Derenzo, Crystal growth and characterization of alkali-earth halide scintillators, *J. Cryst. Growth*, 2012, **352**(1), 78–83, DOI: 10.1016/j.jcrysgro.2012.01.014.

326 J. Brynestad, H. L. Yakel and G. P. Smith, Temperature Dependence of the Absorption Spectrum of Nickel(II)-Doped $KMgCl_3$ and the Crystal Structure of $KMgCl_3$, *J. Chem. Phys.*, 2004, **45**(12), 4652–4664, DOI: 10.1063/1.1727550.

327 G. A. Bukhalova, V. T. Berezhnaya and N. E. Okol'chishena, Some properties of compounds of the type $M^{1+}M^{2+}F_3$, *Russ. J. Inorg. Chem.*, 1969, **14**, 917–921.

328 A. Bulou, J. Nouet, A. W. Hewat and F. J. Schäfer, Structural phase transitions in $KCaF_3$ – DSC, birefringence and neutron powder diffraction results, *Ferroelectrics*, 1980, **25**(1), 375–378, DOI: 10.1080/00150198008207024.

329 F. L. Carter, On the existence of two forms of $NaNiF_3$, *Solid State Commun.*, 1969, **7**(14), 993–995, DOI: 10.1016/0038-1098(69)90070-2.

330 L. Ch'ih-fa and L. S. Morozov, Thermal and tensimetric investigation of systems formed by tin(II) chloride with alkali metal and ammonium chloride, *J. Therm. Anal. Calorim.*, 1963, **8**(3), 708–711.

331 J. C. Cousseins and A. De Kozak, Sur les fluorures doubles de chrome bivalent de potassium ou de rubidium, *C. R. Seances Acad. Sci., Ser. C*, 1966, **263**(25), 1533–1535.

332 D. E. Cox and F. C. Merkert, The preparation, crystal growth and perfection of double halides of $CsNiCl_3$ type, *J. Cryst. Growth*, 1972, **13–14**, 282–284, DOI: 10.1016/0022-0248(72)90170-4.

333 W. J. Crama, *On the cooperative Jahn-Teller effect in ternary chromium(II) and copper(II) halides*, PhD Thesis, Rijksuniversiteit Leiden, Netherlands, 1980.

334 C. Cros, L. Hanebali, L. Latié, G. R. Villeneuve and W. Gang, Structure, ionic motion and conductivity in some solid-solutions of the $LiClMCl_2$ systems (M = Mg, V, Mn), *Solid State Ionics*, 1983, **9–10**, 139–147, DOI: 10.1016/0167-2738(83)90223-0.

335 J.-M. Dance, N. Kerkouri, J.-L. Soubeyroux, J. Darriet and A. Tressaud, Cationic substitutions in fluorides of hexagonal perovskite type. III. The $CsNi_{1-x}Cd_xF_3$ system: Crystal chemistry and trimeric magnetic interactions in $CsNi_{34}Cd_{14}F_3$, *Mater. Lett.*, 1982, **1**(2), 49–52, DOI: 10.1016/0167-577X(82)90004-0.

336 P. Daniel, J. Toulouse, J. Y. Gesland and M. Rousseau, Raman-scattering investigation of the hexagonal perovskite $RbZnF_3$, *Phys. Rev. B: Condens. Matter Mater. Phys.*, 1995, **52**(13), 9129–9132, DOI: 10.1103/PhysRevB.52.9129.

337 P. Demchenko, O. Y. Khyzhun, P. M. Fochuk, S. I. Levkovets, G. L. Myronchuk and O. V. Parasyuk, Single crystal growth, structure and properties of $TlHgBr_3$, *Opt. Mater.*, 2015, **49**, 94–99, DOI: 10.1016/j.optmat.2015.08.026.

338 C. Deschene, *In Situ Monitoring of Cation and Anion Exchange in Perovskite Nanoparticles for Applications in Catalysis, Sensing, and Batteries*, BS Honors thesis, Syracuse University, 2019.

339 K. O. Devaney, M. R. Freedman, G. L. McPherson and J. L. Atwood, Electron paramagnetic resonance studies of manganese(II) and nickel(II) in three structural phases of rubidium magnesium chloride and the crystal structure of 6H-rubidium magnesium chloride, *Inorg. Chem.*, 1981, **20**(1), 140–145, DOI: 10.1021/ic50215a030.

340 R. C. DeVries and R. Roy, Fluoride Models for Oxide Systems of Dielectric Interest. The Systems KF—MgF_2

and AgF-ZnF_2, *J. Am. Chem. Soc.*, 1953, **75**(10), 2479–2484, DOI: 10.1021/ja01106a059.

341 R. Dronskowski, $InFeBr_3$ and $InMnBr_3$: Synthesis, Crystal Structure, Magnetic Properties, and Electronic Structure, *Inorg. Chem.*, 1994, **33**(25), 5927–5933, DOI: 10.1021/ic00103a047.

342 R. Dronskowski, Synthesis, Crystal Structure, and Electronic Structure of $InCdBr_3$, *J. Solid State Chem.*, 1995, **116**(1), 45–52, DOI: 10.1006/jssc.1995.1180.

343 P. G. Dubovoj, Formation of compounds in the RbCl-$BeCl_2$ system, *Ukr. Khem. Zh.*, 1979, **45**(12), 1234–1235.

344 D. E. Eastman and M. W. Shafer, Antiferromagnetic Resonance in Cubic $TlMnF_3$, *J. Appl. Phys.*, 2004, **38**(3), 1274–1276, DOI: 10.1063/1.1709576.

345 H. Ebisu, M. Arakawa and H. Takeuchi, An EPR study of trigonally symmetric Cr^{3+} centres in $TlZnF_3$ single crystals, *J. Phys.: Condens. Matter*, 2005, **17**(29), 4653, DOI: 10.1088/0953-8984/17/29/008.

346 H. Ehrenberg, H. Fuess, S. Hesse, J. Zimmermann, H. von Seggern and M. Knapp, Structures of $CsEuBr_3$ and its degradation product $Cs_2EuBr_5{\cdot}10H_2O$, *Acta Crystallogr., Sect. B: Struct. Sci.*, 2007, **63**(2), 201–204, DOI: 10.1107/S0108768106049032.

347 Å. Engberg and H. Soling, On the crystal structures of $RbCoCl_3$ and Rb_3CoCl_5, *Acta Chem. Scand.*, 1967, **21**, 168–174, DOI: 10.3891/acta.chem.scand.21-0168.

348 G. E. Eperon, S. D. Stranks, C. Menelaou, M. B. Johnston, L. M. Herz and H. J. Snaith, Formamidinium lead trihalide: a broadly tunable perovskite for efficient planar heterojunction solar cells, *Energy Environ. Sci.*, 2014, **7**(3), 982–988, DOI: 10.1039/C3EE43822H.

349 B. Ewald, C. Kudla, P. Heines, H.-L. Keller and C. Lathe, *Investigation of the group subgroup transition in* $AgPbBr_3$, 2002, vol. 2.

350 N. Fedoseeva, I. Spevakova, G. Petrakovskii, V. Chuev and S. Petrov, Magnetic structure and magnetic field behaviour of $NaMnCl_3$, *J. Magn. Magn. Mater.*, 1980, **15–18**, 539–541, DOI: 10.1016/0304-8853(80)91166-X.

351 N. V. Fedoseeva, T. A. Velikanova and A. G. Zvegintsev, High-pressure cubic phase of $RbMnCl_3$ - magnetic properties, *Phys. Status Solidi A*, 1979, **51**(1), K93–K96, DOI: 10.1002/pssa.2210510157.

352 H. Fink and H.-J. Seifert, Über die Systeme des Europium(II)- und Strontiumchlorids mit Alkalimetallchloriden und Thalliumchlorid [1], *Z. Anorg. Allg. Chem.*, 1980, **466**(1), 87–96, DOI: 10.1002/zaac.19804660111.

353 I. Földvári, R. Voszka and Z. Morlin, The Properties of Ni Ions in NaCl Single Crystals. I. Vacuum Ultraviolet, Ionic Conductivity, and X-Ray Diffraction Studies, *Phys. Status Solidi B*, 1978, **89**(1), 235–240, DOI: 10.1002/pssb.2220890130.

354 J. Foulon, J. Durand, A. Larbot, L. Cot and A. Soufiane, Crystal structures of $MSnF_3$ for M = K, Rb, Tl; ionic mobility, *Eur. J. Solid State Inorg. Chem.*, 1993, **30**, 87–99, DOI: 10.1002/chin.199321003.

355 N. Gallo, V. D. Bianco and S. Doronzo, Mercury thiocyanate and cadmium iodide complexes with KCNS and KI in methylmethacrylate, *J. Inorg. Nucl. Chem.*, 1972, **34**(7), 2374–2375, DOI: 10.1016/0022-1902(72)80178-7.

356 J. I. Gómez-Peralta and X. Bokhimi, Ternary halide perovskites for possible optoelectronic applications revealed by Artificial Intelligence and DFT calculations, *Mater. Chem. Phys.*, 2021, **267**, 124710, DOI: 10.1016/j.matchemphys.2021.124710.

357 E. C. Gonzalo, M. L. Sanjuán, M. Hoelzel, M. T. Azcondo, U. Amador, I. Sobrados, J. Sanz, F. García-Alvarado and A. Kuhn, Synthesis and Characterization of $NaNiF_3{\cdot}3H_2O$: An Unusual Ordered Variant of the ReO_3 Type, *Inorg. Chem.*, 2015, **54**(7), 3172–3182, DOI: 10.1021/ic5026262.

358 J. Goodyear, E. M. Ali and H. H. Sutherland, Rubidium tribromomanganate, *Acta Crystallogr., Sect. B: Struct. Crystallogr. Cryst. Chem.*, 1980, **36**(3), 671–672, DOI: 10.1107/S0567740880004074.

359 J. Goodyear and D. J. Kennedy, The crystal structure of $CsMnCl_3$, *Acta Crystallogr., Sect. B: Struct. Crystallogr. Cryst. Chem.*, 1973, **29**(4), 744–748, DOI: 10.1107/S0567740873003286.

360 E. Gordo, G. Z. Chen and D. J. Fray, Toward optimisation of electrolytic reduction of solid chromium oxide to chromium powder in molten chloride salts, *Electrochim. Acta*, 2004, **49**(13), 2195–2208, DOI: 10.1016/j.electacta.2003.12.045.

361 R. G. Grebenshchikov, A study of the RbF–BeF_2 equilibrium diagram and its relation to BaO–SiO_2 system, *Proceedings of the Academy of Sciences*, Institute of Silicate Chemistry of the USSR Academy of Sciences, 1957, vol. 114(2), pp. 316–319.

362 E. Gurewitz, A. Horowitz and H. Shaked, Magnetic spiral structure of $KMnCl_3$—a neutron-diffraction study, *Phys. Rev. B: Condens. Matter Mater. Phys.*, 1979, **20**(11), 4544–4549, DOI: 10.1103/PhysRevB.20.4544.

363 E. Gurewitz, J. Makovsky and H. Shaked, Neutron-diffraction study of the magnetic structure of $KFeCl_3$, *Phys. Rev. B: Solid State*, 1974, **9**(3), 1071–1076, DOI: 10.1103/PhysRevB.9.1071.

364 E. Gurewitz and H. Shaked, Neutron diffraction study of the crystallographic and magnetic structures of potassium tribromoferrate(II), *Acta Crystallogr., Sect. B: Struct. Crystallogr. Cryst. Chem.*, 1982, **38**(11), 2771–2775, DOI: 10.1107/S0567740882009923.

365 I. Hamideddine, N. Tahiri, O. E. Bounagui and H. Ez-Zahraouy, *Ab initio* study of structural and optical properties of the halide perovskite KBX_3 compound, *J. Korean Ceram. Soc.*, 2022, **59**(3), 350–358, DOI: 10.1007/s43207-021-00178-6.

366 M. Harada, Jahn-Teller Phase Transitions in $RbCuCl_3$, *J. Phys. Soc. Jpn.*, 1983, **52**(5), 1646–1657, DOI: 10.1143/JPSJ.52.1646.

367 T. Haseda, N. Wada, M. Hata and K. Amaya, Spin ordering in a triangular X–Y antiferromagnet: $CsFeCl_3$ and $RbFeCl_3$, *Physica B+C*, 1981, **108**(1), 841–842, DOI: 10.1016/0378-4363(81)90725-7.

368 H. J. Haupt, F. Huber and H. Preut, Darstellung und Kristallstruktur von Rubidiumtrijodoplumbat(II), *Z. Anorg. Allg. Chem.*, 1974, **408**(2), 209–213, DOI: 10.1002/zaac.19744080215.

369 A. Hauser, U. Falk, P. Fischer, A. Furrer and H. U. Güdel, Neutron scattering investigation of 1D and 3D magnetic ordering and excitations in AVX_3 (A = Rb, Cs; X = Cl, Br, I), *J. Magn. Magn. Mater.*, 1983, **31–34**, 1139–1140, DOI: 10.1016/0304-8853(83)90832-6.

370 A. Hauser, U. Falk, P. Fischer and H. U. Güdel, Magnetic order in AVX_3 (A = Rb, Cs, $(CD_3)_4$ N; X = Cl, Br, I): A neutron diffraction study, *J. Solid State Chem.*, 1985, **56**(3), 343–354, DOI: 10.1016/0022-4596(85)90184-7.

371 Hayatullah, G. Murtaza, R. Khenata, S. Mohammad, S. Naeem, M. N. Khalid and A. Manzar, Structural, elastic, electronic and optical properties of $CsMCl_3$ (M = Zn, Cd), *Phys. B*, 2013, **420**, 15–23, DOI: 10.1016/j.physb.2013.03.011.

372 C. Hebecker, Neue ternäre Fluoride mit einwertigem Thallium und Silber als Kationen, *Naturwissenschaften*, 1973, **60**(3), 154, DOI: 10.1007/BF00594787.

373 M. Hidaka and S. Hosogi, The crystal structure of $KCdF_3$, *J. Phys. France*, 1982, **43**(8), 1227–1232, DOI: 10.1051/jphys:019820043080122700.

374 K. Hirakawa, H. Yoshizawa and K. Ubukoshi, Magnetic and Neutron Scattering Study of One-Dimensional Heisenberg Antiferromagnet $CsVCl_3$, *J. Phys. Soc. Jpn.*, 1982, **51**(4), 1119–1122, DOI: 10.1143/JPSJ.51.1119.

375 J. B. Hoffman, A. L. Schleper and P. V. Kamat, Transformation of Sintered $CsPbBr_3$ Nanocrystals to Cubic $CsPbI_3$ and Gradient $CsPbBr_xI_{3-x}$ through Halide Exchange, *J. Am. Chem. Soc.*, 2016, **138**(27), 8603–8611, DOI: 10.1021/jacs.6b04661.

376 C. Hohnstedt and G. Meyer, The first ternary iodides with divalent dysprosium, *Naturwissenschaften*, 1991, **78**(10), 462–463, DOI: 10.1007/BF01134384.

377 C. Hohnstedt and G. Meyer, Metallothermische Reduktion des Tribromids und -iodids von Dysprosium mit Alkalimetallen, *Z. Anorg. Allg. Chem.*, 1993, **619**(8), 1374–1378, DOI: 10.1002/zaac.19936190809.

378 W. Hönle, G. Miller and A. Simon, Preparation, crystal structures, and electronic properties of $LiGaCl_3$ and $LiGaI_3$, *J. Solid State Chem.*, 1988, **75**(1), 147–155, DOI: 10.1016/0022-4596(88)90312-X.

379 W. Hönle and A. Simon, Darstellung und Kristallstrukturen von $LiGaBr_4$ und $LiGaBr_3$, *Z. Naturforsch. B*, 1986, **41**(11), 1391–1398, DOI: 10.1515/znb-1986-1113.

380 R. Hoppe, W. Dähne and W. Klemm, Mangantetrafluorid mit einem Anhang über $LiMnF_5$ und $LiMnF_4$, *Justus Liebigs Ann. Chem.*, 1962, **658**(1), 1–5, DOI: 10.1002/jlac.19626580102.

381 R. Hoppe and R. Über Homann, $CsHgF_3$, $RbHgF_3$ und $KHgF_3$, *Z. Anorg. Allg. Chem.*, 1969, **369**(3–6), 212–216, DOI: 10.1002/zaac.19693690312.

382 A. Horowitz, M. Amit, J. Makovsky, L. B. Dor and Z. H. Kalman, Structure types and phase transformations in $KMnCl_3$ and $TlMnCl_3$, *J. Solid State Chem.*, 1982, **43**(2), 107–125, DOI: 10.1016/0022-4596(82)90220-1.

383 R. A. Howie, W. Moser, R. G. Starks, F. W. D. Woodhams and W. Parker, Potassium tin(II) sulphate and related tin apatites: Mössbauer and X-ray studies, *J. Chem. Soc., Dalton Trans.*, 1973, **14**, 1478–1484, DOI: 10.1039/DT9730001478.

384 J. Huang, T. Lei, M. Siron, Y. Zhang, S. Yu, F. Seeler, A. Dehestani, L. N. Quan, K. Schierle-Arndt and P. Yang, Lead-free Cesium Europium Halide Perovskite Nanocrystals, *Nano Lett.*, 2020, **20**(5), 3734–3739, DOI: 10.1021/acs.nanolett.0c00692.

385 S. Huang, H. Shan, W. Xuan, W. Xu, D. Hu, L. Zhu, C. Huang, W. Sui, C. Xiao, Y. Zhao, Y. Qiang, X. Gu, J. Song and C. Zhou, High-Performance Humidity Sensor Based on $CsPdBr_3$ Nanocrystals for Noncontact Sensing of Hydromechanical Characteristics of Unsaturated Soil, *Phys. Status Solidi RRL*, 2022, **16**(6), 2200017, DOI: 10.1002/pssr.202200017.

386 J. Huart, Étude de trois halogénomercurates de thallium, *Bull. Mineral.*, 1965, **88**(1), 65–68, DOI: 10.3406/bulmi.1965.5806.

387 S. Idrissi, O. Mounkachi, L. Bahmad and A. Benyoussef, Study of the electronic and opto-electronic properties of the perovskite $KPbBr_3$ by DFT and TDDFT methods, *Comput. Condens. Matter*, 2022, **33**, e00617, DOI: 10.1016/j.cocom.2021.e00617.

388 H. Jex, J. Maetz and M. Müllner, Cubic-to-tetragonal phase transition in $RbCaF_3$ investigated by diffraction experiments with neutrons, x rays, and γ rays from a Mössbauer source, *Phys. Rev. B: Condens. Matter Mater. Phys.*, 1980, **21**(3), 1209–1218, DOI: 10.1103/PhysRevB.21.1209.

389 L. Jongen, T. Gloger, J. Beekhuizen and G. Meyer, Divalent Titanium: The Halides $ATiX_3$ (A = K, Rb, Cs; X = Cl, Br, I), *Z. Anorg. Allg. Chem.*, 2005, **631**(2–3), 582–586, DOI: 10.1002/zaac.200400464.

390 N. Jouini, L. Guen and M. Tournoux, Structure de $TlFeBr_3$: Distorsion du type perovskite hexagonale 2L, *Mater. Res. Bull.*, 1982, **17**(11), 1421–1427, DOI: 10.1016/0025-5408(82)90228-8.

391 N. Jouini, L. Guen and M. Tournoux, Le systeme TlI-GeI_2 – Structure cristalline de $TlGeI_3$, *Ann. Chim.*, 1982, **7**(1), 45–51.

392 M.-H. Jung, S. H. Rhim and D. Moon, TiO_2/$RbPbI_3$ halide perovskite solar cells, *Sol. Energy Mater. Sol. Cells*, 2017, **172**, 44–54, DOI: 10.1016/j.solmat.2017.07.011.

393 V. Kaiser, M. Otto, F. Binder and D. Babel, Jahn-Teller-Effekt und Kristallstruktur-Verzerrung bei den Kupfer-Fluorperowskiten $NaCuF_3$ und $RbCuF_3$, *Z. Anorg. Allg. Chem.*, 1990, **585**(1), 93–104, DOI: 10.1002/zaac.19905850112.

394 C. Kaladevi, *Studies on some ternary alkali lead bromide crystals*, PhD Thesis, Manonmaniam Sundaranar University, 2011.

395 A. Katrusiak and A. Ratuszna, Phase transitions and the structure of $NaMnF_3$ perovskite crystals as a function of temperature and pressure, *Solid State Commun.*, 1992, **84**(4), 435–441, DOI: 10.1016/0038-1098(92)90492-R.

396 K. Khan, J. Sahariya and A. Soni, Structural, electronic and optical modeling of perovskite solar materials $ASnX_3$ (A = Rb, K; X = Cl, Br): First principle investigations, *Mater.*

Chem. Phys., 2021, **262**, 124284, DOI: 10.1016/j.matchemphys.2021.124284.

397 O. Y. Khyzhun, P. M. Fochuk, I. V. Kityk, M. Piasecki, S. I. Levkovets, A. O. Fedorchuk and O. V. Parasyuk, Single crystal growth and electronic structure of $TlPbI_3$, *Mater. Chem. Phys.*, 2016, **172**, 165–172, DOI: 10.1016/j.matchemphys.2016.01.058.

398 H. Kitagawa, H. Sato, N. Kojima, T. Kikegawa and O. Shimomura, Metallization and phase transitions of the three-dimensional halogen-bridge mixed-valence complex $Cs_2Au_2I_6$ under high pressure, *Solid State Commun.*, 1991, **78**(11), 989–995, DOI: 10.1016/0038-1098(91)90220-P.

399 H. Klasens, P. Zalm and F. Huysman, The manganese emission in ABF_3-compounds, *Philips Res. Rep.*, 1953, **8**, 441–451.

400 K. Knox, Perovskite-like fluorides. I. Structures of $KMnF_3$, $KFeF_3$, $KNiF_3$ and $KZnF_3$. Crystal field effects in the series and in $KCrF_3$ and $KCuF_3$, *Acta Crystallogr.*, 1961, **14**(6), 583–585, DOI: 10.1107/S0365110X61001868.

401 K. Komarek and P. Herasymenko, Equilibria between Titanium Metal and Solutions of Titanium Dichloride in Fused Sodium Chloride, *J. Electrochem. Soc.*, 1958, **105**(4), 216, DOI: 10.1149/1.2428803.

402 E. N. Kovalenko, O. N. Yunakova and N. N. Yunakov, The exciton absorption spectrum of thin films of ternary compounds in the AgBr–$PbBr_2$ system, *Low Temp. Phys.*, 2018, **44**(8), 856–859, DOI: 10.1063/1.5049171.

403 T. A. Kuku, Structure and ionic conductivity of $CuCdCl_3$, *Solid State Ionics*, 1987, **25**(2), 105–108, DOI: 10.1016/0167-2738(87)90109-3.

404 M. H. Kuok, L. S. Tan, Z. X. Shen, C. H. Huan and K. F. Mok, A Raman study of $RbSnBr_3$, *Solid State Commun.*, 1996, **97**(6), 497–501, DOI: 10.1016/0038-1098(95)00625-7.

405 M. H. Kuok and S. H. Tang, A Raman Study of $KCdBr_3$ Single Crystals, *Phys. Status Solidi B*, 1988, **147**(2), K195–K199, DOI: 10.1002/pssb.2221470261.

406 I. Y. Kuznetsova, I. S. Kovaleva and V. A. Fedorov, Cs_2CdBr_4-$CsPbBr_3$ and $CsCdBr_3$-$CsPbBr_3$ joins of the $CdBr_2$-$PbBr_2$-CsBr ternary system, *Zh. Neorg. Khim.*, 2002, **47**(6), 1010–1012.

407 A. Lachgar, D. S. Dudis, P. K. Dorhout and J. D. Corbett, Synthesis and properties of two novel line phases that contain linear scandium chains, lithium scandium iodide ($LiScI_3$) and sodium scandium iodide ($Na_{0.5}ScI_3$), *Inorg. Chem.*, 1991, **30**(17), 3321–3326, DOI: 10.1021/ic00017a019.

408 M. E. Levina and E. V. Yunakovskaya, Phase transitions of the metafluoroberyllates $RbBeF_3$ and $CsBeF_3$, *Moscow Univ. Chem. Bull.*, 1971, **26**(6), 40–42.

409 Q.-J. Li, D. Sprouster, G. Zheng, J. C. Neuefeind, A. D. Braatz, J. McFarlane, D. Olds, S. Lam, J. Li and B. Khaykovich, Complex Structure of Molten NaCl–$CrCl_3$ Salt: Cr–Cl Octahedral Network and Intermediate-Range Order, *ACS Appl. Energy Mater.*, 2021, **4**(4), 3044–3056, DOI: 10.1021/acsaem.0c02678.

410 T.-I. Li and G. D. Stucky, Exchange interactions in polynuclear transition metal complexes. Structural properties of cesium tribromocuprate(II), $CsCuBr_3$, a strongly coupled copper(II) system, *Inorg. Chem.*, 1973, **12**(2), 441–445, DOI: 10.1021/ic50120a040.

411 T.-I. Li and G. D. Stucky, The effect of exchange coupling on the spectra of transition metal ions. The crystal structure and optical spectrum of $CsCrBr_3$, *Acta Crystallogr., Sect. B: Struct. Crystallogr. Cryst. Chem.*, 1973, **29**(7), 1529–1532, DOI: 10.1107/S0567740873004863.

412 T.-I. Li, G. D. Stucky and G. L. McPherson, The crystal structure of $CsMnCl_3$ and a summary of the structures of RMX_3 compounds, *Acta Crystallogr., Sect. B: Struct. Crystallogr. Cryst. Chem.*, 1973, **29**(6), 1330–1335, DOI: 10.1107/S0567740873004450.

413 Y. Li, Y. Ding, Y. Li, H. Liu, X. Meng, Y. Cong, J. Zhang, X. Li, X. Chen and J. Qin, Synthesis, Crystal Structure and Nonlinear Optical Property of $RbHgI_3$, *Crystals*, 2017, **7**(5), 148, DOI: 10.3390/cryst7050148.

414 L. Liang, L. Wencong and C. Nianyi, On the criteria of formation and lattice distortion of perovskite-type complex halides, *J. Phys. Chem. Solids*, 2004, **65**(5), 855–860, DOI: 10.1016/j.jpcs.2003.08.021.

415 A. R. Lim and S.-Y. Jeong, ^{133}Cs nuclear magnetic resonance study in $CsZnCl_3$ single crystals of perovskite ABX_3 type, *Phys. B*, 2008, **403**(18), 3217–3220, DOI: 10.1016/j.physb.2008.04.007.

416 W. Lin, J. He, K. M. McCall, C. C. Stoumpos, Z. Liu, I. Hadar, S. Das, H.-H. Wang, B.-X. Wang, D. Y. Chung, B. W. Wessels and M. G. Kanatzidis, Inorganic Halide Perovskitoid $TlPbI_3$ for Ionizing Radiation Detection, *Adv. Funct. Mater.*, 2021, **31**(13), 2006635, DOI: 10.1002/adfm.202006635.

417 M. R. Linaburg, *Studies of Halide Perovskites $CsPbX_3$, $RbPbX_3$ ($X = Cl^-$, Br^-, I^-), and Their Solid Solutions*, MS thesis, The Ohio State University, 2015.

418 E. v Loef, L. S. Pandian, N. Kaneshige, G. Ciampi, L. Stand, D. Rutstrom, Y. Tratsiak, M. Zhuravleva, C. Melcher and K. S. Shah, Crystal Growth, Density Functional Theory, and Scintillation Properties of $TlCaX_3$ (X = Cl, Br, I), *IEEE Trans. Nucl. Sci.*, 2023, **70**(7), 1378–1383, DOI: 10.1109/TNS.2023.3258065.

419 J. M. Longo, J. A. Kafalas, J. R. O'Connor and J. B. Goodenough, Magnetic and Optical Properties of the High- and Low-Pressure Forms of $CsCoF_3$, *J. Appl. Phys.*, 1970, **41**(3), 935–936, DOI: 10.1063/1.1659031.

420 C. J. J. Loon and D. J. W. Ijdo, The crystal structure of Na_6MnCl_8 and $Na_2Mn_3Cl_8$ and some isostructural compounds, *Acta Crystallogr., Sect. B: Struct. Crystallogr. Cryst. Chem.*, 1975, **31**(3), 770–773, DOI: 10.1107/S0567740875003779.

421 M. M. Lukina and G. P. Klientova, Hydrothermal synthesis of $KZnF_3$ single crystals with a perovskite structure, *Sov. Phys. – Crystallogr.*, 1969, **14**(2), 314–315.

422 S. Lv, Q. Wu, X. Meng, L. Kang, C. Zhong, Z. Lin, Z. Hu, X. Chen and J. Qin, A promising new nonlinear optical

crystal with high laser damage threshold for application in the IR region: synthesis, crystal structure and properties of noncentrosymmetric $CsHgBr_3$, *J. Mater. Chem. C*, 2014, **2**(33), 6796–6801, DOI: 10.1039/C4TC00565A.

423 M. A. Macdonald, E. N. Mel'chakov, I. H. Munro, P. A. Rodnyi and A. S. Voloshinovsky, Radiative core–valence transitions in $CsMgCl_3$ and $CsSrCl_3$, *J. Lumin.*, 1995, **65**(1), 19–23, DOI: 10.1016/0022-2313(95)00051-Q.

424 K. H. Mahendran, S. Nagaraj, R. Sridharan and T. Gnanasekaran, Differential scanning calorimetric studies on the phase diagram of the binary LiCl–$CaCl_2$ system, *J. Alloys Compd.*, 2001, **325**(1), 78–83, DOI: 10.1016/S0925-8388(01)01387-1.

425 G. Maity and S. K. Pradhan, Composition related structural transition between mechanosynthesized $CsPbBr_3$ and $CsPb_2Br_5$ perovskites and their optical properties, *J. Alloys Compd.*, 2020, **816**, 152612, DOI: 10.1016/j.jallcom.2019.152612.

426 K. P. Marshall, S. Tao, M. Walker, D. S. Cook, J. Lloyd-Hughes, S. Varagnolo, A. Wijesekara, D. Walker, R. I. Walton and R. A. Hatton, $Cs_{1-x}Rb_xSnI_3$ light harvesting semiconductors for perovskite photovoltaics, *Mater. Chem. Front.*, 2018, **2**(8), 1515–1522, DOI: 10.1039/C8QM00159F.

427 C. D. Martin, S. Chaudhuri, C. P. Grey and J. B. Parise, Effect of A-site cation radius on ordering of BX_6 octahedra in (K,Na)MgF_3 perovskite, *Am. Mineral.*, 2005, **90**(10), 1522–1533, DOI: 10.2138/am.2005.1693.

428 N. Matsushita, H. Ahsbahs, S. S. Hafner and N. Kojima, Crystal Structure of Mixed-Valence Gold Compound, $Cs_2Au^IAu^{III}Cl_6$ up to 18 GPa, *Rev. High Pressure Sci. Technol.*, 1998, **7**, 329–331, DOI: 10.4131/jshpreview.7.329.

429 N. Matsushita, F. Fukuhara and N. Kojima, A three-dimensional bromo-bridged mixed-valence gold(I,III) compound, $Cs_2Au^IAu^{III}Br_6$, *Acta Crystallogr., Sect. E: Struct. Rep. Online*, 2005, **61**(6), i123–i125, DOI: 10.1107/S1600536805016594.

430 K. M. McCall, D. Friedrich, D. G. Chica, W. Cai, C. C. Stoumpos, G. C. B. Alexander, S. Deemyad, B. W. Wessels and M. G. Kanatzidis, Perovskites with a Twist: Strong In^{1+} Off-Centering in the Mixed-Valent $CsInX_3$ (X = Cl, Br), *Chem. Mater.*, 2019, **31**(22), 9554–9566, DOI: 10.1021/acs.chemmater.9b04095.

431 G. L. McPherson, A. M. McPherson and J. L. Atwood, Structures of $CsMgBr_3$, $CsCdBr_3$ and $CsMgI_3$— diamagnetic linear chain lattices, *J. Phys. Chem. Solids*, 1980, **41**(5), 495–499, DOI: 10.1016/0022-3697(80)90180-8.

432 D. Messer, Die Kristallstruktur von $RbGeCl_3$, *Z. Naturforsch., B: J. Chem. Sci.*, 1978, **33**(4), 366–369, DOI: 10.1515/znb-1978-0403.

433 G. Meyer, Neue Chlor-Perowskite mit zweiwertigen Lanthaniden: $CsLn^{II}Cl_3$ (Ln^{II} = Sm, Eu, Tm, Yb), *Naturwissenschaften*, 1978, **65**(5), 258, DOI: 10.1007/BF00368570.

434 G. Meyer, Reduced ternary rare earth halides: State of the art, *J. Less-Common Met.*, 1983, **93**(2), 371–380, DOI: 10.1016/0022-5088(83)90190-X.

435 G. Meyer and J. D. Corbett, Reduced ternary halides of scandium: $RbScX_3$ (X = chlorine, bromine) and $CsScX_3$ (X = chlorine, bromine, iodine), *Inorg. Chem.*, 1981, **20**(8), 2627–2631, DOI: 10.1021/ic50222a047.

436 G. Meyer, D. J. Hinz and U. Flörke, Crystal structure of caesium titanium tribromide, $CsTiBr_3$, *Z. Kristallogr. – Cryst. Mater.*, 1993, **208**(1–2), 370–371, DOI: 10.1524/zkri.1993.208.12.370.

437 G. Meyer and U. Packruhn, Chlorotitanate(II): $RbTiCl_3$ und $CsTiCl_3$, *Z. Anorg. Allg. Chem.*, 1985, **524**(5), 90–94, DOI: 10.1002/zaac.19855240512.

438 V. J. Minkiewicz, D. E. Cox and G. Shirane, The magnetic structures of $RbNiCl_3$ and $CsNiCl_3$, *Solid State Commun.*, 1970, **8**(12), 1001–1005, DOI: 10.1016/0038-1098(70)90505-3.

439 C. K. Møller, *The structure of cæsium plumbo iodide $CsPbI_3$,* Munksgaard, 1959, vol. 32, p. 18.

440 H. Monzel, M. Schramm, K. Stöwe and H. P. Beck, Zur Neuuntersuchung des Phasendiagramms RbCl/$PbCl_2$, *Z. Anorg. Allg. Chem.*, 2000, **626**(2), 408–411, DOI: 10.1002/(SICI)1521-3749(200002)626:2<408::AID-ZAAC408>3.0.CO;2-A.

441 E. L. Muetterties, Chemistry of the Difluorides of Germanium and Tin, *Inorg. Chem.*, 1962, **1**(2), 342–345, DOI: 10.1021/ic50002a029.

442 I. C. Muñoz, E. Cruz-Zaragoza, A. Favalli and C. Furetta, Thermoluminescence property of $LiMgF_3$ erbium activated phosphor, *Appl. Radiat. Isot.*, 2012, **70**(5), 893–896, DOI: 10.1016/j.apradiso.2012.02.006.

443 S. Nagaraj, C. V. Vishnuvardhan, S. Ghosh and R. Sridharan, Phase diagram study of $CaBr_2$–LiBr system using DTA, *J. Therm. Anal. Calorim.*, 2014, **115**(2), 1835–1839, DOI: 10.1007/s10973-013-3507-3.

444 N. Narsimlu, D. Srinivasu and G. S. Sastry, Study of optical and transport properties of $K_2CuCl_4{\cdot}2H_2O$ single crystal, *Cryst. Res. Technol.*, 1994, **29**(4), 577–582, DOI: 10.1002/crat.2170290423.

445 A. Naskar, R. Khanal and S. Choudhury, Role of Chemistry and Crystal Structure on the Electronic Defect States in Cs-Based Halide Perovskites, *Materials*, 2021, **14**(4), 1032, DOI: 10.3390/ma14041032.

446 M. Natarajan and B. Prakash, Phase transitions in ABX_3 type halides, *Phys. Status Solidi A*, 1971, **4**(3), K167–K172, DOI: 10.1002/pssa.2210040331.

447 M. Natarajan and E. A. Secco, Electrical conductivity and phase transformation studies on the mixed metal halides $RbCdX_3$ (X = Cl, Br, I) and Cs_2CuBr_4, *Phys. Status Solidi A*, 1976, **33**(1), 427–433, DOI: 10.1002/pssa.2210330146.

448 M. Niel, C. Cros, G. Le Flem and M. Pouchard, Sur les chlorures doubles de vanadium+II: les phases $TlVCl_3$ et NH_4VCl_3, *C. R. Acad. Sci.*, 1975, **280**(17), 1093–1095.

449 Y. Nishiwaki and K. Iio, *9aSH-2 Dielectricity and magnetism of hexagonal $RbCoBr_3$ related substance $ACoX_3$ (A = K,Tl B = Cl,Br) (dielectric, region 10),* The Physical Society of Japan Lecture Summary Collection, 2002, p. 830.

450 R. H. Odenthal and R. Hoppe, Fluorargentate(II) der Alkalimetalle, *Monatsh. Chem.*, 1971, **102**(5), 1340–1350, DOI: 10.1007/BF00917190.

451 A. Okazaki, Y. Suemune and T. Fuchikami, The Crystal Structures of $KMnF_3$, $KFeF_3$, $KCoF_3$, $KNiF_3$ and $KCuF_3$, *J. Phys. Soc. Jpn.*, 1959, **14**(12), 1823–1824, DOI: 10.1143/JPSJ.14.1823.

452 D. R. Onken, D. Perrodin, S. C. Vogel, E. D. Bourret and F. Moretti, The crystal structure of $TlMgCl_3$ from 290 K to 725 K, *Acta Crystallogr., Sect. E: Crystallogr. Commun.*, 2020, **76**(11), 1716–1719, DOI: 10.1107/S2056989020013201.

453 V. I. Pakhomov and A. V. Goryunov, On the nature of complex formation in some inorganic halides, *Russ. J. Inorg. Chem.*, 1993, **38**(9), 1402–1408.

454 M. Paul and H. J. Seifert, EMF-measurements with galvanic bromine cells in the systems RBr/MBr_2 (M = Sr, Ba), *J. Therm. Anal.*, 1989, **35**(2), 585–593, DOI: 10.1007/BF01904460.

455 E. Y. Peresh, V. B. Lazarev, V. V. Tsigika, A. V. Orinchaj, I. S. Balog, V. I. Tkachenko and I. I. Pogojda, Homogeneity regions, preparation and analysis of single crystals of certain compounds of Cs(Tl)X-Ge(Sn,Pb,Cd)X_2 systems, where X = Cl, Br, I, *Izv. Akad. Nauk SSSR, Neorg. Mater.*, 1985, **21**(5), 774–778.

456 M. P. Petrov and G. M. Nedlin, Spin-Density Space Oscillations and Hyperfine Interaction in $RbCoF_3$, *J. Appl. Phys.*, 1968, **39**(2), 1012–1014, DOI: 10.1063/1.1656148.

457 N. S. Pidzyrajlo, T. V. Triska and Z. A. Khapko, In *Recombination luminescence of $CsCdI_3$ monocrystals*, Theses of the 23 all-union conference on luminescence, USSR, USSR, 1976, p. 89.

458 A. I. Popov and Y. M. Kiselev, ChemInform Abstract: Synthesis and Characterization of the Higher Fluorides of Silver and Alkali Metals, *Chem. Inf.*, 1988, **19**(27), DOI: 10.1002/chin.198827039.

459 J. Portier, A. Tressaud and J. Dupin, Les Pérovskites Fluorées $AgMeF_3$ (Me = Mg, Mn; Co; Ni; Cu; Zn), *Cr. Acad. Sci. C*, 1970, **270**, 216–218.

460 S. H. Pulcinelli, J. Senegas, B. Tanguy, F. Menil and J. Portier, Préparation et étude structurale par ratons X et RMN d'un fluorure de composition $LiZnF_3$, *Rev. Chim. Miner.*, 1986, **23**(2), 238–249.

461 S. Racine, J. Cipriani and C. Pontikis, Diffusion de la lumiere et excitations magnetiques dans l'antiferromagnetique $KCoF_3$, *C. R. Seances Acad. Sci., Ser. B*, 1972, **274**, 16–18.

462 A. H. Reshak, I. V. Kityk, Z. A. Alahmed, S. Levkovets, A. O. Fedorchuk, G. Myronchuk, K. J. Plucinski, H. Kamarudin and S. Auluck, Experimental and theoretical investigation of the electronic structure and optical properties of $TlHgCl_3$ single crystal, *Opt. Mater.*, 2015, **47**, 445–452, DOI: 10.1016/j.optmat.2015.06.018.

463 M. Retuerto, T. Emge, J. Hadermann, P. W. Stephens, M. R. Li, Z. P. Yin, M. Croft, A. Ignatov, S. J. Zhang, Z. Yuan, C. Jin, J. W. Simonson, M. C. Aronson, A. Pan, D. N. Basov, G. Kotliar and M. Greenblatt, Synthesis and Properties of Charge-Ordered Thallium Halide Perovskites, $CsTl^+_{0.5}Tl^{3+}_{0.5}X_3$ (X = F or Cl): Theoretical Precursors for Superconductivity?, *Chem. Mater.*, 2013, **25**(20), 4071–4079, DOI: 10.1021/cm402423x.

464 R. Riccardi, C. Sinistri, G. Y. Campari and A. Magistris, Binary Systems Formed by Alkali Bromides with Barium or Strontium Bromide, *Z. Naturforsch., A: Astrophys., Phys. Phys. Chem.*, 1970, **25**(5), 781–785, DOI: 10.1515/zna-1970-0536.

465 M. Rousseau, J. Y. Gesland, J. Julliard, J. Nouet, J. Zarembowitch and A. Zarembowitch, Changement de phase structural dans $RbCdF_3$ et $TlCdF_3$, *J. Physique Lett.*, 1975, **36**(5), 121–124, DOI: 10.1051/jphyslet:01975003605012100.

466 W. Rüdorff, G. Lincke and D. Babel, Untersuchungen an ternären Fluoriden. (II). Kobalt(II)- und Kupfer(II)-fluoride, *Z. Anorg. Allg. Chem.*, 1963, **320**(1–4), 150–170, DOI: 10.1002/zaac.19633200119.

467 C. Rüegg, N. Cavadini, A. Furrer, H. U. Güdel, K. Krämer, H. Mutka, A. Wildes, K. Habicht and P. Vorderwisch, Bose–Einstein condensation of the triplet states in the magnetic insulator $TlCuCl_3$, *Nature*, 2003, **423**(6935), 62–65, DOI: 10.1038/nature01617.

468 Sandeep, D. P. Rai, A. Shankar, M. P. Ghimire, R. Khenata, S. Bin Omran, S. V. Syrotyuk and R. K. Thapa, Investigation of the structural, electronic and optical properties of the cubic $RbMF_3$ perovskites (M = Be, Mg, Ca, Sr and Ba) using modified Becke-Johnson exchange potential, *Mater. Chem. Phys.*, 2017, **192**, 282–290, DOI: 10.1016/j.matchemphys.2017.02.005.

469 K. Sawada and M. Tanaka, Formation of bromo complexes of cobalt(II) in acetic acid, *J. Inorg. Nucl. Chem.*, 1977, **39**(2), 339–344, DOI: 10.1016/0022-1902(77)80026-2.

470 V. Scatturin, L. Corliss, N. Elliott and J. Hastings, Magnetic structures of 3d transition metal double fluorides, $KMeF_3$, *Acta Crystallogr.*, 1961, **14**(1), 19–26, DOI: 10.1107/S0365110X61000036.

471 G. Schilling, C. Kunert, T. Schleid and G. Meyer, Metallothermische Reduktion der Tribromide und -iodide von Thulium und Ytterbium mit Alkalimetallen, *Z. Anorg. Allg. Chem.*, 1992, **618**(12), 7–12, DOI: 10.1002/zaac.19926180102.

472 G. Schilling and G. Meyer, Ternäre Bromide und Iodide zweiwertiger Lanthanide und ihre Erdalkali-Analoga vom Typ AMX_3 und AM_2X_5, *Z. Anorg. Allg. Chem.*, 1996, **622**(5), 759–765, DOI: 10.1002/zaac.19966220502.

473 O. Schmitz-Dumont, G. Bergerhoff and E. Hartert, Über den Einfluß des Kationenradius auf die Bildungsenergie von Anlagerungsverbindungen. VII. Die Systeme Alkalifluorid/Bleifluorid, *Z. Anorg. Allg. Chem.*, 1956, **283**(1–6), 314–329, DOI: 10.1002/zaac.19562830131.

474 M. Schölten and R. Dronskowski, Crystal structure of indium magnesium tribromide, $InMgBr_3$, *Z. Kristallogr. – New Cryst. Struct.*, 1997, **212**(1), 5, DOI: 10.1524/ncrs.1997.212.1.5.

475 M. Scholten, R. Dronskowski and H. Jacobs, $InCrBr_3$: A Ternary Indium Bromide Containing Jahn–Teller Unstable Cr^{2+} and the Magnetic Structures of $InCrBr_3$ and $InFeBr_3$, *Inorg. Chem.*, 1999, **38**(11), 2614–2620, DOI: 10.1021/ic981383t.

476 M. Scholten, R. Dronskowski, T. Staffel and G. Meyer, Synthesis and Crystal Structure of Potassium Indium

Tribromide, $KInBr_3$, *Z. Anorg. Allg. Chem.*, 1998, **624**(11), 1741–1745, DOI: 10.1002/(SICI)1521-3749(1998110)624:11<1741::AID-ZAAC1741>3.0.CO;2-W.

477 B. Schüpp, *Präparation und Charakterisierung neuer Halogenopalladate mit besonderem Schwergewicht bezüglich mehrkerniger Halogenopalladatgruppen*, PhD Thesis, Universität Dortmund, 1999.

478 B. Schüpp and H.-L. Keller, $CsPdCl_3$ – eine Verbindung mit $[Pd_2Cl_6]$-Baugruppen und anorganischem Kation, *Z. Anorg. Allg. Chem.*, 1999, **625**(11), 1944–1950, DOI: 10.1002/(SICI)1521-3749(199911)625:11<1944::AID-ZAAC1944>3.0.CO;2-V.

479 M. Sebastian, J. A. Peters, C. C. Stoumpos, J. Im, S. S. Kostina, Z. Liu, M. G. Kanatzidis, A. J. Freeman and B. W. Wessels, Excitonic emissions and above-band-gap luminescence in the single-crystal perovskite semiconductors $CsPbBr_3$ and $CsPbCl_3$, *Phys. Rev. B: Condens. Matter Mater. Phys.*, 2015, **92**(23), 235210, DOI: 10.1103/PhysRevB.92.235210.

480 H.-J. Seifert and E. Dau, Über die Systeme Alkalimetallbromid/Mangan(II)-bromid, *Z. Anorg. Allg. Chem.*, 1972, **391**(3), 302–312, DOI: 10.1002/zaac.19723910311.

481 H.-J. Seifert and P. Ehrlich, Über die Systeme $NaCl/VCl_2$, KCl/VCl_2 und $CsCl/VCl_2$, *Z. Anorg. Allg. Chem.*, 1960, **302**(5–6), 284–288, DOI: 10.1002/zaac.19603020506.

482 H.-J. Seifert, H. Fink, G. Thiel and J. Uebach, Thermodynamische und strukturelle Untersuchungen an den Verbindungen der Systeme KCl/MCl_2 (M = Ca, Cd, Co, Ni), *Z. Anorg. Allg. Chem.*, 1985, **520**(1), 151–159, DOI: 10.1002/zaac.19855200118.

483 H.-J. Seifert and D. Haberhauer, Über die Systeme Alkalimetallbromid/Calciumbromid, *Z. Anorg. Allg. Chem.*, 1982, **491**(1), 301–307, DOI: 10.1002/zaac.19824910139.

484 H.-J. Seifert and K. Klatyk, Über die Systeme Alkalimetallchlorid/Chrom(II)-chlorid, *Z. Anorg. Allg. Chem.*, 1964, **334**(3–4), 113–124, DOI: 10.1002/zaac.19643340302.

485 H.-J. Seifert and K. Klatyk, Über die Systeme $RbCl/FeCl_2$ und $CsCl/FeCl_2$, *Z. Anorg. Allg. Chem.*, 1966, **342**(1–2), 1–9, DOI: 10.1002/zaac.19663420102.

486 H. J. Seifert and K. H. Kischka, Investigations on systems AX/MnX_2 (A = Li–Cs, Tl; X = Cl, Br, I) by DTA and X-ray analysis, *Thermochim. Acta*, 1978, **27**(1), 85–93, DOI: 10.1016/0040-6031(78)85023-0.

487 H. J. Seifert and K. Klatyk, Das System $CsCl/CrCl_2$, *Naturwissenschaften*, 1962, **49**(23), 539, DOI: 10.1007/BF00626806.

488 H. J. Seifert, T. Krimmel and W. Heinemann, Über die Systeme TlX/MnX_2 und AgX/MnX_2 (X = Cl, Br, I), *J. Therm. Anal.*, 1974, **6**(1), 175–182, DOI: 10.1007/BF01911498.

489 H. J. Seifert and U. Langenbach, Thermoanalytische und röntgenographische Untersuchungen an Systemen Alkalichlorid/Calciumchlorid, *Z. Anorg. Allg. Chem.*, 1969, **368**(1–2), 36–43, DOI: 10.1002/zaac.19693680107.

490 M. W. Shafer, The synthesis and characterization of vanadium difluoride, $NaVF_3$, KVF_3, and $RbVF_3$, *Mater. Res. Bull.*, 1969, **4**(12), 905–912, DOI: 10.1016/0025-5408(69)90047-6.

491 K. Sintani, Y. Tomono, A. Tsuchida and K. Siratori, Influence of Magnetic Ordering on the Lattice Vibration of $KNiF_3$, *J. Phys. Soc. Jpn.*, 1968, **25**(1), 99–108, DOI: 10.1143/JPSJ.25.99.

492 J. L. Sommerdijk and A. Bril, Divalent europium luminescence in perovskite-like alkaline-earth alkaline fluorides, *J. Lumin.*, 1976, **11**(5), 363–367, DOI: 10.1016/0022-2313(76)90021-1.

493 J. L. Soubeyroux, C. Cros, W. Gang, R. Kanno and M. Pouchard, Neutron diffraction investigation of the cationic distribution in the structure of the spinel-type solid solutions $Li_{2-2x}M_{1+x}Cl_4$ (M = Mg, V): Correlation with the ionic conductivity and NMR data, *Solid State Ionics*, 1985, **15**(4), 293–300, DOI: 10.1016/0167-2738(85)90132-8.

494 J. Spector, G. Villeneuve, L. Hanebali and C. Cros, NMR Investigations of the Li^+ ion mobility in the double chlorides Li_2MgCl_4 and $LiMgCl_3$, *Mater. Lett.*, 1982, **1**(2), 43–48, DOI: 10.1016/0167-577X(82)90003-9.

495 V. I. Spitsyn, S. V. Kryuchkov, M. S. Grigoriev and A. F. Kuzina, Polynuclear Clusters of Technetium. Part 1. Synthesis, Crystal and Molecular Structure of Bromide Octanuclear Prismatic and Hexanuclear Octahedral Clusters of Technetium, *Dokl. Akad. Nauk SSSR*, 1988, **288**, 389–393, DOI: 10.1002/chin.198849036.

496 M. Steiner, W. Krüger and D. Babel, Proof of ferromagnetic chains in $CsNiF_3$ by neutron diffraction, *Solid State Commun.*, 1971, **9**(3), 227–229, DOI: 10.1016/0038-1098(71)90123-2.

497 H. Steinfink and G. D. Brunton, The crystal structure of $CsBeF_3$, *Acta Crystallogr., Sect. B: Struct. Crystallogr. Cryst. Chem.*, 1968, **24**(6), 807–810, DOI: 10.1107/S0567740868003225.

498 J. Strähle, J. Gelinek and M. Kölmel, Über den thermischen Abbau einiger Alkalimetall- und Ammoniumhalogenoaurate(III) und die Kristallstruktur der Zersetzungsprodukte $Rb_2Au_2Br_6$, $Rb_3Au_3Cl_8$ und $Au(NH_3)Cl_3$, *Z. Anorg. Allg. Chem.*, 1979, **456**(1), 241–260, DOI: 10.1002/zaac.19794560125.

499 I. Sumio and I. Yoshihiro, The congruent melting compounds in the system $KCl–SnCl_2$, *Chem. Lett.*, 1983, (12), 1803–1806, DOI: 10.1246/cl.1983.1803.

500 Y. Syono, S.-i Akimoto and K. Kohn, Structure Relations of Hexagonal Perovskite-Like Compounds ABX_3 at High Pressure, *J. Phys. Soc. Jpn.*, 1969, **26**(4), 993–999, DOI: 10.1143/JPSJ.26.993.

501 R. G. Szlag, L. Suescun, B. D. Dhanapala and F. A. Rabuffetti, Rubidium–Alkaline-Earth Trifluoroacetate Hybrids as Self-Fluorinating Single-Source Precursors to Mixed-Metal Fluorides, *Inorg. Chem.*, 2019, **58**(5), 3041–3049, DOI: 10.1021/acs.inorgchem.8b02988.

502 Y. Takeda, M. Shimada, F. Kanamaru and M. Koizumi, Structure and Properties of $CsFeBr_3$, *J. Phys. Soc. Jpn.*, 1974, **37**(1), 276, DOI: 10.1143/JPSJ.37.276.

503 L. C. Tang, J. Y. Huang, C. S. Chang, M. H. Lee and L. Q. Liu, New infrared nonlinear optical crystal $CsGeBr_3$: synthesis, structure and powder second-harmonic generation properties, *J. Phys.: Condens. Matter*, 2005, **17**(46), 7275, DOI: 10.1088/0953-8984/17/46/011.

504 D. T. Teaney, M. J. Freiser and R. W. H. Stevenson, Discovery of a Simple Cubic Antiferromagnet: Antiferromagnetic Resonance in $RbMnF_3$, *Phys. Rev. Lett.*, 1962, **9**(5), 212–214, DOI: 10.1103/PhysRevLett.9.212.

505 T. Thao Tran and P. Shiv Halasyamani, Synthesis and characterization of $ASnF_3$ ($A = Na^+$, K^+, Rb^+, Cs^+), *J. Solid State Chem.*, 2014, **210**(1), 213–218, DOI: 10.1016/j.jssc.2013.11.025.

506 G. Thiele, H. W. Rotter and K. D. Schmidt, Die Kristallstrukturen und Phasentransformationen von $RbGeBr_3$, *Z. Anorg. Allg. Chem.*, 1988, **559**(1), 7–16, DOI: 10.1002/zaac.19885590101.

507 G. Thiele, H. W. Rotter and K. D. Schmidt, Die Kristallstrukturen und Phasentransformationen des tetramorphen $RbGeI_3$, *Z. Anorg. Allg. Chem.*, 1989, **571**(1), 60–68, DOI: 10.1002/zaac.19895710106.

508 G. Thiele and B. R. Serr, Crystal structure of rubidium triiodostannate(II), $RbSnI_3$, *Z. Kristallogr. – Cryst. Mater.*, 1995, **210**(1), 64, DOI: 10.1524/zkri.1995.210.1.64.

509 J. Tong, C. Lee, M. H. Whangbo, R. K. Kremer, A. Simon and J. Köhler, Cooperative Jahn–Teller distortion leading to the spin-1/2 uniform antiferromagnetic chains in triclinic perovskites $AgCuF_3$ and $NaCuF_3$, *Solid State Sci.*, 2010, **12**(5), 680–684, DOI: 10.1016/j.solidstatesciences.2009.02.028.

510 A. Tressaud, R. De Pape, J. Portier and P. Hagenmuller, Les systemes MF-FeF_2 (M = Li, Na, Rb, Tl), *C. R. Seances Acad. Sci., Ser. C*, 1968, **266**, 984–986.

511 P. V. Tumram, P. R. Kautkar, S. A. Acharya and S. V. Moharil, NIR Emission and $Eu^{2+}Nd^{3+}$ Energy Transfer in $KSrCl_3$:Eu^{2+}, Nd^{3+} phosphor, *Mater. Today: Proc.*, 2017, **4**(14), 12582–12585, DOI: 10.1016/j.matpr.2017.10.065.

512 Y. Vaills, J. Y. Buzaré, A. Gibaud and C. Launay, X-ray investigations of the cubic to tetragonal phase transition in $CsCaCl_3$ at T_c = 95 K, *Solid State Commun.*, 1986, **60**(2), 139–141, DOI: 10.1016/0038-1098(86)90546-6.

513 A. van Roekeghem, J. Carrete, C. Oses, S. Curtarolo and N. Mingo, High-Throughput Computation of Thermal Conductivity of High-Temperature Solid Phases: The Case of Oxide and Fluoride Perovskites, *Phys. Rev. X*, 2016, **6**(4), 041061, DOI: 10.1103/PhysRevX.6.041061.

514 P. C. E. Villars, *SpringerMaterials Landolt-Börnstein database*, Springer Nature, 2023.

515 D. Visser and A. Prodan, Disorder in $KNiCl_3$ as observed by electron diffraction, *Phys. Status Solidi A*, 1980, **58**(2), 481–488, DOI: 10.1002/pssa.2210580218.

516 A. V. Voloshinovskii, P. A. Rodnyi, A. G. Dmitriev, E. N. Melchakov and S. N. Pidzyrailo, Core-valence luminescence of $CsMgCl_3$ and $CsMgF_3$ crystals, *J. Appl. Spectrosc.*, 1993, **59**(1), 560–562, DOI: 10.1007/BF00663370.

517 F. F. Y. Wang and M. Kestigian, Magnetic Properties of $RbFeF_3$, *J. Appl. Phys.*, 1966, **37**(3), 975–976, DOI: 10.1063/1.1708546.

518 H. Wang Shi and M. Zhoa, Phase diagram of YbI_2-RbI binary system and structural investigation of $RbYbI_3$, *J. Less-Common Met.*, 1987, **127**, 219–224, DOI: 10.1016/0022-5088(87)90381-X.

519 J. E. Weidenborner and A. L. Bednowitz, Structures of ferrimagnetic fluorides of ABF_3 type. I. $RbNiF_3$, *Acta Crystallogr., Sect. B: Struct. Crystallogr. Cryst. Chem.*, 1970, **26**(10), 1464–1468, DOI: 10.1107/S0567740870004338.

520 A. Weiss and K. Damm, Notizen: Zur Kenntnis des Natrium-trichloromercurats (II) $Na(HgCI_3)$. Über Quecksilberhalogenide IV, *Z. Naturforsch. B*, 1954, **9**(1), 82, DOI: 10.1515/znb-1954-0116.

521 A. F. Wells, 332. The crystal structure of $CsCuCl_3$ and the crystal chemistry of complex halides ABX_3, *J. Chem. Soc. B*, 1947, 1662–1670, DOI: 10.1039/JR9470001662.

522 R. D. Willett, C. Dwiggins Jr., R. F. Kruh and R. E. Rundle, Crystal Structures of $KCuCl_3$ and NH_4CuCl_3, *J. Chem. Phys.*, 2004, **38**(10), 2429–2436, DOI: 10.1063/1.1733520.

523 R. F. Williamson and W. O. J. Boo, Lower valence fluorides of vanadium. 1. Synthesis and characterization of sodium trifluorovanadate, potassium trifluorovanadate, and rubidium trifluorovanadate, *Inorg. Chem.*, 1977, **16**(3), 646–648, DOI: 10.1021/ic50169a030.

524 G. Wittenburg, *Untersuchungen von Struktur-Eigenschafts-Beziehungen bei Trihalogenometallaten AMX_3 von Germanium(II), Zinn(II) und Blei(II)*, PhD Thesis, Universität Freiburg, Breisgau, 2000.

525 H. T. Witteveen and J. A. R. Van Veen, Magnetic susceptibilities of polycrystalline samples of the compounds $ANiCl_3$ (A = Rb, NH_4, Tl, Cs) and $ANiBr_3$ (A = Rb, Cs), *J. Phys. Chem. Solids*, 1974, **35**(3), 337–346, DOI: 10.1016/S0022-3697(74)80027-2.

526 H. T. Witteveen and J. A. R. van Veen, Magnetic susceptibilities of the compounds $AFeCl_3$ (A = Tl,Rb,NH_4,Cs) with antiferromagnetic linear chains, *J. Chem. Phys.*, 1973, **58**(1), 186–191, DOI: 10.1063/1.1678903.

527 G. Wu and R. Hoppe, Zur Kenntnis der Fluoride zweiwertiger Lanthanoide. II. Über die Synthese von $MLnF_3$ aus $MLnF_4$, *Z. Anorg. Allg. Chem.*, 1984, **514**(7), 92–98, DOI: 10.1002/zaac.19845140712.

528 G.-Q. Wu and R. Hoppe, Neue Fluoro-Perowskite zweiwertiger Lanthaniden. Zur Kenntnis von $CsEuF_3$, $CsYbF_3$ und $RbYbF_3$, *Z. Anorg. Allg. Chem.*, 1983, **504**(9), 55–59, DOI: 10.1002/zaac.19835040907.

529 Y. Xie, S. Wang and X. Zhao, Phase diagram and structure of $CsSm_{(1-x)}Yb_xI_3$ systems, *J. Alloys Compd.*, 1996, **241**(1), 40–43, DOI: 10.1016/0925-8388(96)02196-2.

530 S. Yakovlev, M. Avdeev and M. Mezouar, High-pressure structural behavior and equation of state of $NaZnF_3$, *J. Solid State Chem.*, 2009, **182**(6), 1545–1549, DOI: 10.1016/j.jssc.2009.03.031.

531 Y. Yamane, K. Yamada and K. Inoue, Mechanochemical synthesis and order–disorder phase transition in fluoride ion conductor $RbPbF_3$, *Solid State Ionics*, 2008, **179**(17), 605–610, DOI: 10.1016/j.ssi.2008.04.022.

532 T. Yanagida, Y. Fujimoto, M. Arai, M. Koshimizu, T. Kato, D. Nakauchi and N. Kawaguchi, Comparative studies of scintillation properties of Tl-based crystals, *Sens. Mater.*, 2020, **32**(4), 1351–1356.

533 H. W. Zandbergen, Neutron powder diffraction and magnetic measurements on $TlMnI_3$ and $TlFeI_3$, *J. Solid State*

Chem., 1981, **37**(2), 189–203, DOI: **10.1016/0022-4596(81)90085-2**.

534 H. W. Zandbergen, Neutron powder diffraction and magnetic measurements on $RbTiI_3$, $RbVI_3$, and $CsVI_3$, *J. Solid State Chem.*, 1981, **37**(3), 308–317, DOI: **10.1016/0022-4596(81)90492-8**.

535 H. W. Zandbergen, G. C. Verschoor and D. J. W. IJdo, The structures of thallium cadmium triiodide and dirubidium iron tetraiodide, *Acta Crystallogr., Sect. B: Struct. Crystallogr. Cryst. Chem.*, 1979, **35**(6), 1425–1427, DOI: **10.1107/S0567740879006580**.

536 J. Zhang and J. D. Corbett, Synthesis and structure of The Novel Layered Phase $CsTi_2Cl_7$, *Z. Anorg. Allg. Chem.*, 1990, **580**(1), 36–44, DOI: **10.1002/zaac.19905800105**.

537 J. Zhang and G. Hong, Luminescence properties of Ce^{3+} in KMF_3 (M = Mg,Ca,Sr,Ba) hosts with perovskite structure, *J. Rare Earths*, 1997, **2**, 75–78.

538 J. Zhang, R. Y. Qi and J. D. Corbett, Two novel titanium halide phases: KTi_4Cl_{11} and $CsTi_{4.3}I_{11}$, *Inorg. Chem.*, 1991, **30**(25), 4794–4798, DOI: **10.1021/ic00025a022**.

539 A. Zodkevitz, J. Makovsky and Z. H. Kalman, The Preparation and Crystal Structure of $TlMnCl_3$, $TlFeCl_3$, $TlCoCl_3$ and $TlNiCl_3$, *Isr. J. Chem.*, 1970, **8**(5), 755–762, DOI: **10.1002/ijch.197000095**.

540 G. Bergerhoff and L. Goost, Ammoniumtrifluorostannat(II), *Acta Crystallogr., Sect. B: Struct. Crystallogr. Cryst. Chem.*, 1973, **29**(3), 632–633, DOI: **10.1107/S0567740873003031**.

541 P. Charpin, N. Roux and J. Ehnetsmann, *Compt. Rend.*, 1968, **267 C**, 484–486.

542 T. Das, G. Di Liberto and G. Pacchioni, Density Functional Theory Estimate of Halide Perovskite Band Gap: When Spin Orbit Coupling Helps, *J. Phys. Chem. C*, 2022, **126**(4), 2184–2198, DOI: **10.1021/acs.jpcc.1c09594**.

543 R. Hoppe, W. Liebe and W. Dähne, Über Fluoromanganate der Alkalimetalle, *Z. Anorg. Allg. Chem.*, 1961, **307**(5–6), 276–289, DOI: **10.1002/zaac.19613070507**.

544 T. D. Huan, V. N. Tuoc and N. V. Minh, Layered structures of organic/inorganic hybrid halide perovskites, *Phys. Rev. B*, 2016, **93**(9), 094105, DOI: **10.1103/PhysRevB.93.094105**.

545 A. Kozak, *Rev. Chim. Miner.*, 1971, **8**, 301–335.

546 V. G. Krishnan, S.-q Dou and A. Weiss, Structure and Bonding of Tribromocadmates, $ACdBr_3$, A = NH_4, Rb, Cs, CH_3NH_3, $(CH_3)_2NH_2$, $(CH_3)_4N$], $[H_2NNH_3$, and $(H_2N)_3C$. An X-ray Diffraction and $^{79\text{-}81}$Br NQR Study, *Z. Naturforsch., A: Phys. Sci.*, 1991, **46**(12), 1063–1082, DOI: **10.1515/zna-1991-1212**.

547 A. Le Bail, J. L. Fourquet, J. Rubín, E. Palacios and J. Bartolomé, NH_4CdF_3: Structure of the low temperature phase, *Phys. B*, 1990, **162**(3), 231–236, DOI: **10.1016/0921-4526(90)90017-O**.

548 G. Meyer and N. Böhmer, Korrosion von Messing und Bronze durch Ammoniumhalogenide, *Z. Anorg. Allg. Chem.*, 2000, **626**(6), 1332–1334, DOI: **10.1002/(SICI)1521-3749(200006)626:6<1332::AID-ZAAC1332>3.0.CO;2-X**.

549 M. J. Portier, A. Tressaud, J. L. Dupin and R. de Pape, Structures et proprietes magnetiques de quelques composes de formule M Fe F_3 (M = Na, K, Rb, Cs, NH_4, T1), *Mater. Res. Bull.*, 1969, **4**(1), 45–50, DOI: **10.1016/0025-5408(69)90015-4**.

550 M. M. Rolies and C. J. De Ranter, A new investigation of ammonium cadmium chloride, *Acta Crystallogr., Sect. B: Struct. Crystallogr. Cryst. Chem.*, 1978, **34**(10), 3057–3059, DOI: **10.1107/S0567740878010018**.

551 W. Rüdorbf, J. Kandler and D. Babel, Untersuchungen an ternären Fluoriden. I. Struktur, Magnetismus und Reflexionsspektren von Alkali-, Ammonium- und Thallium-Nickel(II)-fluoriden, *Z. Anorg. Allg. Chem.*, 1962, **317**(5–6), 261–287, DOI: **10.1002/zaac.19623170502**.

552 G. Shachar, J. Makovsky and H. Shaked, Neutron diffraction and magnetic measurements of polycrystalline NH_4MnCl_3, *Solid State Commun.*, 1971, **9**(9), 493–495, DOI: **10.1016/0038-1098(71)90131-1**.

553 D. Smith, Hindered Rotation of the Ammonium Ion in the Solid State, *Chem. Rev.*, 1994, **94**(6), 1567–1584, DOI: **10.1021/cr00030a005**.

554 C. C. Stoumpos, L. Frazer, D. J. Clark, Y. S. Kim, S. H. Rhim, A. J. Freeman, J. B. Ketterson, J. I. Jang and M. G. Kanatzidis, Hybrid Germanium Iodide Perovskite Semiconductors: Active Lone Pairs, Structural Distortions, Direct and Indirect Energy Gaps, and Strong Nonlinear Optical Properties, *J. Am. Chem. Soc.*, 2015, **137**(21), 6804–6819, DOI: **10.1021/jacs.5b01025**.

555 C. C. Stoumpos, L. Mao, C. D. Malliakas and M. G. Kanatzidis, Structure–Band Gap Relationships in Hexagonal Polytypes and Low-Dimensional Structures of Hybrid Tin Iodide Perovskites, *Inorg. Chem.*, 2017, **56**(1), 56–73, DOI: **10.1021/acs.inorgchem.6b02764**.

556 J. Tian, D. B. Cordes, C. Quarti, D. Beljonne, A. M. Z. Slawin, E. Zysman-Colman and F. D. Morrison, Stable 6H Organic–Inorganic Hybrid Lead Perovskite and Competitive Formation of 6H and 3C Perovskite Structure with Mixed A Cations, *ACS Appl. Energy Mater.*, 2019, **2**(8), 5427–5437, DOI: **10.1021/acsaem.9b00419**.

557 S. I. Troyanov, I. V. Morozov and Y. M. Korenev, The synthesis and crystal structure of ammonium fluorocuprates NH_4CuF_3 and $(NH_4)_2CuF_4$, *Russ. J. Inorg. Chem.*, 1993, **38**(6), 909–913, DOI: **10.1002/chin.199352035**.

558 K. Yamada, T. Matsui, T. Tsuritani, T. Okuda and S. Ichiba, ^{127}I-NQR, ^{119}Sn Mössbauer Effect, and Electrical Conductivity of $MSnI_3$ (M = K, NH_4, Rb, Cs, and CH_3NH_3), *Z. Naturforsch., A: Phys. Sci.*, 1990, **45**(3–4), 307–312, DOI: **10.1515/zna-1990-3-416**.

559 A. Jain, S. P. Ong, G. Hautier, W. Chen, W. D. Richards, S. Dacek, S. Cholia, D. Gunter, D. Skinner, G. Ceder and K. A. Persson, Commentary: The Materials Project: A materials genome approach to accelerating materials innovation, *APL Mater.*, 2013, **1**(1), 011002, DOI: **10.1063/1.4812323**.

560 V. I. Hegde, C. K. H. Borg, Z. del Rosario, Y. Kim, M. Hutchinson, E. Antono, J. Ling, P. Saxe, J. E. Saal and B. Meredig, Quantifying uncertainty in high-throughput density functional theory: A comparison of AFLOW, Materials Project, and OQMD, *Phys. Rev. Mater.*, 2023, **7**(5), 053805, DOI: **10.1103/PhysRevMaterials.7.053805**.

561 K. V. Sopiha, C. Comparotto, J. A. Márquez and J. J. S. Scragg, Chalcogenide Perovskites: Tantalizing Prospects, Challenging Materials, *Adv. Opt. Mater.*, 2022, **10**(3), 2101704, DOI: **10.1002/adom.202101704**.

562 G. Kresse and J. Furthmüller, Efficiency of *ab initio* total energy calculations for metals and semiconductors using a plane-wave basis set, *Comput. Mater. Sci.*, 1996, **6**(1), 15–50, DOI: **10.1016/0927-0256(96)00008-0**.

563 G. Kresse and J. Furthmüller, Efficient iterative schemes for *ab initio* total-energy calculations using a plane-wave basis set, *Phys. Rev. B: Condens. Matter Mater. Phys.*, 1996, **54**(16), 11169–11186, DOI: **10.1103/PhysRevB.54.11169**.

564 J. P. Perdew, K. Burke and M. Ernzerhof, Generalized Gradient Approximation Made Simple, *Phys. Rev. Lett.*, 1996, **77**(18), 3865–3868, DOI: **10.1103/PhysRevLett.77.3865**.